Nuclear Science
NEA/NSC/DOC(2010)10

ISBN 978-92-64-99152-1

NEA Nuclear Science Committee
NEA Committee on the Safety of Nuclear Installations

VVER-1000 Coolant Transient Benchmark

Phase 2 (V1000CT-2)

Summary Results of Exercise 1 on Vessel Mixing Simulation

N.P. Kolev, I. Spasov
INRNE, Bulgaria

E. Royer
Commissariat à l'énergie atomique, France

NEA No. 6964

NUCLEAR ENERGY AGENCY
Organisation for Economic Co-operation and Development

ORGANISATION FOR ECONOMIC CO-OPERATION AND DEVELOPMENT

The OECD is a unique forum where the governments of 33 democracies work together to address the economic, social and environmental challenges of globalisation. The OECD is also at the forefront of efforts to understand and to help governments respond to new developments and concerns, such as corporate governance, the information economy and the challenges of an ageing population. The Organisation provides a setting where governments can compare policy experiences, seek answers to common problems, identify good practice and work to co-ordinate domestic and international policies.

The OECD member countries are: Australia, Austria, Belgium, Canada, Chile, the Czech Republic, Denmark, Finland, France, Germany, Greece, Hungary, Iceland, Ireland, Israel, Italy, Japan, Korea, Luxembourg, Mexico, the Netherlands, New Zealand, Norway, Poland, Portugal, the Slovak Republic, Slovenia, Spain, Sweden, Switzerland, Turkey, the United Kingdom and the United States. The European Commission takes part in the work of the OECD.

OECD Publishing disseminates widely the results of the Organisation's statistics gathering and research on economic, social and environmental issues, as well as the conventions, guidelines and standards agreed by its members.

NUCLEAR ENERGY AGENCY

The OECD Nuclear Energy Agency (NEA) was established on 1st February 1958 under the name of the OEEC European Nuclear Energy Agency. It received its present designation on 20th April 1972, when Japan became its first non-European full member. NEA membership today consists of 28 OECD member countries: Australia, Austria, Belgium, Canada, the Czech Republic, Denmark, Finland, France, Germany, Greece, Hungary, Iceland, Ireland, Italy, Japan, Korea, Luxembourg, Mexico, the Netherlands, Norway, Portugal, the Slovak Republic, Spain, Sweden, Switzerland, Turkey, the United Kingdom and the United States. The European Commission also takes part in the work of the Agency.

The mission of the NEA is:

- to assist its member countries in maintaining and further developing, through international co-operation, the scientific, technological and legal bases required for a safe, environmentally friendly and economical use of nuclear energy for peaceful purposes, as well as
- to provide authoritative assessments and to forge common understandings on key issues, as input to government decisions on nuclear energy policy and to broader OECD policy analyses in areas such as energy and sustainable development.

Specific areas of competence of the NEA include safety and regulation of nuclear activities, radioactive waste management, radiological protection, nuclear science, economic and technical analyses of the nuclear fuel cycle, nuclear law and liability, and public information.

The NEA Data Bank provides nuclear data and computer program services for participating countries. In these and related tasks, the NEA works in close collaboration with the International Atomic Energy Agency in Vienna, with which it has a Co-operation Agreement, as well as with other international organisations in the nuclear field.

Corrigenda to OECD publications may be found online at: *www.oecd.org/publishing/corrigenda*.

Cover photo: Kozloduy NPP (Bulgaria).

Foreword

The Nuclear Energy Agency (NEA) of the Organisation for Economic Co-operation and Development (OECD) has completed, under United States Nuclear Regulatory Commission (US NRC) sponsorship, the PWR main steam line break (MSLB) and BWR turbine trip benchmarks for coupled thermal-hydraulics/neutron kinetics codes. Over the course of these benchmarks a systematic approach has been established to validate best-estimate coupled codes. This approach employs a multi-level methodology that not only allows for a consistent and comprehensive validation process, but also contributes to determine additional requirements and to prepare a basis for licensing applications of the coupled calculations for a specific reactor type, *i.e.* to establish a safety expertise in the analysis of reactivity transients.

The OECD VVER-1000 Coolant Transient Benchmark project was started in 2002 with an overall objective to assess computer codes for safety analysis of VVER power plants, specifically for their use in reactivity transients. It consists of two phases. Phase 1, labelled V1000CT-1 and led by Pennsylvania State University (PSU) is a main coolant pump (MCP) start-up while three other MCP are in operation. Phase 2, labelled V1000CT-2 and led by the French Commissariat à l'énergie atomique (CEA) includes calculation of coolant mixing experiments and a main steam line break (MSLB) analysis. The V1000CT-2 benchmark team is from the Institute for Nuclear Research and Nuclear Energy (INRNE, Bulgaria), the CEA and PSU. The V1000CT-2 benchmark sponsors are the OECD/NEA and the CEA. Kozloduy nuclear power plant is providing technical support.

The V1000CT-2 benchmark reports are being published by the NEA in four volumes. The first two volumes provide the specifications of the VVER-1000 vessel mixing and MSLB benchmarks. In addition, the transient boundary conditions, cross-section libraries and decay heat values as a function of time are available on the NEA website and on CD-ROM (upon request). The present volume summarises the results for V1000CT-2 Exercise 1 (single phase vessel mixing calculation) and identifies important modelling issues. The reference problem is a nuclear power plant flow mixing experiment. The fourth volume will present the results for Exercises 2 and 3 (coupled code MSLB analysis using validated flow mixing models).

Readers are kindly invited to note that, although this report is printed in black and white, many of the figures included were prepared in colour. The colour versions will be made available on the NEA website.

Acknowledgements

This report is the sum of many efforts: those of the participants, the benchmark team and the funding agencies – CEA France and the OECD/NEA and their staff. Special thanks are due to D. Caruge and R. Lenain from CEA Saclay whose support and encouragement in establishing and preparing this benchmark were invaluable. Particular appreciation goes to U. Bieder from CEA Grenoble who participated in preparing the specifications.

The authors would like to thank Professor J. Aragonés from Universidad Politécnica de Madrid – member of the NSC/NEA and Professor F. d'Auria from the University of Pisa, member of the NEA Committee on the Safety of Nuclear Installations, for their support in establishing the OECD benchmark on VVER vessel mixing and MSLB.

Special thanks are due to the personnel of Kozloduy NPP for providing plant data, simulator time and expertise. Of particular note is the support of J. Kostadinov, former Executive Director of KNPP.

The authors thank the V1000CT-2 benchmark participants and the members of the AER Working Groups D and C for their valuable support, comments and feedback. Special appreciation goes to the report reviewers: U. Bieder (CEA), T. Hoehne (FZD) and M. Boetcher (FZK).

The authors wish to express their sincere appreciation for the outstanding support offered by Dr. Enrico Sartori, who provided efficient administration, organisation and valuable technical recommendations.

Table of contents

List of tables

List of figures

List of abbreviations

ANS	American Nuclear Society
BOC	Beginning of cycle
BPG	Best practice guidelines
BST	Block of shielding tubes
CEA	Commissariat à l'énergie atomique
DES	Detached eddy simulation
DTC	Doppler temperature coefficient
EFPD	Effective full power days
EREC	Electrogorsk Research and Experimental Centre
FA	Fuel assembly
FZD	Forschung Zentrum Dresden
FZK	Forschung Zentrum Karlsruhe (Karlsruhe Institute of Technology)
GRS	Geselschaft für Reaktorsicherheit
HP	Hot power
HZP	Hot zero power
INRNE	Institute for Nuclear Research and Nuclear Energy
KI	Kurchatov Institute
KNPP	Kozloduy nuclear power plant
KU	Kiev University
LES	Large eddy simulation
LWR	Light water reactor
MCP	Main coolant pump
MSH	Main steam header
MSLB	Main steam line break
NEA	Nuclear Energy Agency
NRC	Nuclear Regulatory Commission
OECD	Organisation for Economic Co-operation and Development
ORNL	Oak Ridge National Laboratory
PSU	Pennsylvania State University
PWR	Pressurised water reactor
RCS	Reactor coolant system
RPLC	Reactor power limitation controller
RPC	Reactor power controller
SG	Steam generator
SST	Shear stress transport
TH	Thermal-hydraulics
UNIPI	University of Pisa

Chapter 1: Introduction

Recently developed best-estimate computer code systems for modelling of 3-D coupled neutronics/ thermal-hydraulic transients and for the coupling of core and system dynamics need to be validated against experimental results and compared against each other. International benchmark studies have been set up for this purpose.

Coupled code benchmarks such as the OECD PWR MSLB problem (NEA, 1999) identified the coolant mixing as an unresolved issue in the analysis of complex plant transients with reactivity insertion. Phase 2 of the VVER-1000 Coolant Transient Benchmarks (V1000CT-2) (NEA, 2010a, 2010b; Topalov, 2004; Bieder, 2004) was thus defined aiming at providing a framework for:

- assessment of single-phase vessel mixing models;
- assessment of coupled codes in MSLB simulations using validated mixing models.

The benchmark includes a complete set of input data and consists of three exercises as summarised below.

1.1 Exercise 1 – Computation of a vessel mixing experiment

The vessel mixing problem is based on VVER-1000 plant experiments. The objective is to test the capability of reactor vessel thermal-hydraulic models to represent single-phase flow mixing. The specific objectives are:

- understanding the main physics;
- qualification of the available data;
- understanding the hard point of modelling;
- understanding the actual limits of CFD and coarse-mesh simulation.

The reference problem is a coolant transient initiated by steam generator isolation at low power, considered as a pure thermal-hydraulic problem. The available plant data permit code validation on different scales:

- separate effects;
- component level (reactor pressure vessel);
- system level.

Regarding CFD codes the task is to assess the ability of CFD to reproduce the experimentally observed angular turn of the loop flow centres (swirl) and the core inlet temperature distribution, given the vessel boundary conditions and the pressure above the core. The calculation of the vessel outlet parameters (loop-to-loop mixing) is an option.

Regarding system codes, the task is to assess the ability of multi-1-D vessel models with cross-flow and coarse 3-D models to reproduce the swirl and the core inlet temperature distribution, as well as the vessel outlet temperatures. Given vessel boundary conditions or full plant simulation can be used.

1.2 Exercise 2 – Computation of a VVER-1000 MSLB transient with given vessel boundary conditions

The task is to model the core and the vessel only, using the validated coolant mixing models and pre-calculated vessel MSLB boundary conditions. A realistic and a pessimistic scenario are considered. The primary objective is to evaluate the response of the coupled 3-D neutronics/core-vessel thermal-hydraulics in code-to-code comparison. A specific objective is to provide an additional test of the vessel mixing models with MSLB boundary conditions, by comparing coarse-mesh solutions and reference CFD results for the core inlet distributions. For this purpose, a CFX-5 transient solution for the assembly inlet parameters was made available by FZD (Hoehne, 2007b). Supplementary plant estimated data from the Kozloduy-6 mixing experiments (NEA, 2010a) can also be used for semi-quantitative comparison of the disturbed sector formation and the angular turn of the loop flows.

1.3 Exercise 3 – Best-estimate coupled core-plant MSLB simulation

This exercise is a best-estimate analysis of the transient in its entirety, for a realistic and a pessimistic scenario.

The V1000CT-2 benchmark is documented in four volumes. The first two volumes in the series contain the specifications of the vessel mixing problem and MSLB problem correspondingly. The present volume summarises the comparative analysis of the submitted results for Exercise 1 (computation of a vessel mixing experiment). The fourth volume will contain the summary results of Exercises 2 and 3 (MSLB simulation).

A total of 13 results for Exercise 1 have been submitted by 11 organisations from 8 countries as listed in Table 1.1 below. Chapter 2 of this report presents a summary description of Exercise 1. Chapter 3 discusses the metrics used to quantify the comparison of the results. Chapter 4 presents the comparison of CFD results. Chapter 5 shows the comparison of coarse-mesh results using system codes. Appendices A and B describe the codes used by the participants. Appendices C and D present user-provided calculation details. Appendices E and F provide selected CFD and coarse mesh results in table format.

Table 1.1: List of participants in Exercise 1 of V1000CT-2

Organisation	Country	Code	Type	Model
BUTE	Hungary	CFX-10	CFD	SST
CEA	France	TRIO_U	CFD	LES
EREC	Russia	REMIX 1.0	CFD	k-ε
FZK	Germany	CFX-10	CFD	k-ε
FZD	Germany	CFX-10	CFD	SST
ORNL	USA	FLUENT	CFD	k-ω
UNIPI	Italy	CFX-10	CFD	k-ε
INRNE	Bulgaria	CATHARE2	System	Multi-1-D
GRS/KI	Germany/Russia	ATHLET/BIPR8	System	Multi-1-D
KU	Ukraine	RELAP3D	System	Coarse 3-D
PSU	USA	TRACE	System	Coarse 3-D
UNIPI	Italy	RELAP3D	System	Coarse 3-D

Chapter 2: The investigated mixing problem

This chapter summarises the main features of the vessel mixing problem based on plant experiments. The reference plant is Kozloduy-6 with VVER-1000 V320 in Bulgaria. This is a four loop pressurised water reactor with hexagonal fuel assemblies, horizontal steam generators and 3 000 MW thermal power. Figures 2.1 through 2.3 and Table 2.1 illustrate the reactor vessel and internals, and the location of the main coolant inlet nozzles.

During the plant-commissioning phase of Kozloduy NPP units 5 and 6 special experiments were conducted to study the mixing of loop flows in the reactor vessel of VVER-1000 V320 (NEA, 2010a; Topalov, 2004). Starting from nearly symmetric hydraulic states, thermal asymmetric loop operation in different combinations was caused by disturbing the steam flow of one or more steam generators (SG). During the tests all main coolant pumps (MCP) were in operation. Both loop heat-up and loop cool-down were considered in the experiments. For the heat-up tests the pressure in the steam generator was first increased by closing the steam isolation valve (SIV) and isolating the SG from feedwater. Then, the pressure was stabilised by steam dump to the atmosphere.

Non-uniform and asymmetric loop flow mixing in the reactor vessel has been observed in the event of such thermal asymmetric loop operation. For certain flow conditions a swirl was formed in the downcomer and the lower plenum causing an azimuth shift of the main loop flows with respect to the cold leg axes.

One of the tests involving single loop heat-up and conducted at Kozloduy-6 was chosen as the reference problem for Exercise 1 of the V1000CT-2 benchmark. The conditions were selected so that the reactivity feedback effects were small enough and the thermal-hydraulics could be approximately separated from neutron kinetics. The objective of the plant experiment was to determine the following characteristics:

- Mixing coefficients for two in-vessel flow paths:
  - from cold legs to the fuel assembly outlets;
  - from cold legs to hot legs.
- The angular turn of the loop flows relative to the cold leg axes.

The mixing experiment was initiated by isolating SG #1. Three states were considered: initial, transient and final stabilised state. These states are described below. After the stabilisation of the pressure and the core outlet temperature, the experiment was repeated for loop #2. The transient caused by disturbing loop #1 is selected for the coolant mixing analysis and the data of the second experiment is used indirectly to support the analysis.

2.1 Initial state

The reactor core is at the beginning of life (BOL) with an average exposure of 0.4 effective full power days. All four MCP and four steam generators are in operation. The main operational parameters are as follows:

- Thermal power of the reactor: 281 MW/9.36% of the nominal according to primary circuit balance.
- Pressure above the core is 15.59 MPa (close to the nominal value of 15.7 MPa).
- Coolant temperature at the reactor inlet is 268.6°C/541.8 K (about 20° lower than the nominal value).

- Boron acid concentration is 7.2 g/kg, near the value of 7.5 g/kg at which the coolant temperature reactivity coefficient is zero.
- Control rod groups #9 and #10 are fully inserted and groups #1-7 are fully withdrawn. The position of the regulating rod group #8 is ≈84% from the bottom of the core.
- The automatic power controller and the power limitation controller are turned off.
- Steam generator levels are equal to the nominal ones and there is no letdown flow. The main steam header pressure is 5.07 MPa, about 1.0 MPa lower than the nominal value.

2.2 Transient

The transient is initiated by closure of a steam isolation valve (SIV-1) and isolating SG-1 from feedwater. The pressure in SG-1 increases and stabilises to 6.47 MPa in about 20 min. The MSH pressure is maintained approximately constant during the transient by operating the steam dump to condenser (BRU-K) in regulating mode.

The coolant temperature in loop #1 rises by 13.6° and the mass flow rate decreases by ≈3.6%. The temperature in the other loops increases slightly due to the mixing of loop flows. The mass flow through the reactor decreases by 1%. Reverse heat transfer occurs in the isolated SG-1. At about 90 s transient time the temperature of cold leg #1 exceeds that of the hot leg. The difference stabilises to 0.6-0.8° in about 25 min.

During the transient the position of control rods is fixed. The reactor power is c low – about 9.4%, and changes by 0.16%. The initially symmetric core power distribution does not change significantly and remains nearly symmetric within the error tolerance. Analysis has shown that in most of the assembly powers the change is less than 2%. Only four deviations exceed 3% and are 3.1%, 3.3%, 3.5% and 4.3% correspondingly. This permits to assume an approximately constant power distribution during the considered coolant transient. In addition, the total power remains very low, about 9.4%.

2.3 Final state

The stabilised state at 1 800 s from the onset of the transient is considered as “final state”. Table 2.2 shows the integral parameters for the initial and final state. Time histories are given in NEA (2010a).

2.4 Plant data

The following measured data (NEA, 2010a; Topalov, 2004) from Kozloduy-6 are available for code validation:

- core, vessel and plant integral parameters and time histories;
- pressure line in the vessel;
- 2-D distributions of the fuel assembly outlet temperatures in 95 out of 163 assemblies;
- core power distribution (assumed constant during the transient).

Other plant data, *e.g.* the assembly inlet temperatures, full core distributions and loop-to-assembly flow mixing coefficients, have been derived from the direct measurements. The full core outlet temperatures (for 163 assemblies) were obtained by symmetry considerations or cross-interpolation from the 95 measured values. Note that the core has 60° rotational symmetry in the initial state at BOL. The corresponding relative temperature rise distribution is shown in Figure 2.5. A measured core inlet velocity profile in Kozloduy-5 (another plant unit) is used for qualitative comparison.

It is important to note that because of the specific design of the assembly heads, the outlet measured temperatures are about 0.5 K less than the bulk flow temperatures at the end of the heated parts of the assemblies and the reactor outlet. This is due to the cooler jets of bypass flow through the control rod guide channels into the assembly heads (see Figure 2.2). A correct comparison with the assembly outlet temperatures requires precise modelling of the mixing in the assembly heads.

In order to reduce the uncertainty associated with the modelling of local flow mixing and the quasi-stagnation zone in the assembly head, the *assembly inlet* temperatures Tin,k were estimated from the outlet measurements and used for comparison with the calculations instead of the outlet temperatures. For this purpose the assembly flows were assumed uniform (the actual non-uniformity is maximum 1-1.5%), and the assembly powers or temperature rise were assumed constant during the transient (the actual local power changes during the transient were less than 2% according to SPND readings except for two assemblies where the changes exceeded 3%).

The mixing coefficient Cnk from cold leg #*n* to the outlet of FA #*k* is defined as the ratio of coolant flow from loop *n* into assembly *k*, to the total flow through assembly *k*. In general, the flow into assembly #*k* has contributions from all four loops and correspondingly there are four mixing coefficients C1k, C2k, C3k and C4k. These coefficients have been determined by means of the Least Squares Method from flow and temperature balance using the measured temperatures at the assembly outlets and integral parameters.

Experimentally determined loop-to-assembly mixing coefficients Cnk are shown in per cent in Figure 2.4. Note that the centrelines of "non-mixing zones" with Cnk = 90-100% mark the corresponding loop flows "centres". Azimuth angular turn of the loop flow centres relative to the cold leg axes is observed as shown in Table 2.3 below. Results from Kozloduy Unit 5 are shown for comparison.

Figure 2.1: Reactor vessel and internals

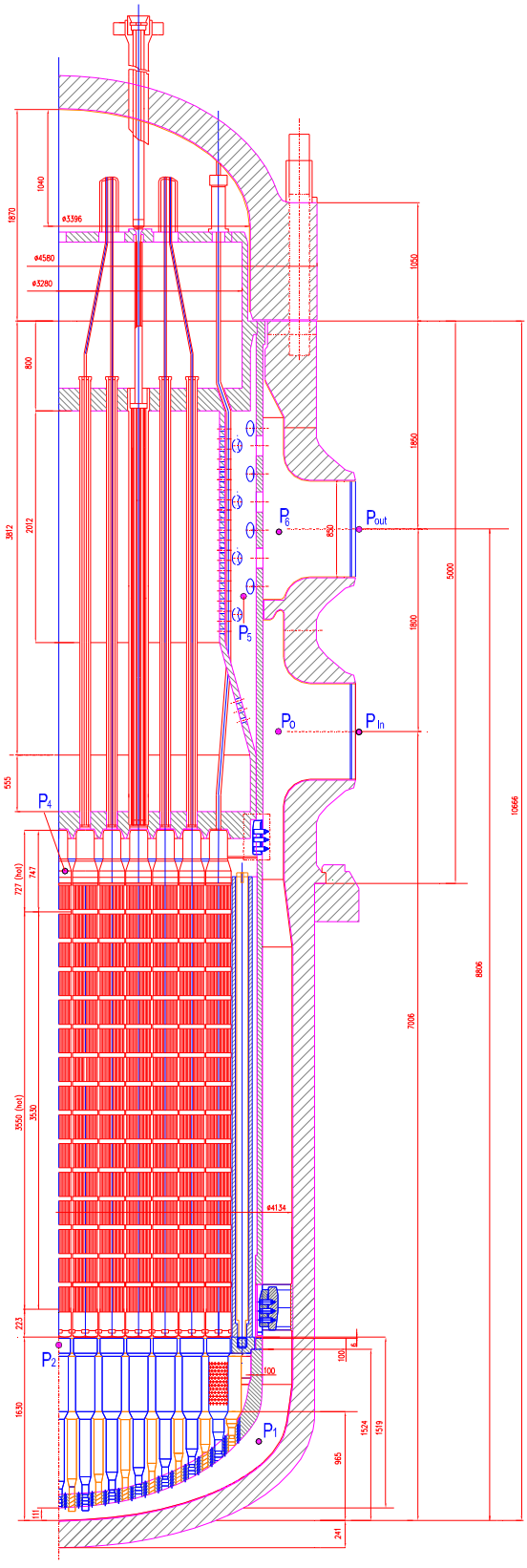

Figure 2.2: Flow paths at the fuel assembly head

1 – thermocouple, 2 – control rod, 3 – guide tube

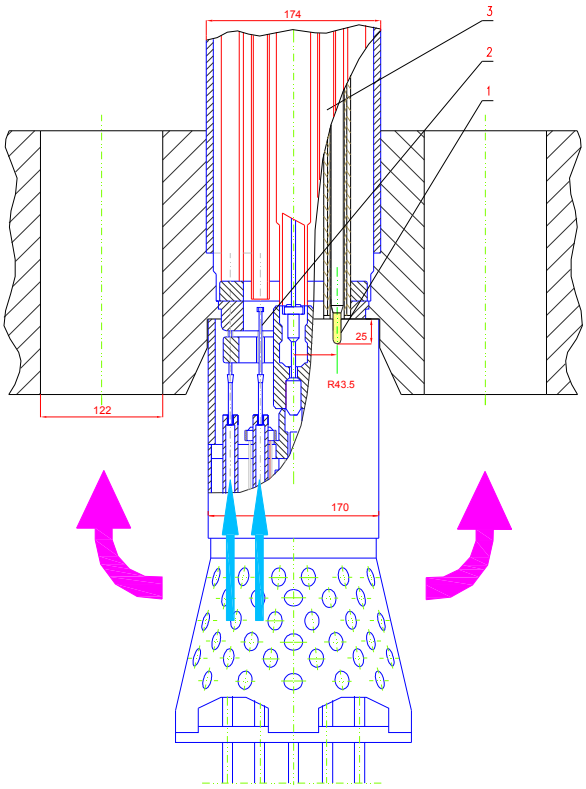

Figure 2.3: Location of the VVER-1000 vessel inlet nozzles by design

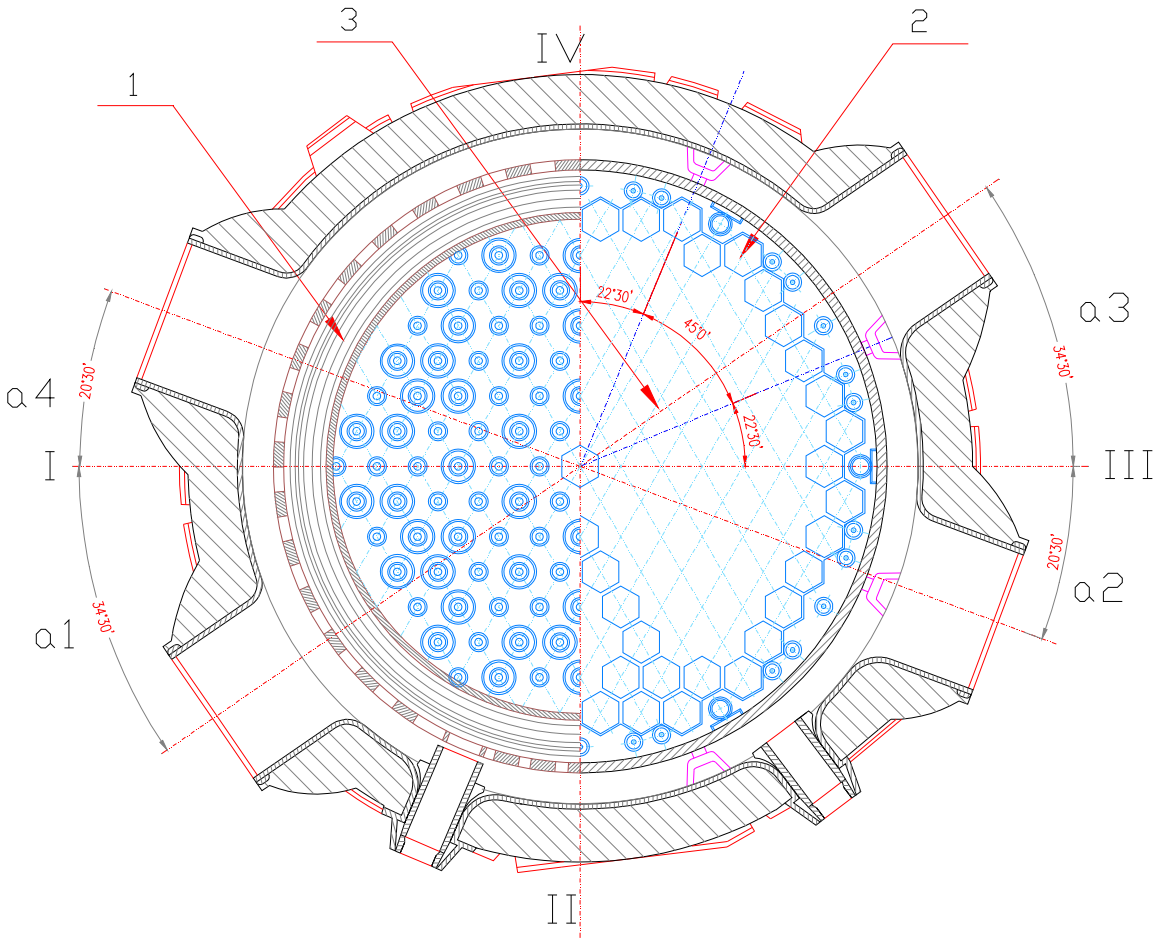

Table 2.1: Actual location of the vessel inlet nozzles of Kozloduy-6

Inlet nozzle	Angle	Concept. design	Actual	Deviation
1	α1	34°30’	34°39’	-7%
2	α2	20°30’	20°18’	+10%
3	α3	34°30’	34°38’	+6%
4	α4	20°30’	20°29’	-1%

Table 2.2: Integral parameters in the initial and final state

Parameter	Initial state before closing SIV-1	Final stabilised state SIV-1 closed	Uncertainty
Exposure, FPD	0.4	0.4	
Core power, MW (primary balance)	281	286	± 60 MW
Boron acid concentration, g/kg	7.20	7.20	
Position of CR group #8, %	84	84	± 1%
Reactor inlet pressure, P0, MPa	15.97 [1]	15.97 [1]	
Reactor pressure drop, P0-P6, MPa	0.418	0.417	± 0.043 MPa
Core pressure drop, MPa (design/plant)	0.142/0.149	0.142/0.149	
Upper plenum losses, MPa (estimated)	0.042 [2]	0.042 [2]	
V1000CT-2 Exercise 1 boundary conditions			
Pressure above the core, P4, MPa	15.593	15.593	± 0.3 MPa
Reactor outlet pressure, P6, MPa	15.55 [1]	15.55 [1]	
Cold leg #1 coolant temperature, C/K	268.6/541.75	282.2/555.35	± 1.5 K
Cold leg #2 coolant temperature, C/K	268.7/541.85	269.9/543.05	± 1.5 K
Cold leg #3 coolant temperature, C/K	268.6/541.75	269.0/542.15	± 1.5 K
Cold leg #4 coolant temperature, C/K	268.6/541.75	269.2/542.35	± 1.5 K
Mass flow rate 1, kg/s	4 737	4 566	±110 kg/s
Mass flow rate 2, kg/s	4 718	4 676	±110 kg/s
Mass flow rate 3, kg/s	4 682	4 669	±110 kg/s
Mass flow rate 4, kg/s	4 834	4 819	±110 kg/s
Inlet velocity 1, m/s (dv1/0.56745)	10.64705	10.57362	
Inlet velocity 2, m/s	10.60788	10.53935	
Inlet velocity 3, m/s	10.52466	10.50601	
Inlet velocity 4, m/s	10.86734	10.84775	
MCP #1 pressure head, MPa	0.620	0.607	±0.02-0.04 MPa
MCP #2 pressure head, MPa	0.609	0.609	±0.02-0.04 MPa
MCP #3 pressure head, MPa	0.606	0.603	±0.02-0.04 MPa
MCP #4 pressure head, MPa	0.615	0.612	±0.02-0.04 MPa
Coolant flow 1, m^3/h	21 750	21 600	±490 m^3/h
Coolant flow 2, m^3/h	21 670	21 530	±490 m^3/h
Coolant flow 3, m^3/h	21 500	21 460	±490 m^3/h
Coolant flow 4, m^3/h	22 200	22 160	±490 m^3/h
Reactor coolant flow, m3/h	87 120	86 750	±1550m3/h
Reactor mass flow rate, kg/s	18 970	18 730	±450 kg/s
Hot leg #1 coolant temperature, C/K	271.86/545.0	281.7/554.85	± 1.5 K
Hot leg #2 coolant temperature, C/K	271.83/545.0	275.4/548.55	± 1.5 K
Hot leg #3 coolant temperature, C/K	271.76/544.9	272.6/545.75	± 1.5 K
Hot leg #4 coolant temperature, C/K	271.86/545.0	273.3/546.45	± 1.5 K
Pressure in SG #1, MPa	5.11	6.51	±0.2 MPa
Pressure in SG #2, MPa	5.13	5.14	±0.2 MPa
Pressure in SG #3, MPa	5.15	5.15	±0.2 MPa
Pressure in SG #4, MPa	5.13	5.14	±0.2 MPa
Main steam header pressure, MPa	5.07	5.07	±0.2 MPa

[1] Obtained from measured dPr-r, pressure above the core and estimated pressure losses (P4-P6).

[2] At P ≈ 15.6 MPa, T ≈ 272°C.

Figure 2.4: Plant data: flow mixing coefficients from cold leg #1 to fuel assembly outlets

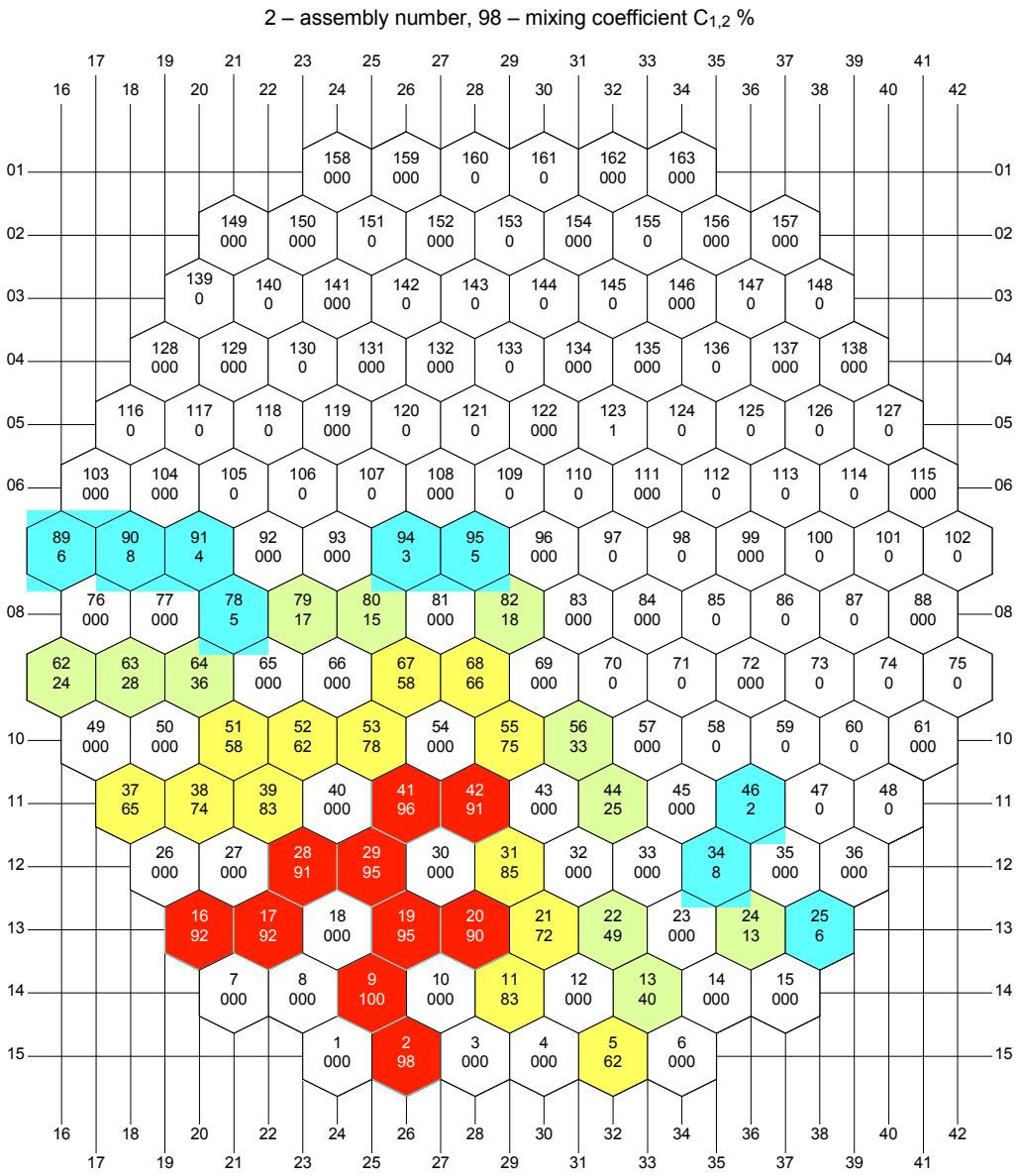

Table 2.3: Plant-estimated angular turn of the loop flow centres

	Kozloduy Unit 6	Kozloduy Unit 5
Loop 1	-24°	-26°
Loop 2	+8°	+9°
Loop 3	-30°	-23°
Loop 4	+8°	+9°

Figure 2.5: Relative assembly-wise temperature rise distribution in the initial state

Yellow – measured data, no colour – estimated values

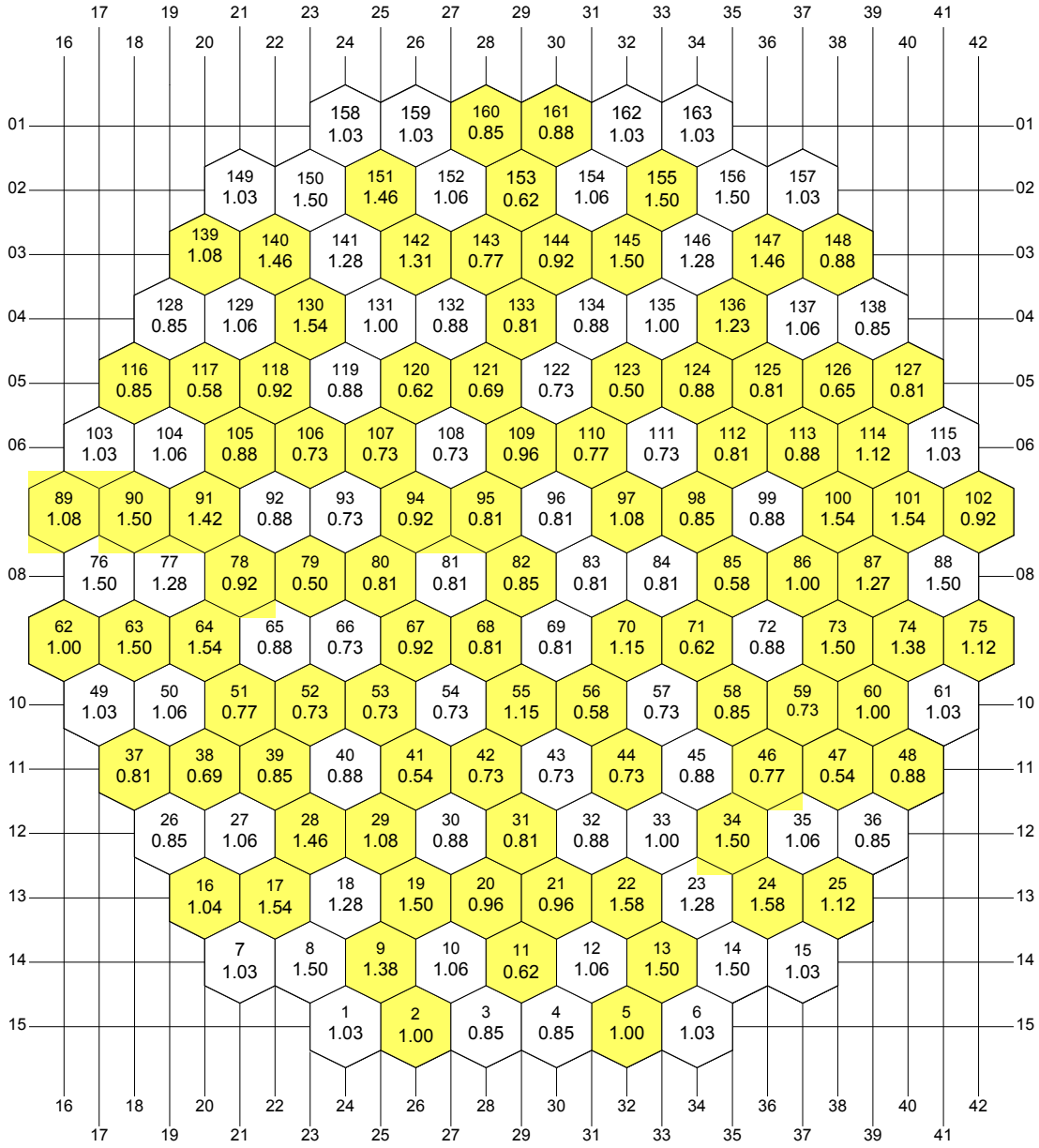

Chapter 3: Methodology of comparison

This work contains several types of submitted results for analysis, such as integral parameters, two-dimensional distributions and time history data. The analysis includes a test of the ability of the considered models to reproduce key phenomena and detailed quantitative comparison in terms of suitable target variables and metrics. Code-to-experiment comparison and intercomparison of the deviations for different codes and models are considered.

3.1 Target variables

For the assessment of computed results, in accordance with the Best Practice Guidelines (BPG) (Menter, 2002; Mahaffy, 2007) we consider:

- The code/model ability to reproduce the main features of the vessel flow such as the observed sector formation and angular turn of the loop flows.
- The following target variables:
  - azimuth distributions of the downcomer velocities and temperatures:
    - 24 points at elevation 5 800 mm – just before the diffuser, above each of the 8 consoles and ±10°;
    - 24 points at elevation 2 500 mm – above each of the 8 consoles and ±10°;
  - 2-D temperature and velocity distributions at the core inlet;
  - 2-D distributions of the differences between computed parameters and plant data at the core inlet;
  - integral parameters (core, vessel and plant depending on the considered scale);
  - time histories of integral parameters.

The angular turn of the loop flow is defined as the angle from the loop axis to the centreline of the sector of minimal mixing. It is determined and visualised using the 2-D distribution of the loop to assembly temperature difference:

$$\delta T_{n,i} = T_n - T_i,\ n = 1,\ i = 1,163 \tag{3.1}$$

where n is the loop number and i is the assembly number.

3.2 Metrics

The results are analysed in terms of:

1) Maximum in modulus error:

$$e_{i,max} = \max\left|x_i - x_{i,meas}\right|$$

where $e_{i,max}$ is the maximum in modulus error of the participant results from measured data, x_i is the computed value and $x_{i,meas}$ is the experimental value.

2) Average in modulus error (ME_{ABS}):

$$ME_{ABS} = \frac{1}{N}\left\{\sum_{i=1}^{N}\left|\left(x_i - x_{i,meas}\right)\right|\right\}$$

where N is the number of data values.

3) Mean error (ME):

$$ME = \frac{1}{N}\left\{\sum_{i=1}^{N}\left(x_i - x_{i,meas}\right)\right\}$$

4) Variance of error (VE):

$$\sigma^2 = VE = \frac{1}{(N-1)}\left\{\sum_{i=1}^{N}\left(x_{i,meas} - x_i - ME\right)^2\right\}$$

5) Mean square error (MSE):

$$MSE = \frac{1}{N}\left\{\sum_{i=1}^{N}\left(x_{i,meas} - x_i\right)^2\right\}$$

6) Figures of merit:

$$FOM_{ME} = \frac{1}{(ME+1)}$$

$$FOM_{VE} = \frac{1}{(VE+1)}$$

$$FOM_{MSE} = \frac{1}{(MSE+1)}$$

Criteria 1, 2, 3 and 5 were used for the 2-D distributions. The figures of merit for the ME, VE and MSE methods were used for integral parameters and indicate whether the participant results are close to the reference data. A FOM closer to unity indicates a better agreement.

3.3 Uncertainties

The experiments were conducted at the beginning of core life, just after calibration of the sensors. The initial state core power distribution has a 60° rotational symmetry.

The uncertainties in plant measured data are given in Table 2.1. The uncertainties in thermal sensor readings refer to a temperature range of 250-350°C. For the purposes of this analysis the loop flows were determined from pump head and coolant temperature measurements, taking into account all necessary corrections. Flow stratification or impeller induced effects in the main coolant loops were not considered. The boundary conditions were assumed flat over the nozzle cross-section. The loop temperatures were obtained as weighted averages of the readings of two thermocouples and one thermo-resistor at each nozzle. In the initial and final states a series of 6-10 measurements has been used for reliable determination of the integral parameters. The uncertainty in thermocouple measurements at the assembly outlets is ±1.0 K.

The uncertainty in the assembly inlet temperatures derived from outlet measurements includes contributions from the measurement uncertainties and from the assumptions made (uniform assembly by assembly volumetric flow, small mixing in the core and constant relative assembly temperature rise during the transient).

Chapter 4: CFD results and discussion

This chapter presents the post-test CFD results for the final state of the V1000CT-2 vessel mixing transient. The domain of solution is from the reactor inlet to the core inlet. The task is to calculate the final state flow parameters in the downcomer and at the core inlet, given the vessel boundary conditions and the pressure above the core. The vessel boundary conditions are assumed flat over the cross-section of the nozzles. The analysis includes:

- code-to-code comparison of the flow parameters in selected points in the downcomer;
- code-to-experiment comparison of the core inlet temperature distributions and the angular turn of the loop flow centres with respect to the cold leg axes.

Plant data for the assembly inlet temperatures and the angular turn of the loop flow were estimated from the measured core outlet temperatures as described in the first volume of the *VVER-1000 Coolant Transient Benchmark (V1000CT-2)* (NEA, 2010a) and discussed in this chapter.

The TRIO_U code (CEA, 2005) was used to develop and validate the specifications and to provide support calculations.

A total of seven contributions from eight organisations were submitted. FZK presented full vessel CFD simulation results. In addition to these results some participants have published additional studies (Bieder, 2005, 2007; Boettcher, 2008a, 2008b; Hoehne, 2007a; Yamaji, 2006) and comparisons of different turbulence models in accordance with the BPG (Mahaffy, 2008; Menter, 2002).

4.1 Modelling assumptions

Participant-provided calculation details are given in Table 4.1 and in Appendix C.

Table 4.1: Summary of the V1000CT-2 CFD modelling assumptions

Organi-sation	Code	Turbu-lence model	Discretisation	Advection scheme	Mesh type	Plant specific data	Use of CEA CAD geom. data
BUTE	CFX 10	SST	3 266 140	Upwind	Unstructured tetrahedral	Yes	Yes
CEA	TRIO_U	LES	10 000 000 contr. volumes	High resolution	Unstructured tetrahedral	Yes	Yes
EREC	REMIX 1.0	k-ε	311 394 cells 332 940 vertices	Upwind	Unstructured hexahedral	Yes	Yes
FZK	CFX 5	k-ε	14 000 000 whole RPV	Upwind	Unstructured/ hybrid; core: structured	Yes	Yes
FZD	CFX 10	SST	4 700 000	Upwind	Unstructured tetrahedral	Yes	Yes
PSU/ ORNL	FLUENT	k-ω	541 000	Upwind	Unstructured	Yes	Yes
UNIPI	CFX 10	k-ε	930 000 nodes 4 200 000 elem.	Upwind	Unstructured tetrahedral	Yes	Yes

In order to facilitate the participants' input preparation and to ensure a reliable comparison using consistent geometry data, a qualified CAD geometry file was prepared by U. Bieder from CEA Grenoble and provided to the participants upon request. This file is based on the actual geometry of the vessel

and not the conceptual design geometry. It was tested in TRIO_U LES validation runs and in a sensitivity study (Bieder, 2004, 2005, 2007) which indicated the importance of using the actual vessel geometry for reliable results.

4.2 Comparative analysis

For the assessment of CFD results, in accordance with the Best Practice Guidelines (Mahaffy, 2008; Menter, 2002) we consider:

- the code/model ability to reproduce the main features of the flow in the final stabilised state, such as sector formation and the angular turn of the loop flow;
- choice of target variables and metrics as described in Chapter 3.

The results are visualised in 2-D core maps and graphs representing azimuth, radial and assembly-by-assembly distributions.

The computed angular turn of loop #1 flow is determined as the angle between the loop axis and the centreline of the zone of minimal mixing in the disturbed sector. The zone of minimal mixing is shown in terms of loop to assembly inlet temperature difference. The smaller the difference, the lower the mixing. In order to fit the original plant data (NEA, 2010a) presented in terms of loop to assembly mixing coefficients (see Figure 2.3), four temperature intervals were used. The temperature difference below 1.2 K is presented in red, the range of 1.2-5 K in yellow, 5-8 K in green and over 8 K in blue.

For the analysis of the gradients at the borders of the disturbed sector, the 2-D maps are supplemented by charts displaying the assembly-by-assembly inlet temperatures in comparison with the plant estimated data. The core maps, representing the relative difference between computed and plant estimated assembly inlet temperatures are given in Appendix E.

For precise quantitative and qualitative comparison of the results, the assembly-by-assembly deviations from the experimental data are shown in separate graphs in Figures 4.23-4.35. These graphs are supplemented by 2-D core maps in Appendix E representing the differences between computed and plant estimated assembly inlet temperatures.

Finally, the results of the statistical evaluation are given in Table 4.11.

The CFX results of different participants obtained with the same turbulence models [k-ε or shear stress transport (SST)] allow a study of the user effects and the impact of specific assumptions. The verified CFX simulations with minimised numerical errors and with different turbulence models allow a comparison of the performance of the turbulence models. Finally, the submitted and published participants' results give insight into the overall performance of current CFD codes using turbulence models from k-ε to detached eddy simulation (DES) and LES.

4.3 Initial state results

Figures 4.1 and 4.2 show the FZK CFX 5 computed assembly-by-assembly core inlet and outlet temperatures in the initial state. Note that the computed assembly outlet temperatures refer to the end of the heated part of the assemblies and not to the thermocouple tips.

4.4 Final state results

4.4.1 Coolant mixing from the reactor inlet to the upper and lower downcomer

Table 4.2 shows the integral parameters, including the RPV boundary conditions and the measured hot leg temperatures.

Regarding the requested distributions, several CFX results from different users and with the same or different turbulence models were submitted. This enables an informative comparison if the user-provided information about the modelling assumptions is sufficiently detailed.

Figure 4.1: FZK CFX 5 results – core inlet temperatures at the initial state

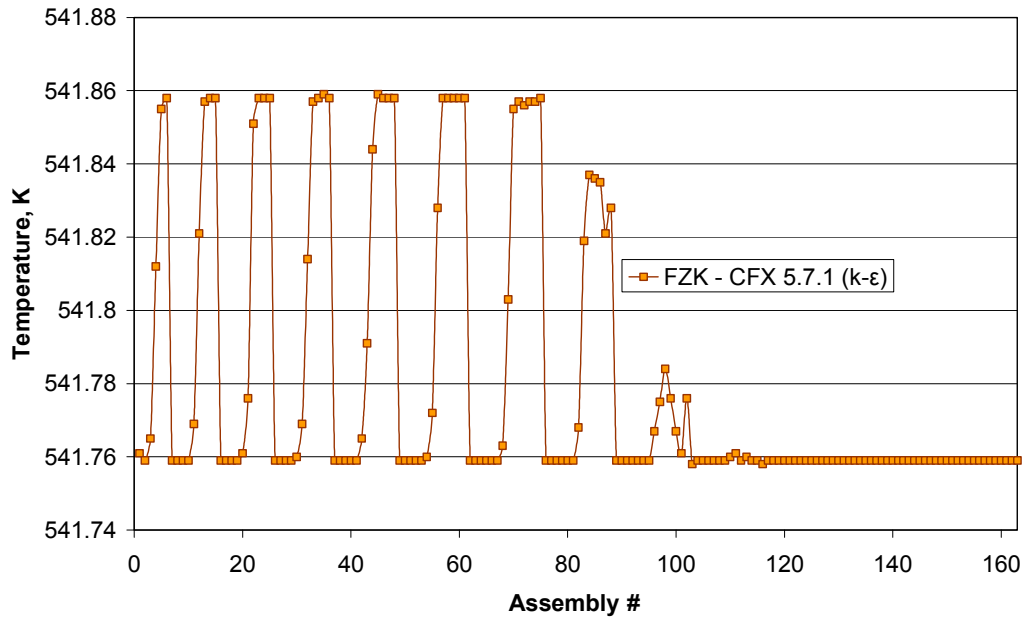

Figure 4.2: FZK CFX 5 results – core outlet temperatures at the initial state

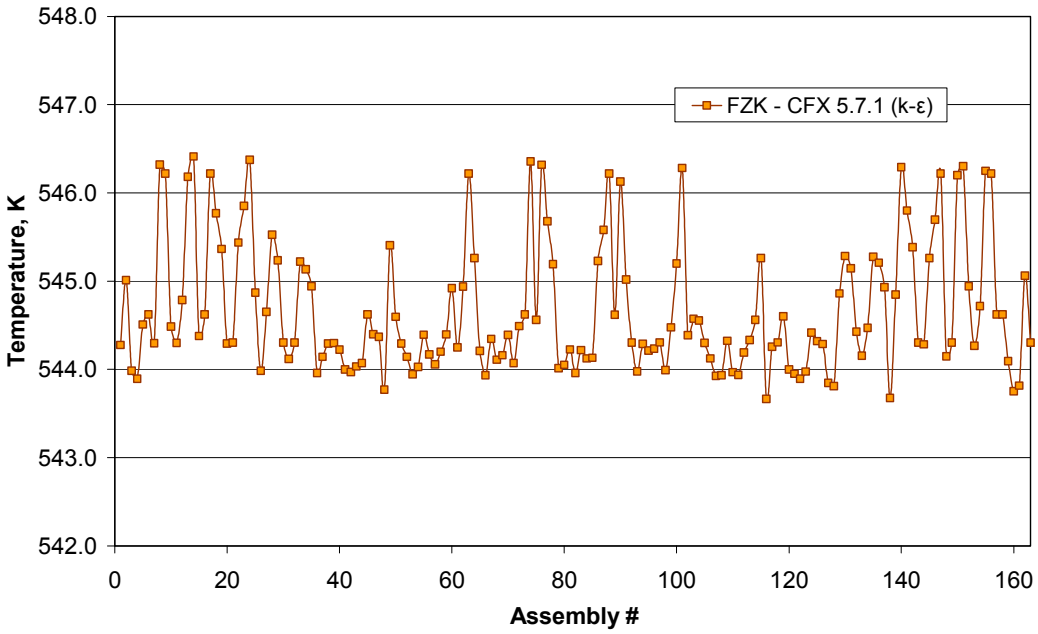

Table 4.2: Final state integral parameters

Parameter	Plant data	CEA TRIO_U	EREC REMIX	ORNL FLUENT	FZK CFX 5	FZD CFX 10	BUTE CFX 10	BUTE CFX 10	Uncertainty
Boundary conditions									
Cold leg #1 temperature, K	555.35	555.35	555.35	555.35	555.47	555.35	555.35	555.35	±1.5 K
Cold leg #2 temperature, K	543.05	543.05	543.05	543.05	543.28	543.05	543.05	543.05	±1.5 K
Cold leg #3 temperature, K	542.15	542.35	542.15	542.15	542.38	542.35	542.15	542.15	±1.5 K
Cold leg #4 temperature, K	542.35	542.35	542.35	542.35	542.47	542.35	542.35	542.35	±1.5 K
Loop #1 mass flux, kg/s	4 566	0	4 566	4 566	4 566	0	4 566	0	±110 kg/s
Loop #2 mass flux, kg/s	4 676	0	4 676	4 676	4 676	0	4 676	0	±110 kg/s
Loop #3 mass flux, kg/s	4 669	0	4 669	4 669	4 669	0	4 669	0	±110 kg/s
Loop #4 mass flux, kg/s	4 819	0	4 819	4 819	4 819	0	4 819	0	±110 kg/s
Cold leg #1 velocity, m/s	10.574	10.574	10.57	0	10.65	10.574	10.616	10.57	
Cold leg #2 velocity, m/s	10.539	10.539	10.54	0	10.6	10.539	10.880	10.54	
Cold leg #3 velocity, m/s	10.506	10.506	10.5	0	10.58	10.506	10.855	10.51	
Cold leg #4 velocity, m/s	10.848	10.848	10.85	0	10.58	10.848	11.206	10.85	
Pressure above the core, MPa	15.593								±0.3 MPa
Reactor outlet pressure, MPa	15.55	–	–	–	15.60	–		–	

Figure 4.3 illustrates the available results for the downcomer temperature distribution at 5 800 mm from the bottom of the reactor vessel (just above the diffuser). Participants' results in digital format are shown in Table 4.3. Generally good agreement is observed, with the exception of the results at 12°30' from direction I of axis I-III of the core co-ordinate system. A certain grouping of the FZD SST and UNIPI k-ε results on one hand, and FZK k-ε and BUTE SST results on the other is observed in the disturbed sector. The largest temperature difference is 3.9 K, between REMIX and BUTE CFX 10 results.

Figure 4.4 shows a comparison of the computed azimuth temperature distributions in the lower downcomer at 2 500 mm from the bottom of the reactor vessel. Participants' results for this elevation are given in digital format in Table 4.4. Generally good agreement is displayed, with the exception of some results at 12°30' and 22°30' counter-clockwise of direction I. The largest differences are 3.2 K between FZK k-ε and UNIPI k-ε results. A certain grouping of the FZD and UNIPI results on one hand, and the FZK and BUTE results on the other is observed in the disturbed sector.

Table 4.5 shows the temperature deviations between the two considered elevations in the downcomer, which are indicative of the flow mixing.

Figure 4.5 illustrates the azimuth velocity distribution at elevation 5 800 mm. Participants' results in digital format are shown in Table 4.6. The comparison shows a good agreement of the results, except that of FZK k-ε. It is interesting to note that the FZD SST and UNIPI k-ε results are close. The REMIX results are not visualised because of its significant difference from the others (see Table 4.6). This difference requires further analysis.

Figure 4.6 and Table 4.7 show a comparison of the azimuth velocity distribution at elevation 2 500 mm, just above the consoles. All CFD results except those of REMIX are close to each other.

4.4.2 Coolant mixing from the reactor inlet to the core inlet

Figure 4.7 shows the plant estimated sector of disturbance and the angular turn of the loop #1 flow centre, in terms of temperature differences from nozzle #1 to the assembly inlets. Small differences below 1.2 K indicate a minimal mixing and correspond to loop-to-assembly mixing coefficients of 90-100% (see the corresponding core outlet map in Figure 2.4, Chapter 2). The angular turn at the core inlet is estimated at 26° counter-clockwise of axis I. Note that the 2-D colour map in Figure 4.7 shows only assemblies with outlet measurements.

In the following, the results will be discussed in terms of absolute values and absolute deviations of computed to plant data. The maximum and average in modulus deviations refer to 95 assemblies with temperature measurements. The corresponding values for the whole core distributions (163 assemblies) are also given for information in Table 4.11, but are affected by larger uncertainties due to the reconstruction of the outlet temperatures in assemblies without measurements.

Figure 4.8 shows the CEA-TRIO_U LES predicted disturbed sector and angular turn of the loop #1 flow centre. Good agreement with the plant data is observed. The angular turn is 26°. Figure 4.9 presents the assembly-by-assembly comparison of the core inlet temperatures with plant data. Figures 4.23-4.25 and Figure E.1 in Appendix E visualise the corresponding discrepancies at the core inlet. The comparison shows an accurate prediction of the angular turn of loop #1 flow and relatively smooth transition at the disturbed sector borders. Note that this result is obtained with a high resolution advection scheme. For assemblies with thermal measurements, the maximal and average in modulus deviations are 2.90 K and 0.575 K, respectively, which is the second best result.

A sensitivity study was performed with TRIO_U LES (Bieder, 2004, 2005, 2007) to analyse the significance of different modelling hypotheses. The results indicate the importance of the use of the actual vessel geometry. With the conceptual design data the predicted angular turn is about half of the experimental value. Adding part of the core region to the domain of solution resulted in a core inlet velocity distribution closer to the expected one.

Figure 4.10 shows the EREC-REMIX k-ε predicted disturbed sector and angular turn of the loop #1 flow centre. The results are in good agreement with the plant data, but display a wider disturbed sector. The angular turn is around 24°. Figure 4.11 indicates a good agreement of the core inlet temperatures around the core centre and at the disturbed sector border between the first and fourth nozzle. Figures 4.26 and 4.27 show the corresponding temperature deviations in comparison with the TRIO_U LES results. The maximal and average in modulus deviations are 4.16 K and 0.688 K respectively.

Figures 4.12 and 4.13 show the ORNL-FLUENT k-ω results. The predicted disturbed sector is wider than the experimental one and is characterised by radial temperature stratification which is not observed in the experiment. The angular turn is about 23°. The assembly inlet temperatures in Figure 4.13 indicate a generally good agreement with the plant data in the core centre and at the sector border between the first and fourth nozzle. Figures 4.28, 4.29 show the corresponding temperature deviations. The maximal and average in modulus deviations are 4.85 K and 0.852 K respectively.

Figures 4.14 and 4.15 show the FZK CFX 5 k-ε results for the assembly inlet temperatures. The angular turn is 27°. The results are close to the plant estimated data, in terms of sector formation and angular turn. Figures 4.23, 4.32 and 4.33 show the temperature deviations at the core inlet. The results are in good overall agreement with the plant data, with some differences at the sector borders. The maximal and average in modulus deviations are 3.01 K and 0.598 K respectively.

Figure 4.36 shows the FZK CFX 5 k-ε results for the assembly outlets in comparison with the corresponding measured/reconstructed temperatures. The deviations are somewhat larger than those at the inlet, as expected, because the local mixing in the assembly heads was not modelled. In this case, computed values at the end of the heated part are compared with the measured ones in the assembly head, which are lower because of the cooler jets through the control rod guide channels.

Figures 4.16 and 4.17 show the FZD CFX 10 SST results. The angular turn is about 21°. A certain radial stratification is seen, and the predicted zone of minimal mixing is a bit narrower than the experimental one. Figures 4.23, 4.30 and 4.31 show the temperature deviations at the core inlet. The maximal in modulus deviation is 4.55 K and the average in modulus deviation is 0.888 K. Part of the deviations seems to be related with the underestimated angular turn of the zone of minimal mixing causing large gradients at the disturbed sector borders.

Hoehne (2007a) has compared the performance of different advanced turbulence models in CFX 10: SST, DES and LES. The CFD simulations were performed according to the BPG (NEA, 2010b). Best results in terms of mixing scalar at the core inlet were obtained using DES.

Figures 4.18 and 4.19 show the BUTE CFX 10 SST results. The computed disturbed sector is close to the experimental one and the angular turn is about 24°. Figures 4.23, 4.24 and 4.25 show the temperature deviations at the core inlet. The comparison demonstrates a good overall agreement in the assembly inlet temperatures, with a maximal deviation of 2.85 K and average in modulus deviation 0.549 K.

Figures 4.20 and 4.21 show the comparison of UNIPI CFX 10 k-ε results for the angular flow rotation and core inlet temperatures. The angular turn is about 20°. Figures 4.23, 4.34 and 4.35 show the temperature differences at the core inlet. The maximal in modulus deviation is 3.56 K and the average in modulus deviation is 0.813 K. Part of the deviations seems to be related with the underestimated angular turn of the zone of minimal mixing causing large gradients at the disturbed sector borders.

Tables 4.8-4.10 show selected radial temperature distributions which may be useful in the analysis. Table 4.8 illustrates the assembly inlet temperatures along the centreline of the sector of minimal mixing and Tables 4.9 and 4.10 show the assembly inlet temperatures along the borders of the disturbed sector where large gradients occur.

Figures 4.37 and 4.38 show the assembly-by-assembly inlet velocities (at 1 630 mm from the inner vessel bottom, just above the core support plate). Supplementary plant data from Kozloduy-5 are given in Figure 4.38 for a qualitative comparison. It should be noted that there are two FZK results for the core inlet velocities, using different modelling. Figure 4.38 shows the FZK CFX 10 SST calculation (Hoehne, 2007a) with explicit modelling of the elliptical sieve plate while Figure 4.37 shows the FZK CFX k-ε result assuming porous medium. The comparison reveals some qualitative differences in the assembly-by-assembly velocity distributions which require further attention.

Figure 4.39 shows a comparison of the corresponding mass flow rates at the assembly inlets.

Additional 2-D maps in terms of absolute temperature differences at the assembly inlets [Eq. (3.1)] are given in Appendix E, for the analysis of the sector formation and the transitional border zones.

4.4.3 Radial distributions at the core inlet

Figure 4.40 shows the computed radial velocity profiles at the core inlet, in qualitative comparison with measured plant data from Kozloduy-5. For this comparison, the radial velocity profile was obtained by averaging over each concentric row of fuel assemblies. The FZK result for the velocity profile in Figure 4.40 was obtained from a recent CFX 10 SST calculation (Boettcher, 2008a, 2008b) with explicit modelling of the elliptic plate in the lower plenum.

The comparison of the radial velocity profile at the core inlet shows:

- good agreement of the UNIPI CFX SST results and the experimental profile;
- qualitative agreement of the FZK CFX 10 SST results;
- a qualitative difference of the FZD and BUTE results from the plant data that requires further analysis.

4.5 Conclusions

- The analysis shows that the results are in reasonable agreement for each parameter, with some exceptions for the core inlet velocity. This agreement was achieved under the following conditions: use of the actual and not the conceptual design geometry of the reactor vessel + appropriate treatment of turbulence + compliance with the Best Practice Guidelines.
- CFD simulations predict qualitatively well the flow rotation, but the sector formation is characterised by more diffusion than in the measurements.
- The accuracy of CFD for temperature prediction at the core inlet is in the range 1-4 K.
- The observed differences depend on the modelling assumptions, summarised in Table 4.1 and Appendix C, and on the degree of compliance with the BPG. The TRIO_U LES results show the best agreement in the angular turn of the loop flow. The BUTE CFX SST simulation is the best in terms of maximum and average in modulus temperature deviations at the core inlet. The UNIPI CFX 10 k-ε predicted core inlet radial velocity profile is closest to that expected.
- The qualitative difference between the computed and plant estimated core inlet velocity distribution requires additional analysis. Further improvement of the core inlet velocity distribution is possible by explicit modelling of the elliptical sieve plate, as well as modelling of the fuel assemblies and using appropriate boundary conditions.
- CFD codes still have limitations but the development work for single phase mixing is moving in the proper direction. The quality of the results depends on the experience of the user and the compliance with the Best Practice Guidelines.

Figure 4.3: Downcomer temperature distribution at z = 5 800 mm

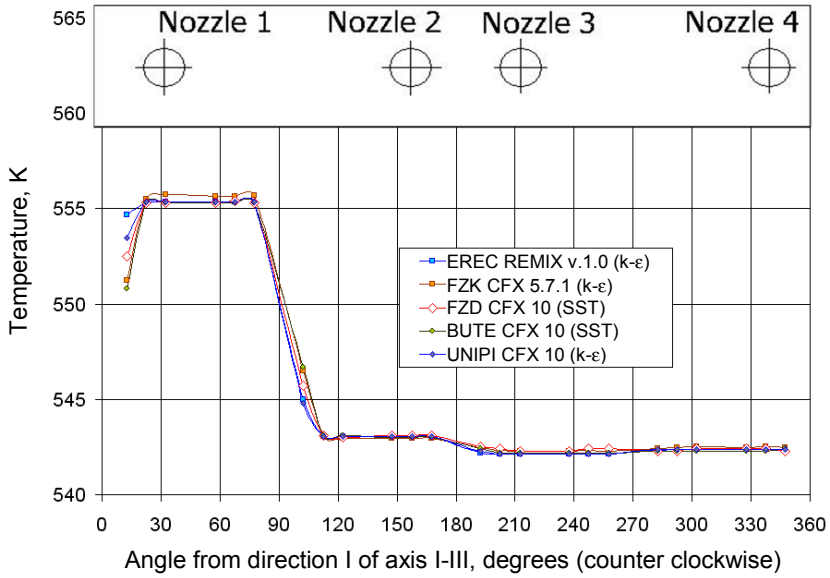

Table 4.3: Downcomer temperature distribution at z = 5 800 mm

	BUTE CFX 10	FZK CFX 5	EREC REMIX	UNIPI CFX 10	FZD CFX 10
θ, °	**T, K**	**T, K**	**T, K**	**T, K**	**T,K**
12°30'	550.8	551.3	554.7	553.44	552.5
22°30'	555.3	555.5	555.3	555.34	555.3
32°30'	555.3	555.7	555.3	555.35	555.3
57°30'	555.3	555.7	555.3	555.35	555.3
67°30'	555.3	555.6	555.3	555.35	555.4
77°30'	555.3	555.7	555.3	555.35	555.3
102°30'	546.7	546.5	545.0	544.82	545.7
112°30'	543.1	543.1	543.0	543.06	543.1
122°30'	543.1	543.0	543.1	543.05	543.0
147°30'	543.0	542.9	543.1	543.05	543.1
157°30'	543.0	543.0	543.1	543.05	543.1
167°30'	543.0	543.0	543.0	543.05	543.1
192°30'	542.4	542.5	542.2	542.26	542.5
202°30'	542.2	542.3	542.2	542.15	542.4
212°30'	542.2	542.3	542.2	542.15	542.3
237°30'	542.2	542.3	542.2	542.15	542.3
247°30'	542.2	542.3	542.2	542.15	542.4
257°30'	542.2	542.3	542.2	542.15	542.4
282°30'	542.3	542.4	542.3	542.36	542.3
292°30'	542.3	542.5	542.4	542.35	542.3
302°30'	542.3	542.5	542.4	542.35	542.4
327°30'	542.3	542.5	542.4	542.35	542.4
337°30'	542.3	542.5	542.4	542.35	542.4
347°30'	542.4	542.5	542.4	542.35	542.3

Figure 4.4: Downcomer temperature distribution at z = 2 500 mm

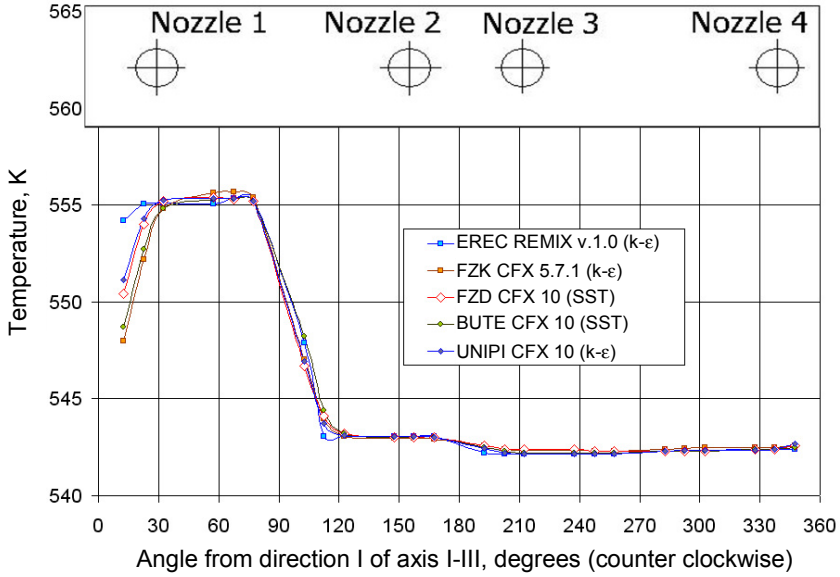

Table 4.4: Downcomer temperature distribution at z = 2 500 mm

	BUTE CFX 10	FZK CFX 5	EREC REMIX	UNIPI CFX 10	FZD CFX 10
θ, °	**T, K**	**T, K**	**T, K**	**T, K**	**T,K**
12°30'	548.7	548.0	554.2	551.14	550.4
22°30'	552.7	552.2	555.0	554.28	554.0
32°30'	554.8	554.8	555.1	555.25	555.2
57°30'	555.3	555.7	555.0	555.35	555.4
67°30'	555.3	555.7	555.3	555.35	555.3
77°30'	555.2	555.4	555.3	555.21	555.2
102°30'	548.2	547.0	547.9	546.92	546.7
112°30'	544.4	544.0	543.1	543.74	544.1
122°30'	543.2	543.1	543.1	543.09	543.2
147°30'	543	543.0	543.0	543.05	543.0
157°30'	543	543.0	543.0	543.05	543.0
167°30'	543	542.9	543.0	543.03	543.0
192°30'	542.5	542.6	542.2	542.43	542.6
202°30'	542.3	542.4	542.2	542.22	542.4
212°30'	542.2	542.3	542.2	542.16	542.4
237°30'	542.2	542.3	542.2	542.15	542.4
247°30'	542.2	542.3	542.2	542.15	542.3
257°30'	542.2	542.3	542.2	542.16	542.3
282°30'	542.3	542.4	542.3	542.32	542.3
292°30'	542.3	542.5	542.4	542.35	542.3
302°30'	542.3	542.5	542.4	542.35	542.3
327°30'	542.4	542.5	542.4	542.35	542.4
337°30'	542.4	542.5	542.4	542.37	542.4
347°30'	542.5	542.6	542.4	542.68	542.6

Table 4.5: Temperature differences between the upper and lower downcomer (at 5 800 and 2 500 mm)

	BUTE CFX 10	FZK CFX 5	EREC REMIX	UNIPI CFX 10	FZD CFX 10
θ, °	T, K	T, K	T, K	T, K	T,K
12°30'	-2.1	-3.3	-0.5	-2.3	-2.1
22°30'	-2.6	-3.3	-0.3	-1.1	-1.3
32°30'	-0.5	-0.9	-0.2	-0.1	-0.1
57°30'	0.0	0.0	-0.3	0.0	0.1
67°30'	0.0	0.1	0.0	0.0	-0.1
77°30'	-0.1	-0.3	0.0	-0.1	-0.1
102°30'	1.5	0.5	2.9	2.1	1.0
112°30'	1.3	0.9	0.1	0.7	1.0
122°30'	0.1	0.1	0.0	0.0	0.2
147°30'	0.0	0.1	-0.1	0.0	-0.1
157°30'	0.0	0.0	-0.1	0.0	-0.1
167°30'	0.0	-0.1	0.0	0.0	-0.1
192°30'	0.1	0.1	0.0	0.2	0.1
202°30'	0.1	0.1	0.0	0.1	0.0
212°30'	0.0	0.0	0.0	0.0	0.1
237°30'	0.0	0.0	0.0	0.0	0.1
247°30'	0.0	0.0	0.0	0.0	-0.1
257°30'	0.0	0.0	0.0	0.0	-0.1
282°30'	0.0	0.0	0.0	0.0	0.0
292°30'	0.0	0.0	0.0	0.0	0.0
302°30'	0.0	0.0	0.0	0.0	-0.1
327°30'	0.1	0.0	0.0	0.0	0.0
337°30'	0.1	0.0	0.0	0.0	0.0
347°30'	0.1	0.1	0.0	0.3	0.3

Figure 4.5: Downcomer velocity distribution at z = 5 800 mm

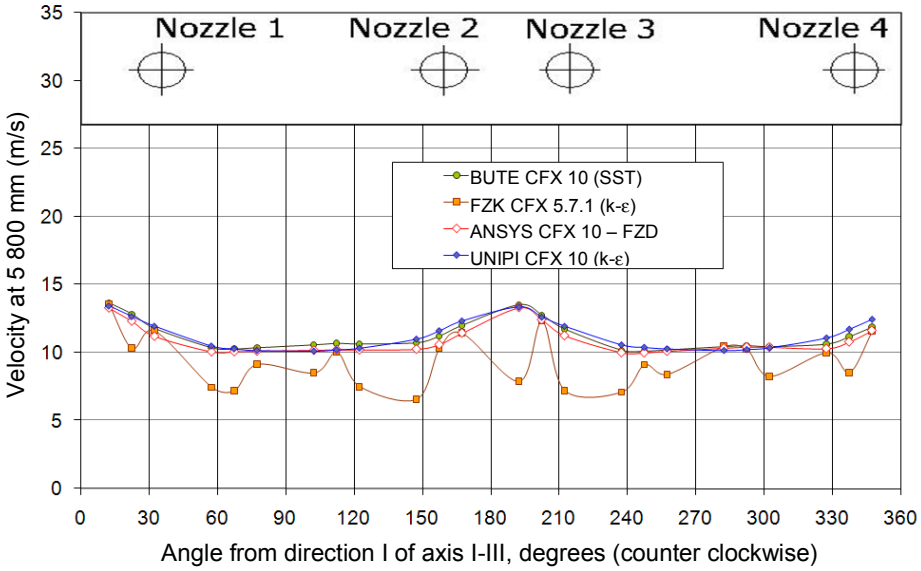

Table 4.6: Downcomer velocity distribution at z = 5 800 mm

	BUTE CFX 10	FZK CFX 5	EREC REMIX	UNIPI CFX 10	FZD CFX 10
θ, °	**v,m/s**	**v,m/s**	**v,m/s**	**v,m/s**	**v,m/s**
12°30'	13.64	13.54	17.71	13.44	13.27
22°30'	12.82	10.31	13.94	12.65	12.3
32°30'	11.76	11.61	5.59	11.94	11.19
57°30'	10.34	7.44	7.86	10.47	10.05
67°30'	10.24	7.18	10.30	10.25	10.06
77°30'	10.33	9.13	13.02	10.13	10.1
102°30'	10.55	8.50	17.25	10.09	10.17
112°30'	10.66	10.01	14.67	10.19	10.2
122°30'	10.62	7.49	12.67	10.31	10.19
147°30'	10.71	6.56	6.08	10.98	10.24
157°30'	11.21	10.32	4.34	11.60	10.58
167°30'	12.00	11.43	9.93	12.33	11.43
192°30'	13.52	7.87	17.46	13.36	13.3
202°30'	12.75	12.31	13.66	12.61	12.4
212°30'	11.71	7.19	5.41	11.93	11.24
237°30'	10.15	7.09	7.92	10.55	9.99
247°30'	10.09	9.11	10.87	10.37	9.979
257°30'	10.17	8.39	13.50	10.25	10.09
282°30'	10.42	10.44	16.82	10.13	10.32
292°30'	10.49	10.23	14.30	10.21	10.4
302°30'	10.42	8.25	12.27	10.34	10.39
327°30'	10.61	9.98	6.20	11.07	10.28
337°30'	11.16	8.53	4.55	11.71	10.78
347°30'	11.87	11.58	9.60	12.45	11.62

Figure 4.6: Downcomer velocity distribution at z = 2 500 mm

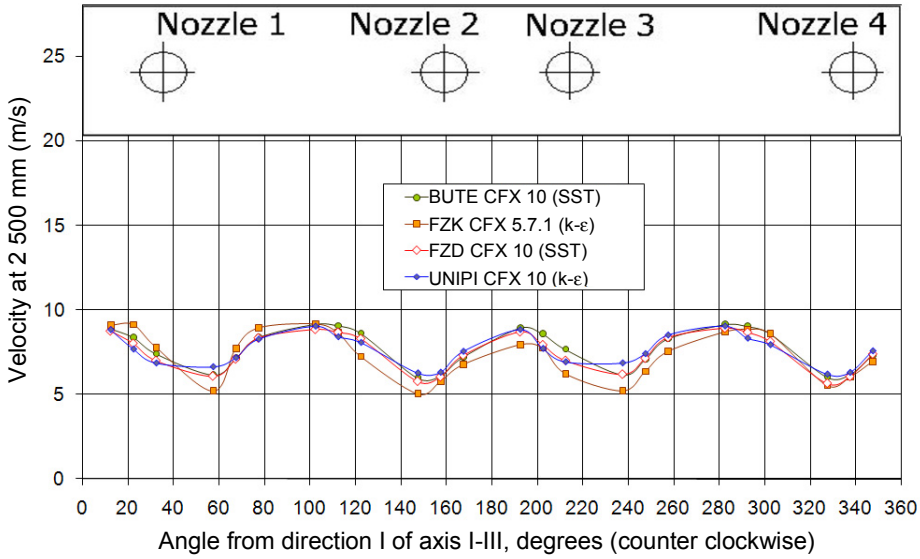

Table 4.7: Downcomer velocity distribution at z = 2 500 mm

	BUTE CFX 10	FZK CFX 5	EREC REMIX	UNIPI CFX 10	FZD CFX 10
θ, °	**v,m/s**	**v,m/s**	**v,m/s**	**v,m/s**	**v,m/s**
12°30'	8.88	9.11	12.98	8.81	8.755
22°30'	8.37	9.14	8.41	7.67	8.019
32°30'	7.39	7.79	1.89	6.86	6.996
57°30'	6.15	5.20	2.20	6.64	6.076
67°30'	7.12	7.73	4.91	7.17	7.093
77°30'	8.35	8.95	8.73	8.26	8.342
102°30'	9.15	9.18	17.27	9.02	8.849
112°30'	9.06	8.66	12.05	8.39	8.678
122°30'	8.61	7.25	8.57	8.06	8.3
147°30'	5.96	5.04	0.73	6.28	5.77
157°30'	6.09	5.78	0.55	6.32	6.036
167°30'	7.20	6.78	4.18	7.54	7.312
192°30'	8.93	7.95	12.58	8.82	8.703
202°30'	8.57	7.76	7.54	7.71	7.933
212°30'	7.65	6.23	1.34	6.93	7.006
237°30'	6.16	5.22	2.49	6.86	6.189
247°30'	7.05	6.36	5.62	7.40	7.133
257°30'	8.28	7.55	9.64	8.50	8.364
282°30'	9.13	8.71	16.37	9.02	8.921
292°30'	9.02	8.86	11.27	8.31	8.674
302°30'	8.58	8.61	7.67	7.93	8.133
327°30'	6.02	5.54	0.78	6.21	5.651
337°30'	6.16	6.02	0.22	6.31	6.051
347°30'	7.31	6.96	3.51	7.57	7.385

Figure 4.7: Plant data – angular turn of loop #1 flow centre in the final state, determined by the centreline of the sector of minimal mixing (where $dT_i = T_{cold\ leg1} - T_i$, i = 1,163)

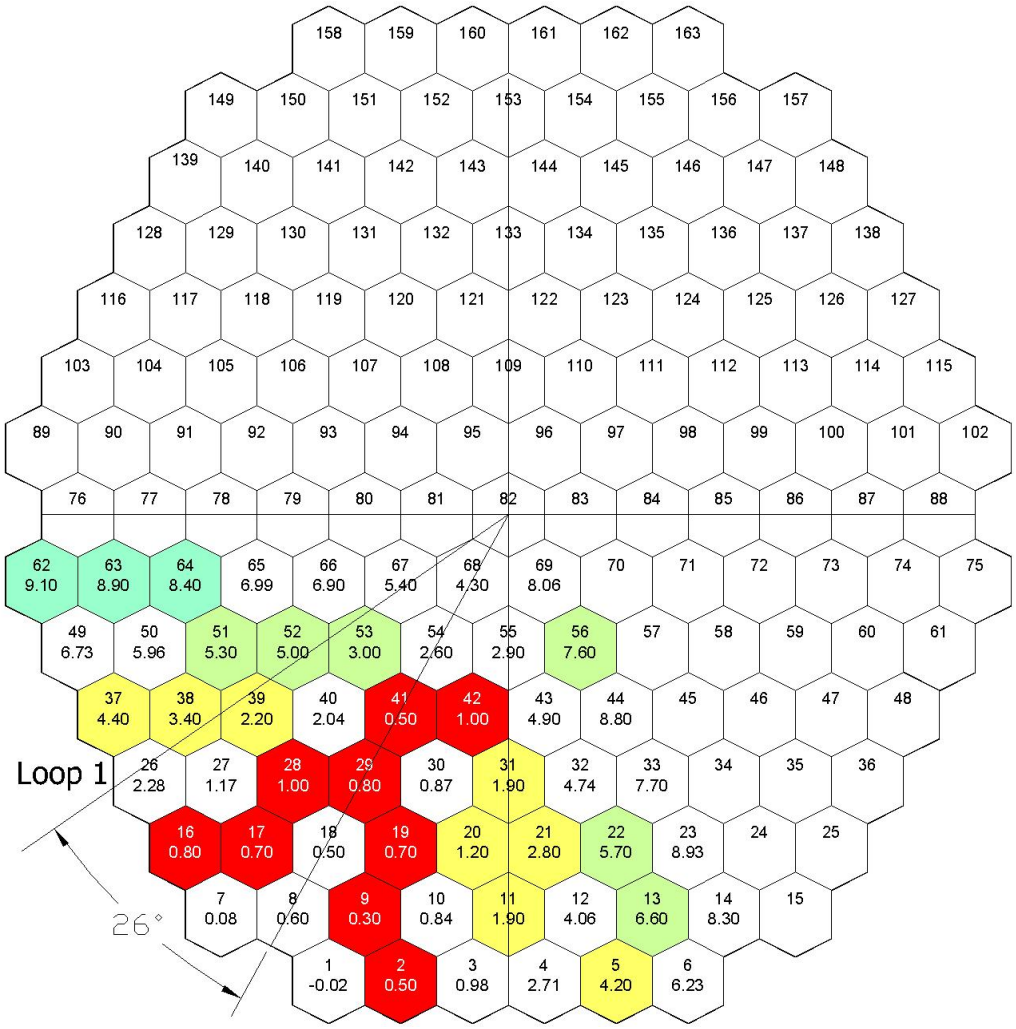

Figure 4.8: CEA TRIO_U results – angular turn of the loop #1 flow centre

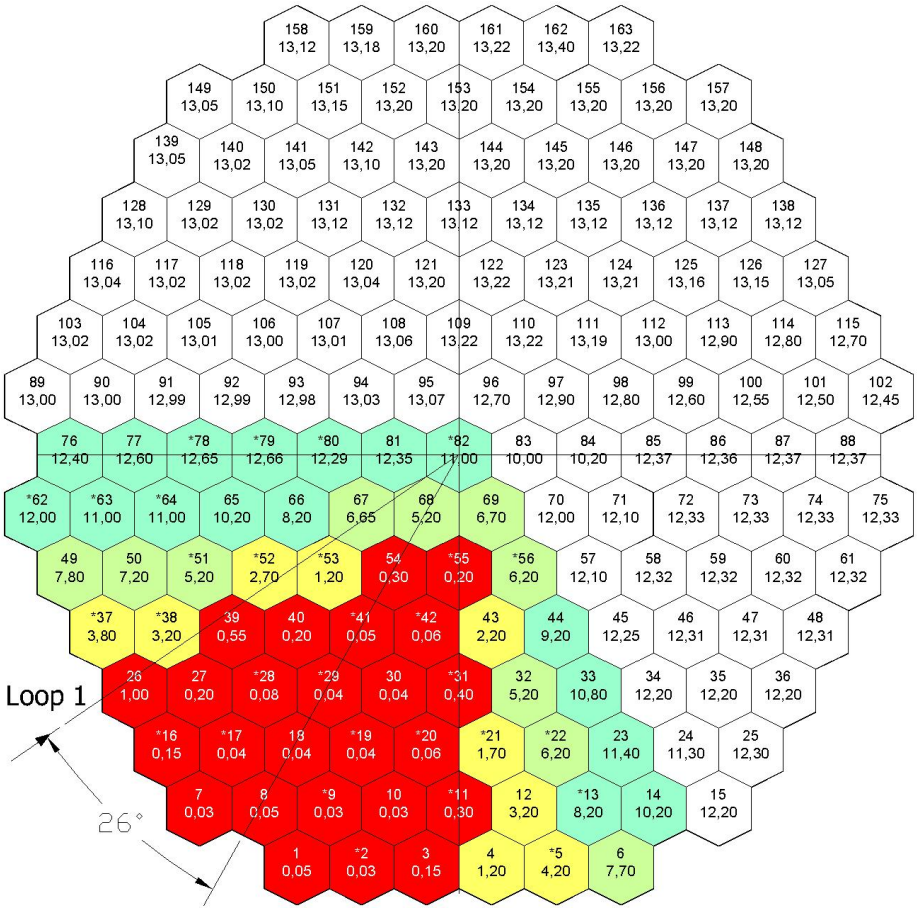

Figure 4.9: CEA TRIO_U calculated core inlet temperatures in comparison with plant data

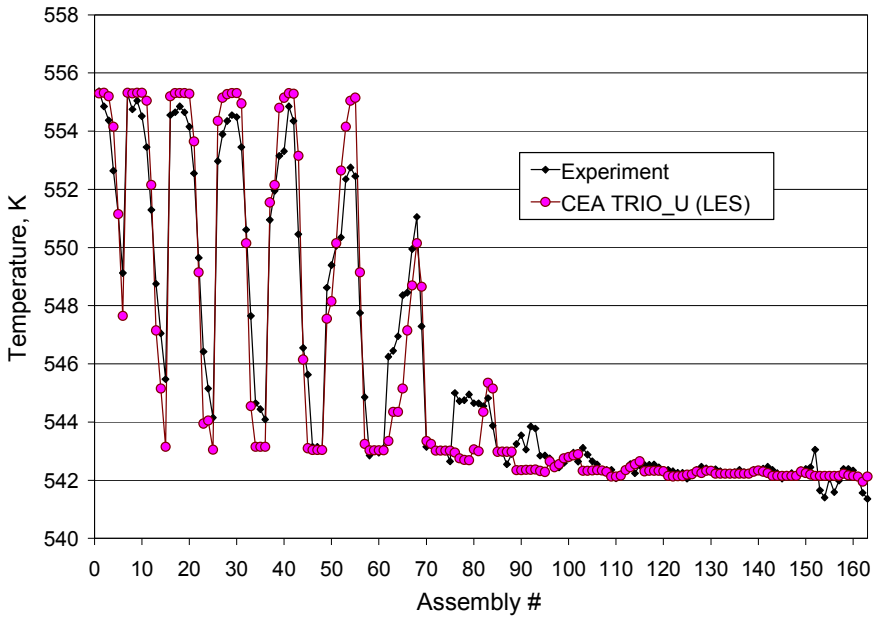

Figure 4.10: EREC REMIX results – angular turn of the loop #1 flow centre

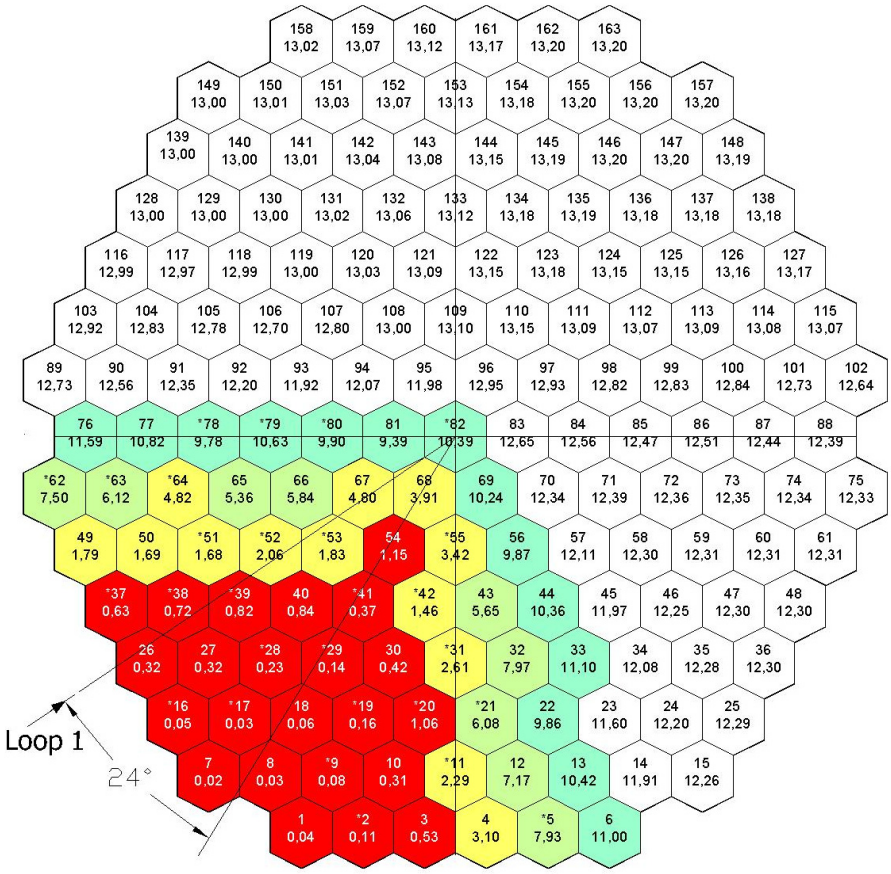

Figure 4.11: EREC REMIX calculated core inlet temperatures in comparison with plant data

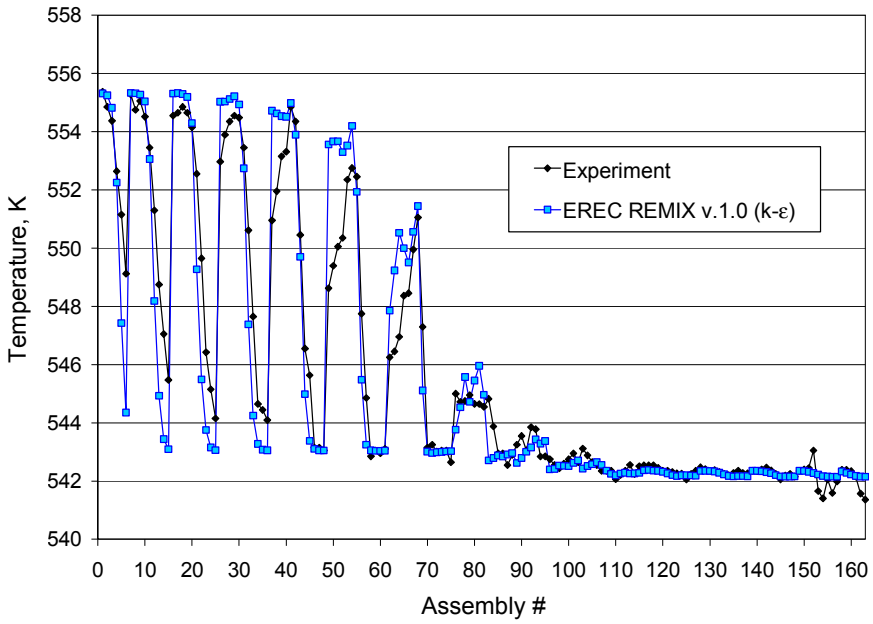

Figure 4.12: ORNL FLUENT results – angular turn of the loop #1 flow centre

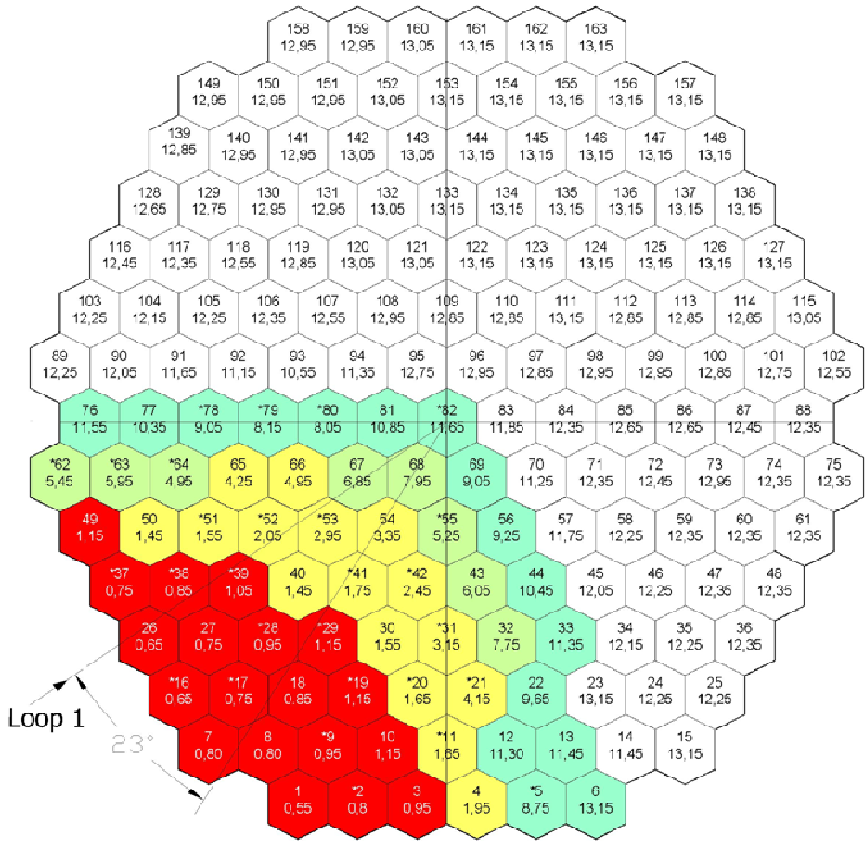

Figure 4.13: ORNL FLUENT calculated core inlet temperatures in comparison with plant data

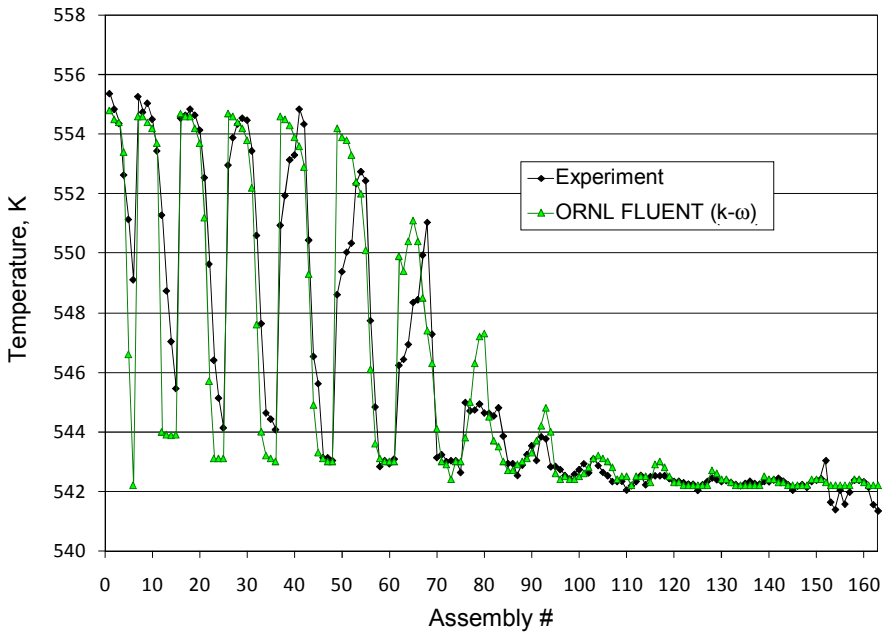

Figure 4.14: FZK CFX 5 results – angular turn of the loop #1 flow centre

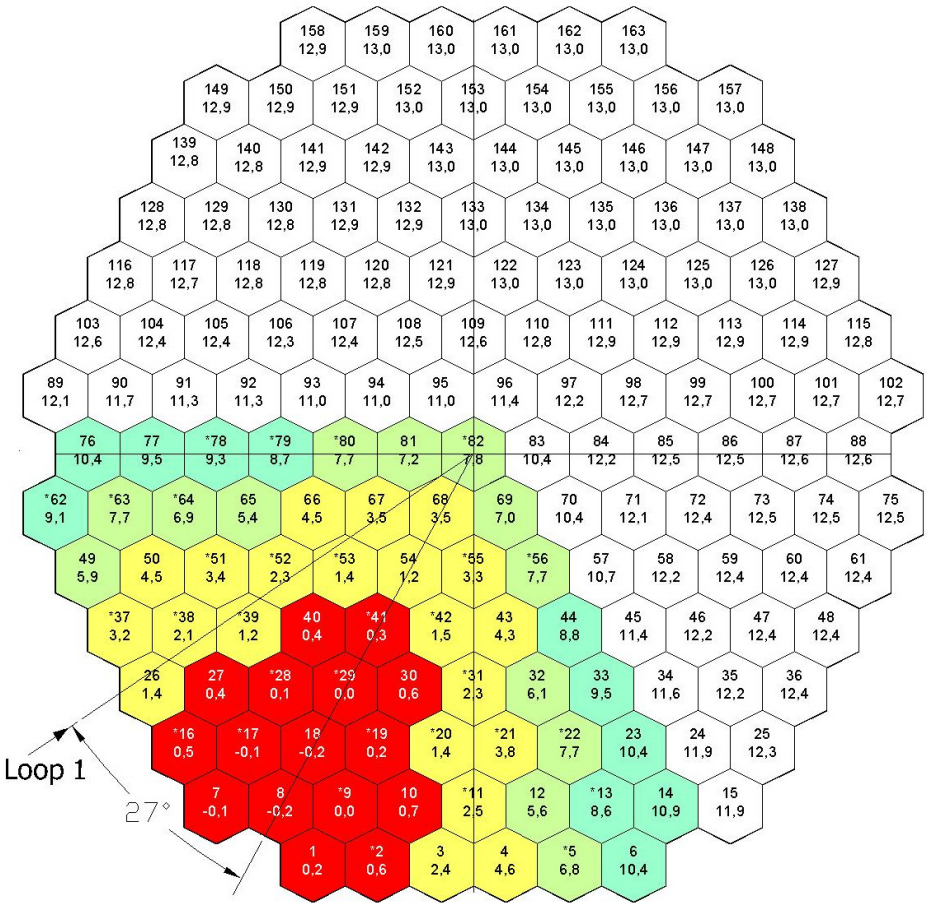

Figure 4.15: FZK CFX 5 calculated core inlet temperatures in comparison with plant data

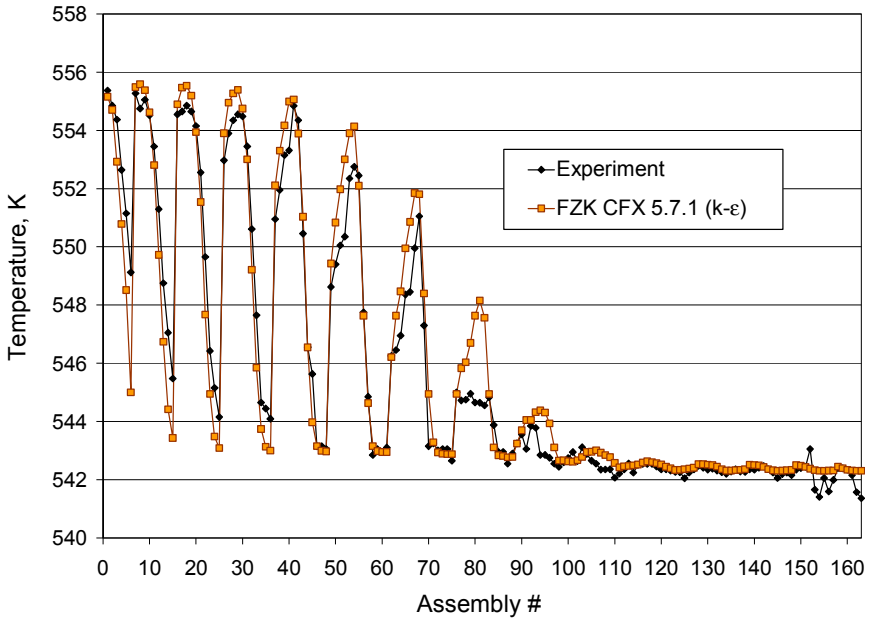

Figure 4.16: FZD CFX 10 results – angular turn of the loop #1 flow centre

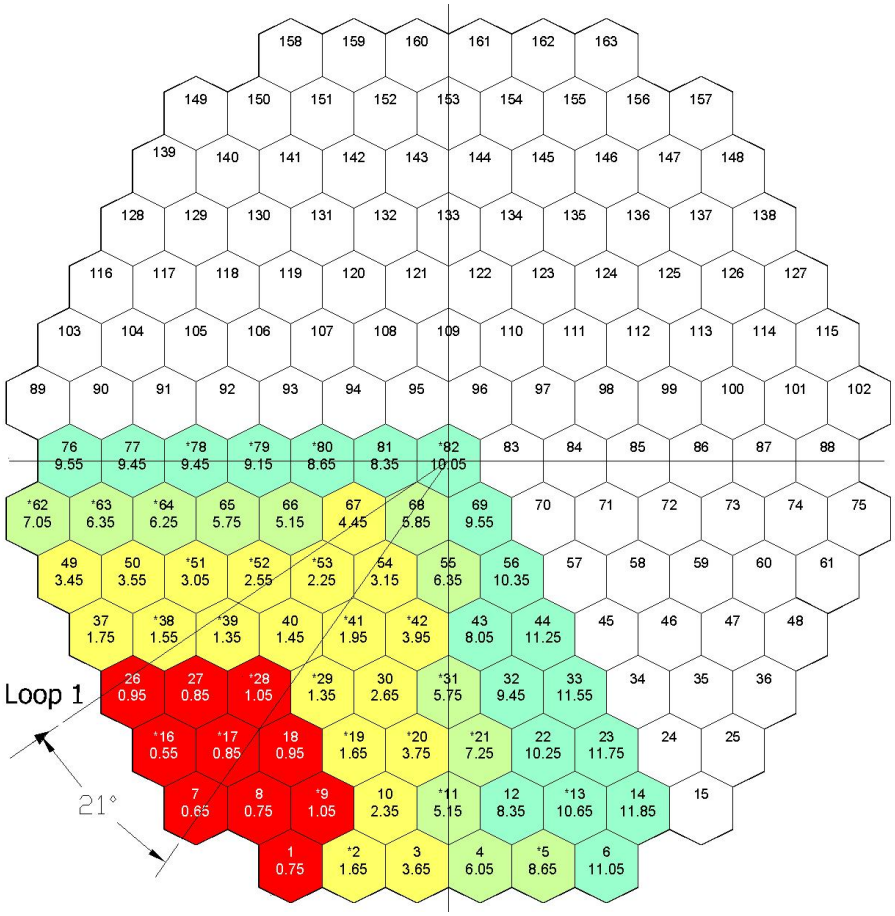

Figure 4.17: FZD CFX 10 calculated core inlet temperatures in comparison with plant data

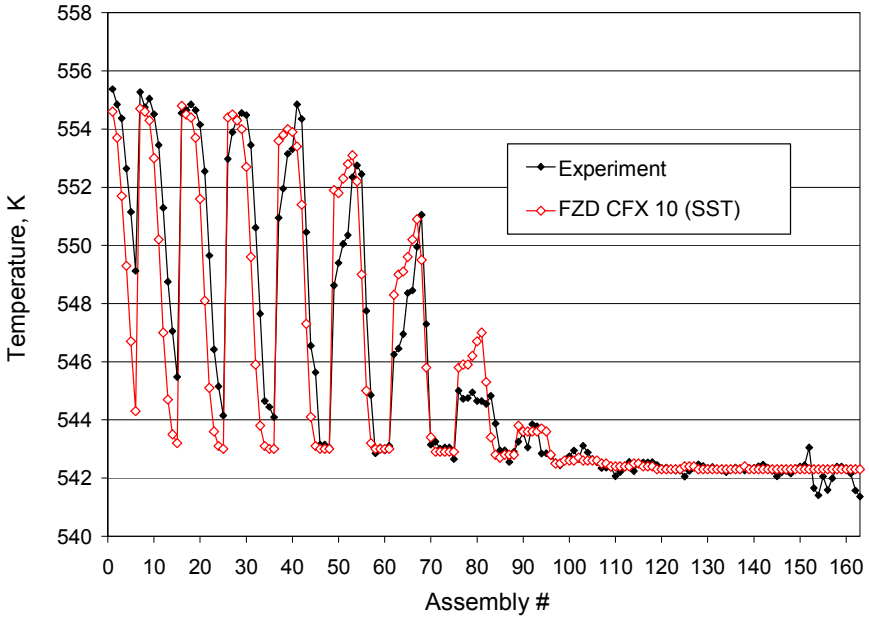

Figure 4.18: BUTE CFX 10 results – angular turn of the loop #1 flow centre

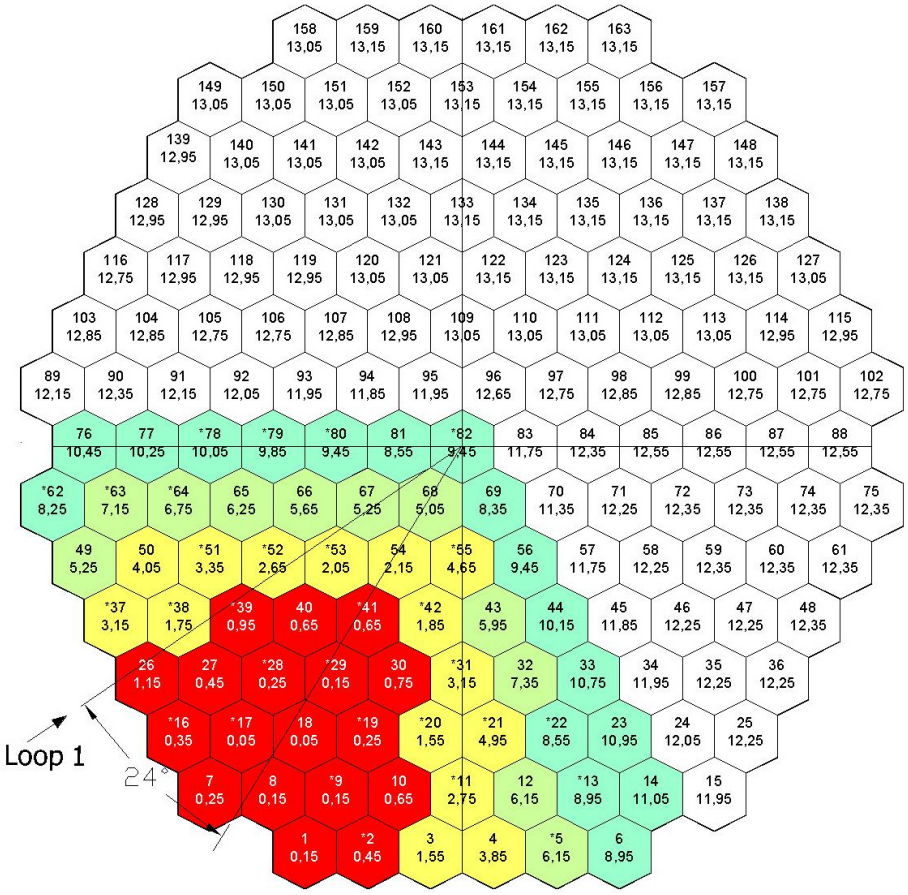

Figure 4.19: BUTE CFX 10 calculated core inlet temperatures in comparison with plant data

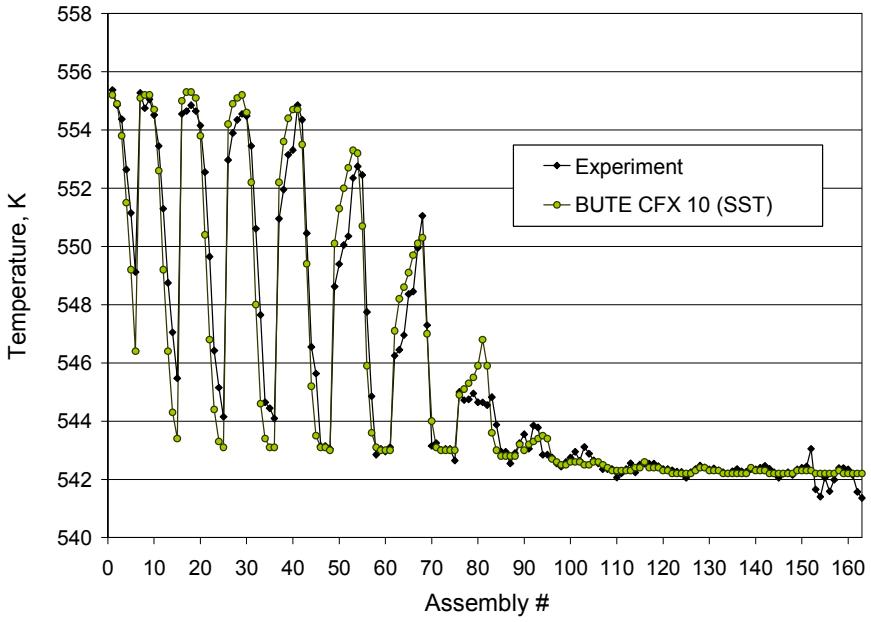

Figure 4.20: UNIPI CFX 10 results – angular turn of the loop #1 flow centre

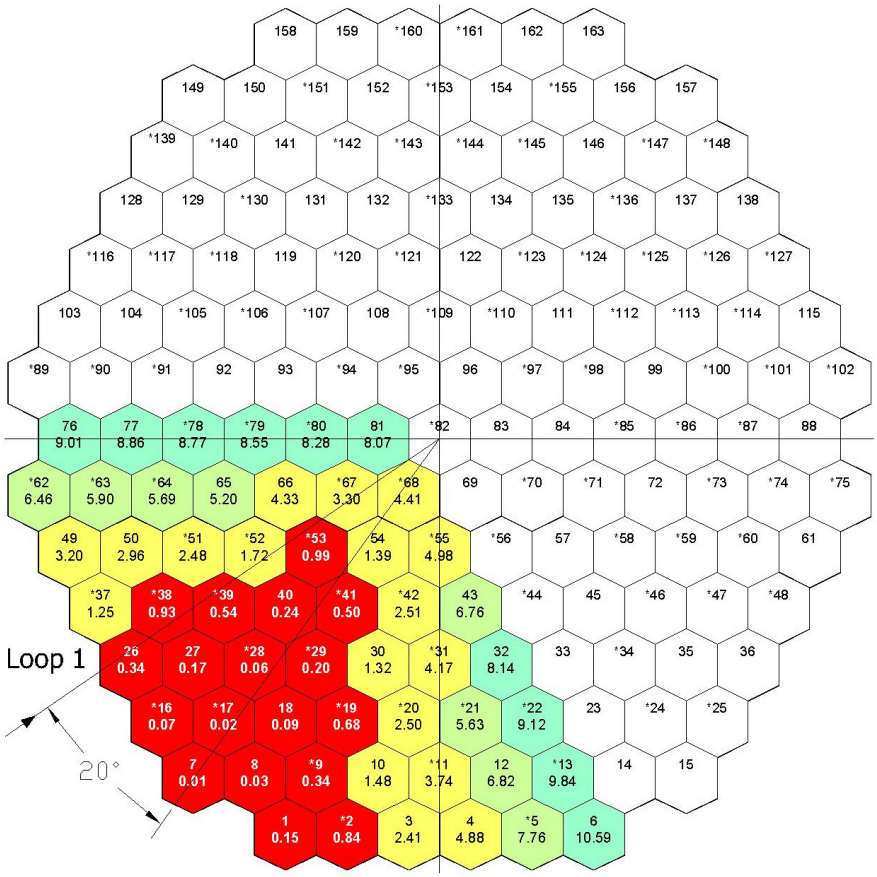

Figure 4.21: UNIPI CFX 10 calculated core inlet temperatures in comparison with plant data

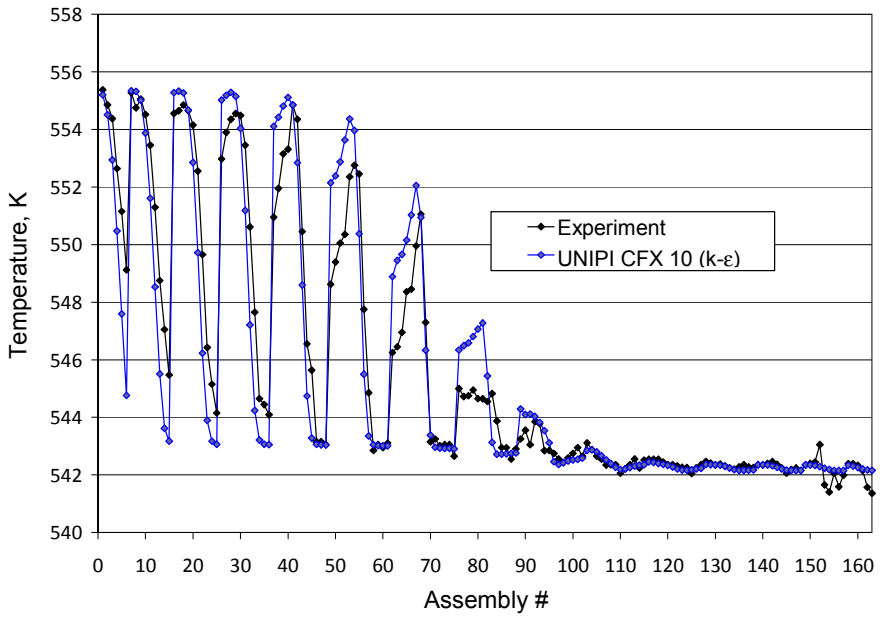

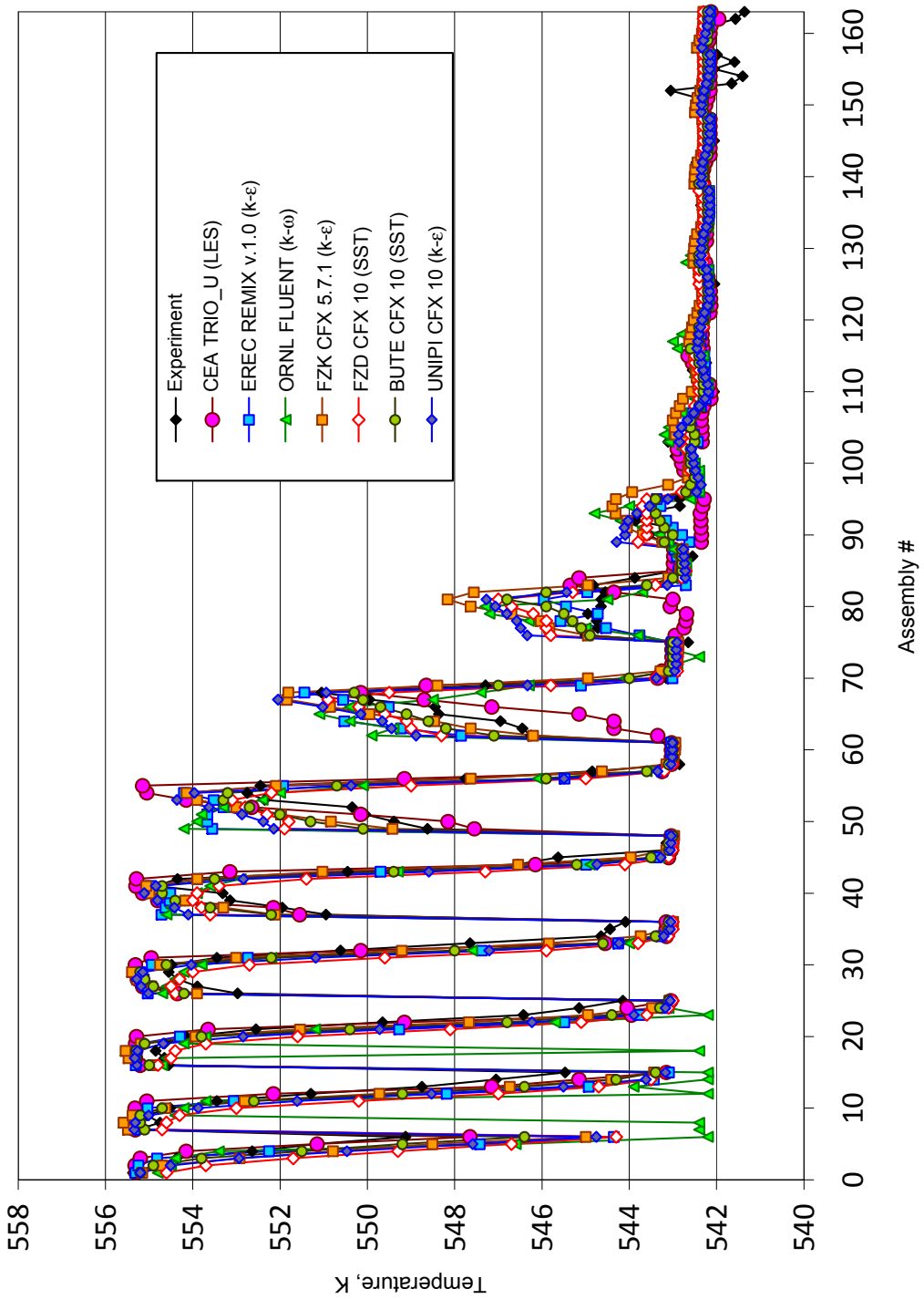

Figure 4.22: Assembly-by-assembly comparison of all core inlet temperature results

Table 4.8: Comparison of loop-to-assembly temperature differences along the centreline of the zone of minimal mixing

Code	Assembly #						
	8	18	29*	41*	54	68*	82*
Experiment	0.6	0.5	0.80	0.50	2.60	4.30	10.8
CEA	0.05	0.04	0.04	0.05	0.30	5.20	11.0
BUTE	0.15	0.05	0.15	0.65	2.15	5.05	9.45
EREC	0.03	0.06	0.14	0.37	1.15	3.91	10.39
FZD	0.75	0.95	1.35	1.95	3.15	5.85	10.05
FZK	0.02	0.02	0.00	0.30	1.2	3.5	7.8
ORNL	0.80	0.85	1.15	1.75	3.35	7.95	11.65
UNIPI	0.03	0.09	0.20	0.50	1.39	4.41	9.91

* Assembly with temperature measurement.

Table 4.9: Comparison of loop-to-assembly temperature differences along the border between the perturbed sector #1 and the non-perturbed sector #4

Code	Assembly #						
	76	77	78*	79*	80*	81	82*
Experiment	10.35	10.63	10.60	10.40	10.70	10.71	10.80
CEA	12.4	12.6	12.65	12.66	12.29	12.35	11.00
BUTE	10.45	10.25	10.05	9.85	9.45	8.55	9.45
EREC	11.59	10.82	9.78	10.63	9.90	9.39	10.39
FZD	9.55	9.45	9.45	9.15	8.65	8.35	10.05
FZK	10.4	9.5	9.3	8.7	7.7	7.2	7.8
ORNL	11.55	10.35	9.05	8.15	8.05	10.85	11.65
UNIPI	9.01	8.86	8.77	8.55	8.28	8.07	9.91

* Assembly with temperature measurement.

Table 4.10: Comparison of loop-to-assembly temperature differences along the border between the perturbed sector #1 and the non-perturbed sector #2

Code	Assembly #						
	14	23	33	44*	56*	69	82*
Experiment	8.30	8.93	7.70	8.80	7.60	8.06	10.80
CEA	10.20	11.40	10.80	9.20	6.20	6.70	11.00
BUTE	11.05	10.95	10.75	10.15	9.45	8.35	9.45
EREC	11.91	11.60	11.10	10.36	9.87	10.24	10.39
FZD	11.85	11.75	11.55	11.25	10.35	9.55	10.05
FZK	10.9	10.4	9.5	8.8	7.7	7.0	7.8
ORNL	13.15	13.15	11.35	10.45	9.25	9.05	11.65
UNIPI	11.37	11.46	11.12	10.61	9.85	9.02	9.91

* Assembly with temperature measurement.

Figure 4.23: Comparison of the deviations of all computed core inlet temperatures from plant-estimated data (163 assemblies)

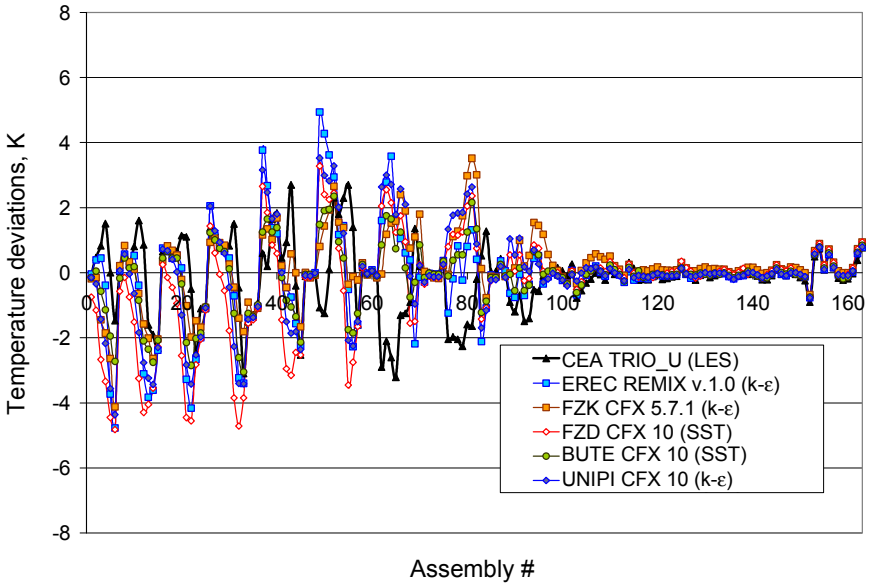

Table 4.11: Comparison of maximum and average deviations in assembly inlet temperatures

95 instrumented assemblies	TRIO_U	BUTE CFX 10	EREC REMIX	FZD CFX 10	FZK CFX 5	ORNL FLUENT	UNIPI CFX 10
Mean error (ME)	0.052	0.009	-0.036	0.237	-0.278	0.016	-0.071
Average in modulus error	0.575	0.549	0.688	0.888	0.598	0.852	0.813
Maximum in modulus error	2.90	2.85	4.163	4.55	3.011	4.85	3.56
Mean square error (MSE)	0.828	0.754	1.573	2.197	0.885	2.112	1.734

163 instrumented assemblies	TRIO_U	BUTE CFX 10	EREC REMIX	FZD CFX 10	FZK CFX 5	ORNL FLUENT	UNIPI CFX 10
Mean error (ME)	0.130	0.106	0.087	0.354	-0.178	0.405	0.049
Average in modulus error	0.699	0.622	0.810	0.979	0.671	1.191	0.898
Maximum in modulus error	3.21	3.05	4.93	4.82	4.13		4.36
Mean square error (MSE)	1.101	0.927	1.935	2.464	1.066	5.940	1.974

Figure 4.24: CEA TRIO_U and BUTE CFX 10 results – comparison of the core inlet temperature deviations from plant data (95 assemblies)

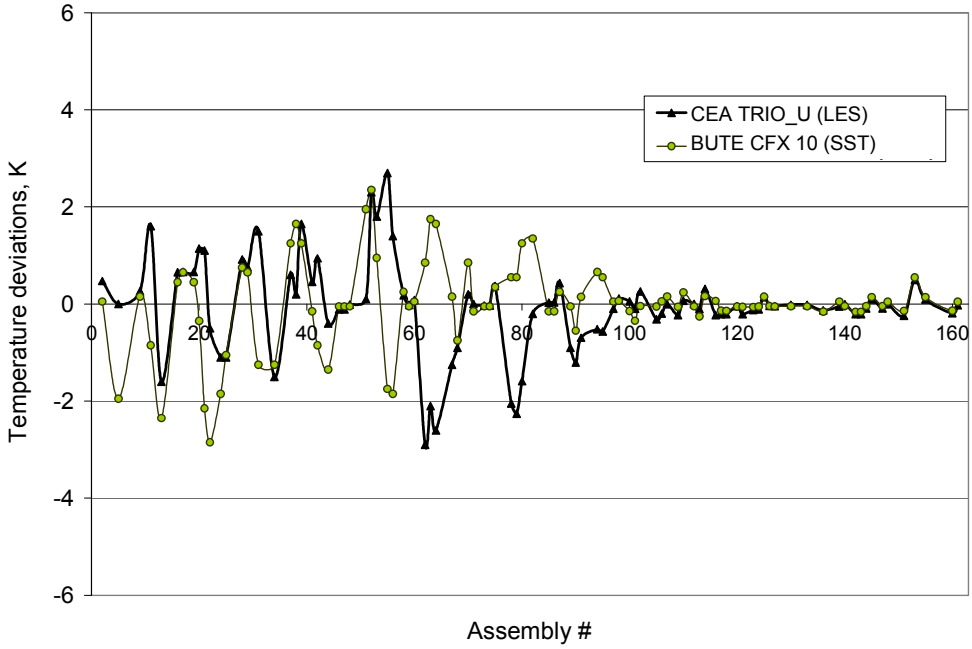

Figure 4.25: CEA TRIO_U and BUTE CFX 10 results – comparison of the core inlet temperature deviations from plant data (163 assemblies)

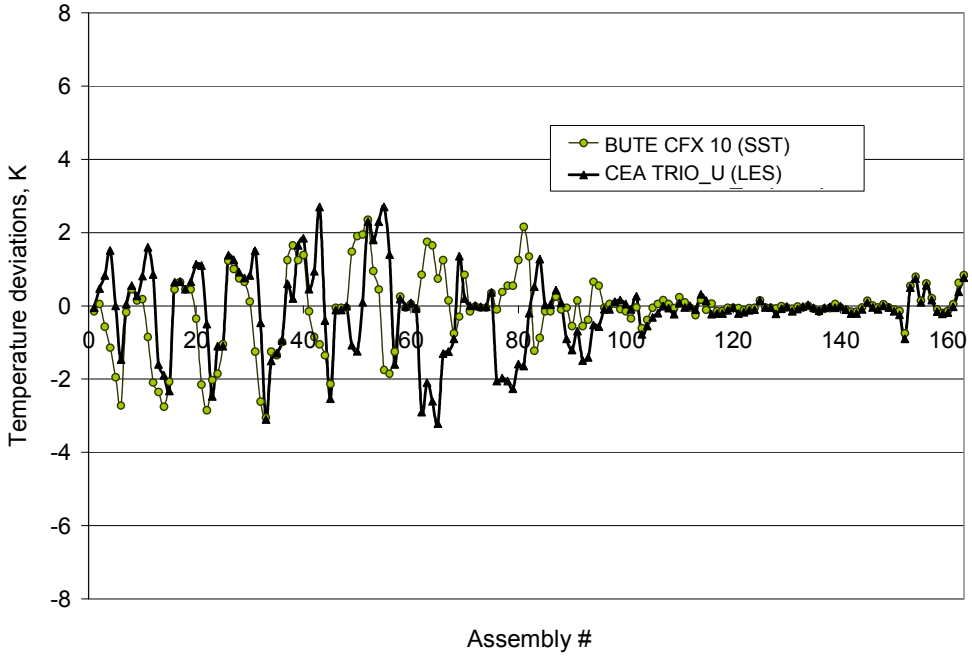

Figure 4.26: CEA TRIO_U and EREC REMIX results – comparison of the core inlet temperature deviations from plant data (95 assemblies)

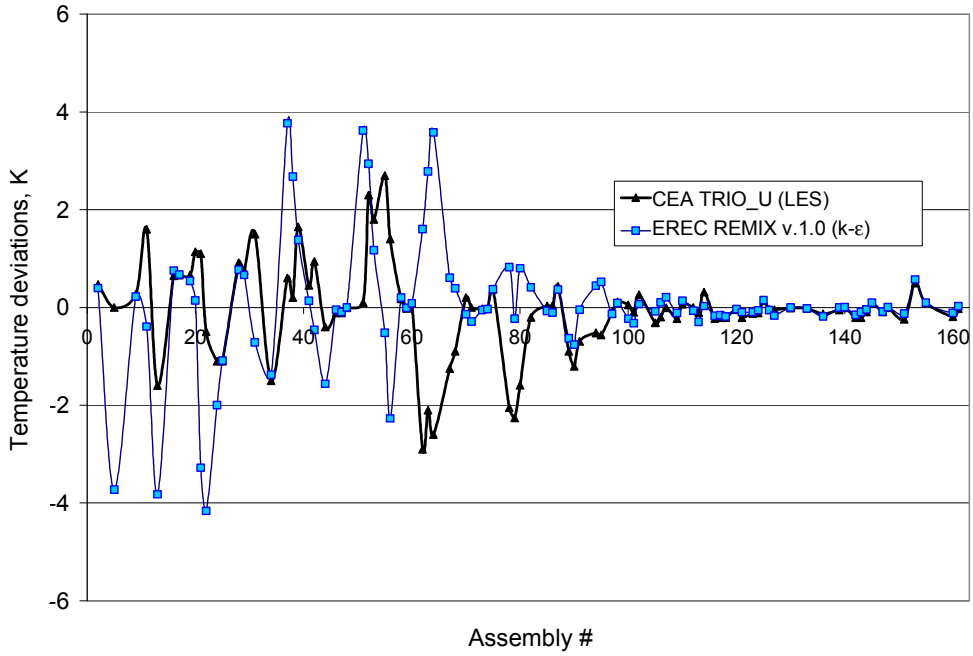

Figure 4.27: CEA TRIO_U and EREC REMIX results – comparison of the core inlet temperature deviations from plant data (163 assemblies)

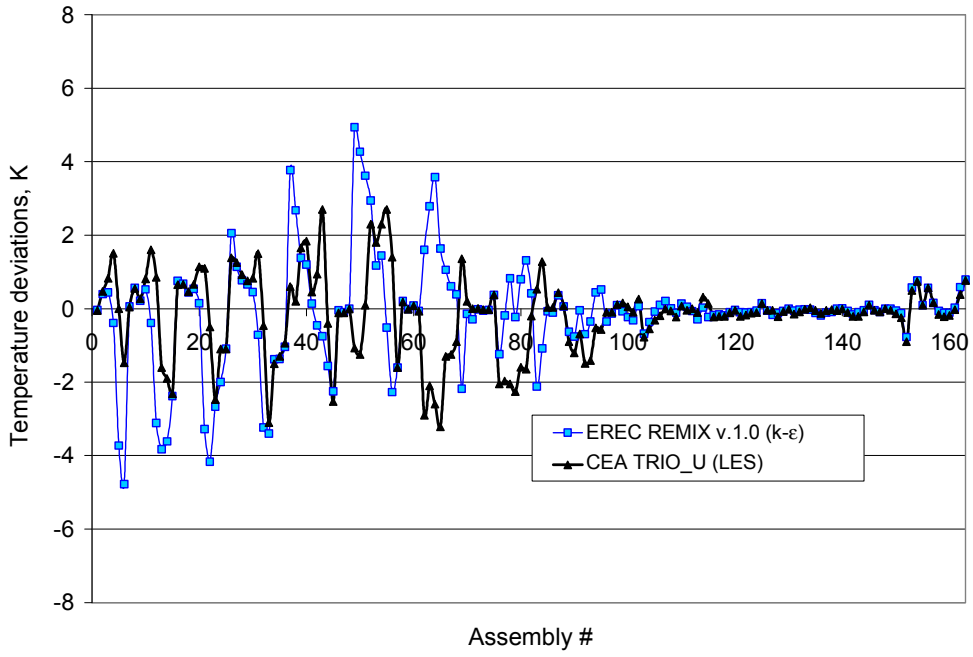

Figure 4.28: CEA TRIO_U and ORNL FLUENT results – comparison of the core inlet temperature deviations from plant data (95 assemblies)

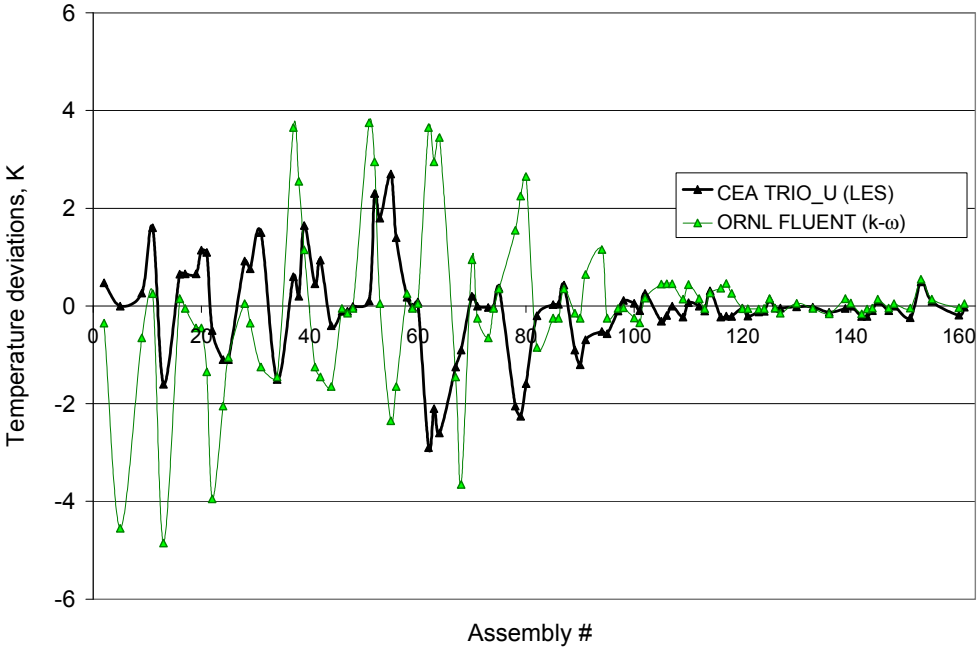

Figure 4.29: CEA TRIO_U and ORNL FLUENT results – comparison of the core inlet temperature deviations from plant data (163 assemblies)

Values in the template for assemblies # 7, 8 and 18 are not filled

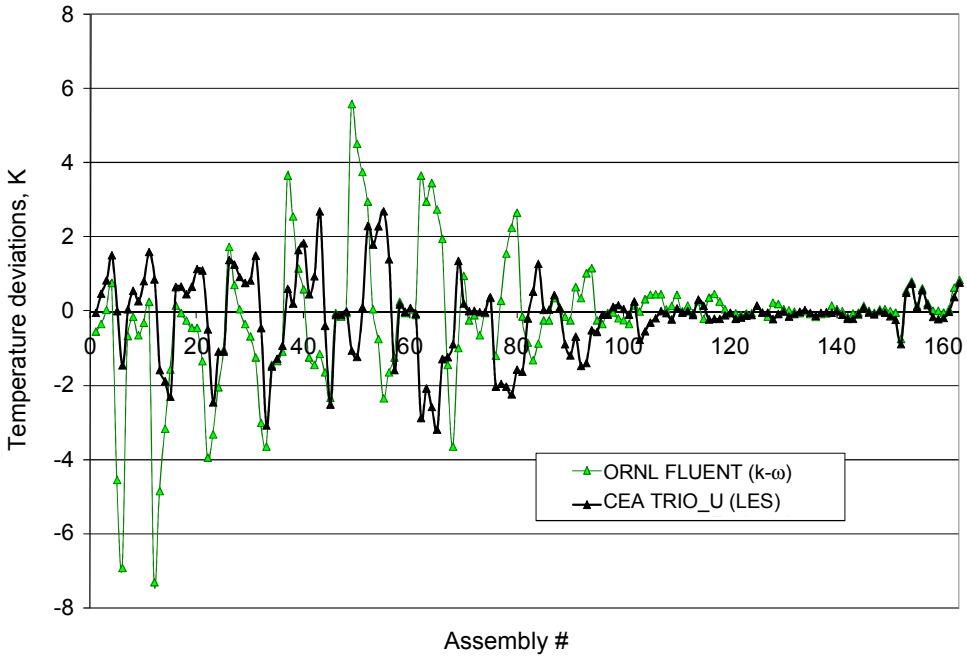

Figure 4.30: CEA TRIO_U and FZD CFX 10 results – comparison of the core inlet temperature deviations from plant data (95 assemblies)

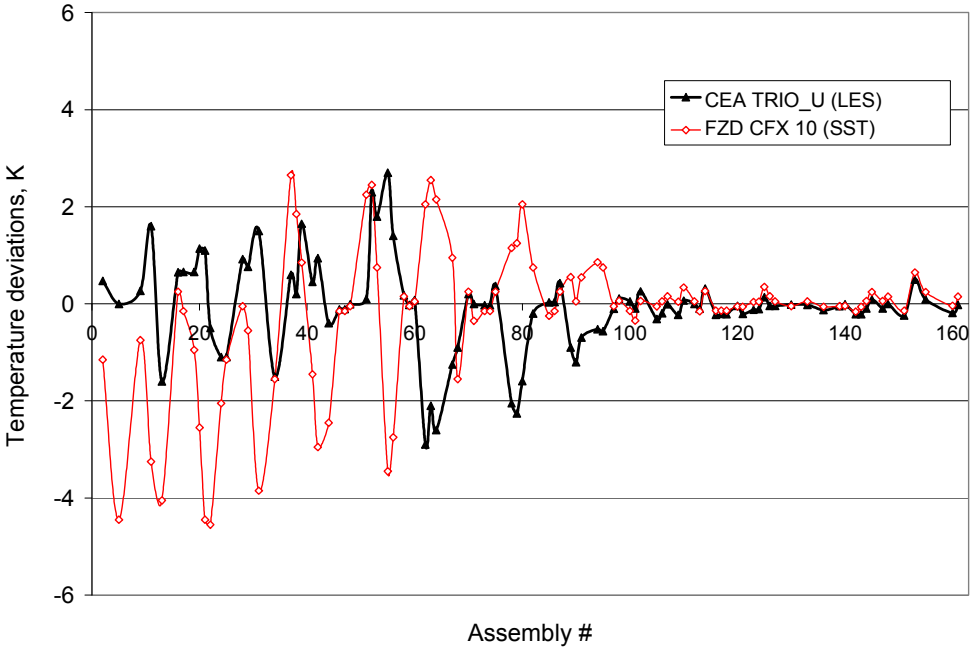

Figure 4.31: CEA TRIO_U and FZD CFX 10 results – comparison of the core inlet temperature deviations from plant data (163 assemblies)

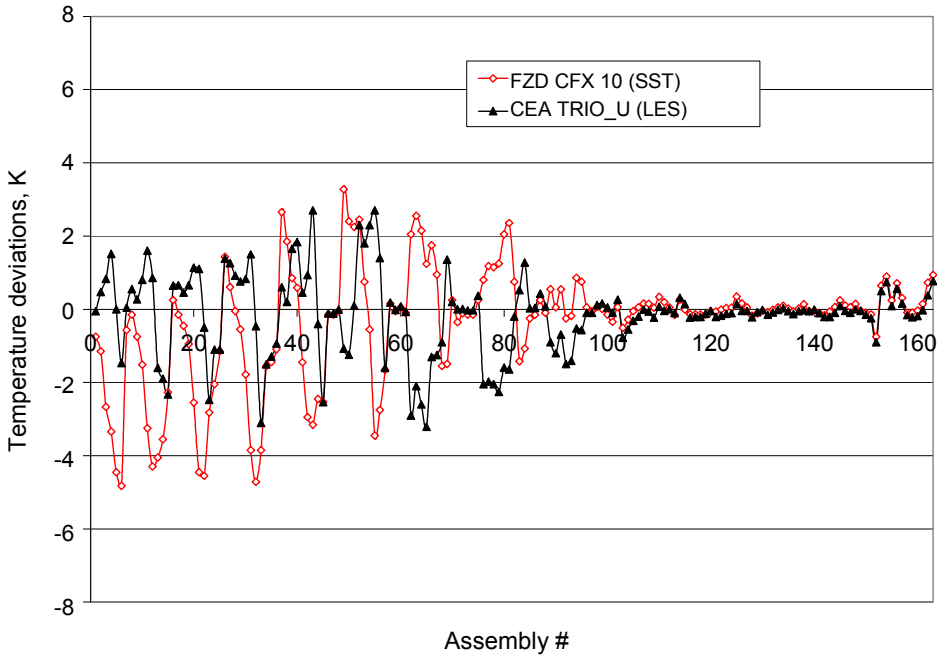

Figure 4.32: CEA TRIO_U and FZK CFX 5 results – comparison of the core inlet temperature deviations from plant data (95 assemblies)

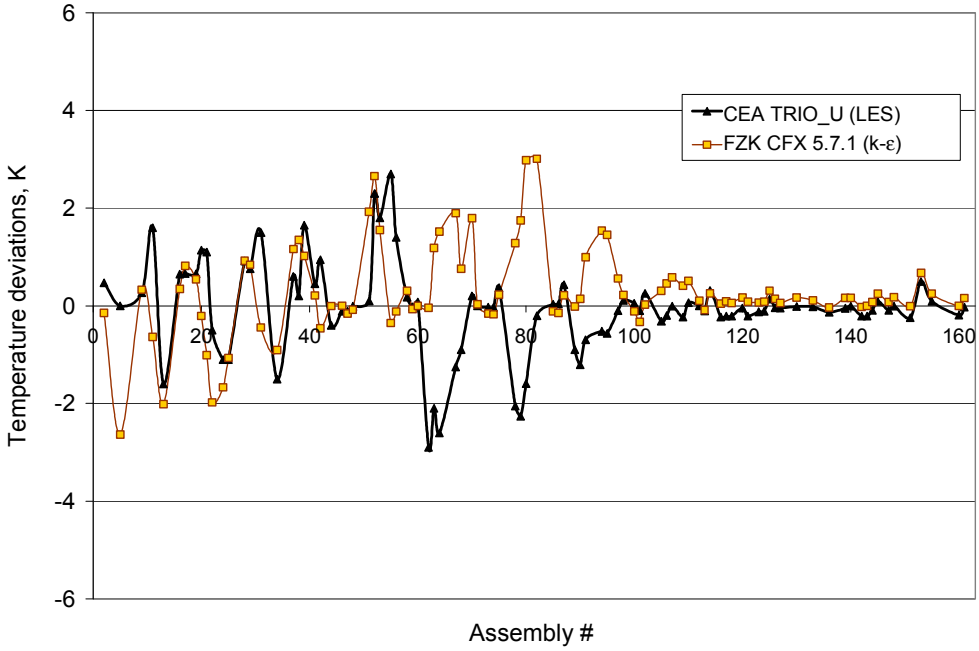

Figure 4.33: CEA TRIO_U and FZK CFX 5 results – comparison of the core inlet temperature deviations from plant data (163 assemblies)

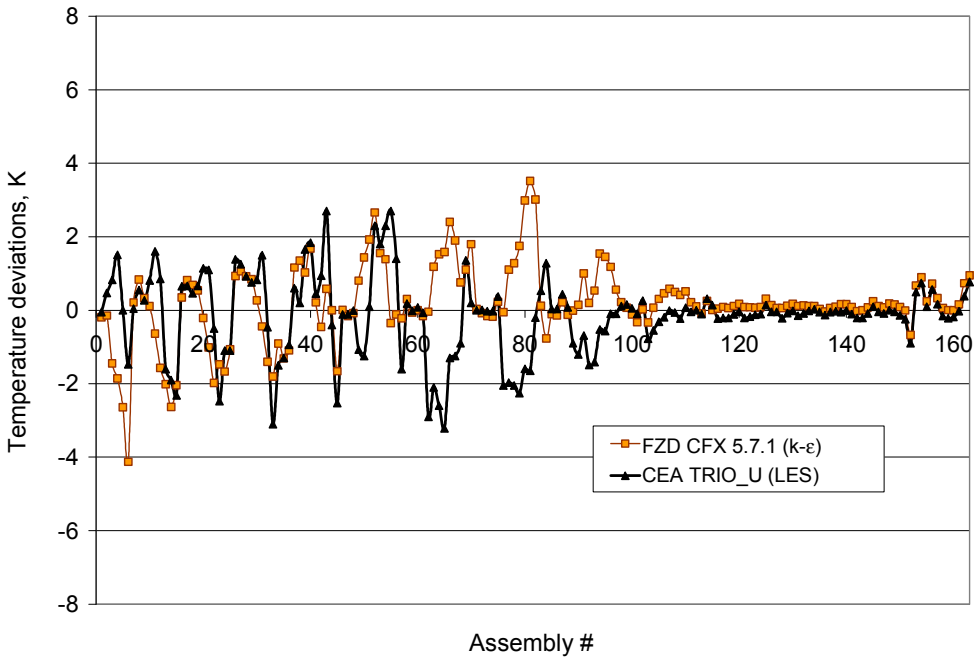

Figure 4.34: CEA TRIO_U and UNIPI CFX 10 results – comparison of the core inlet temperature deviations from plant data (95 assemblies)

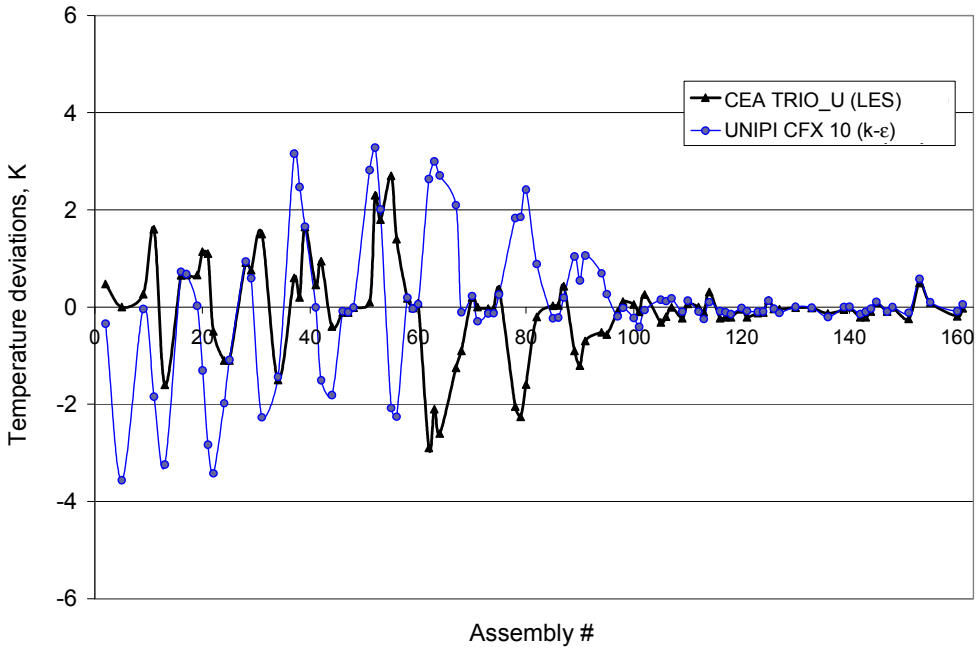

Figure 4.35: CEA TRIO_U and UNIPI CFX 10 results – comparison of the core inlet temperature deviations from plant data (163 assemblies)

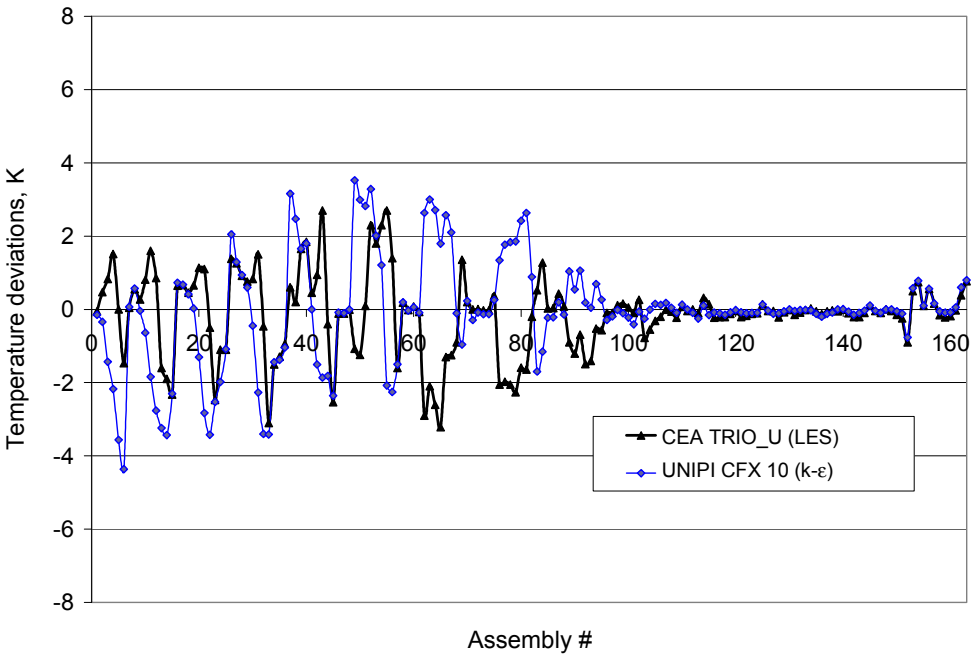

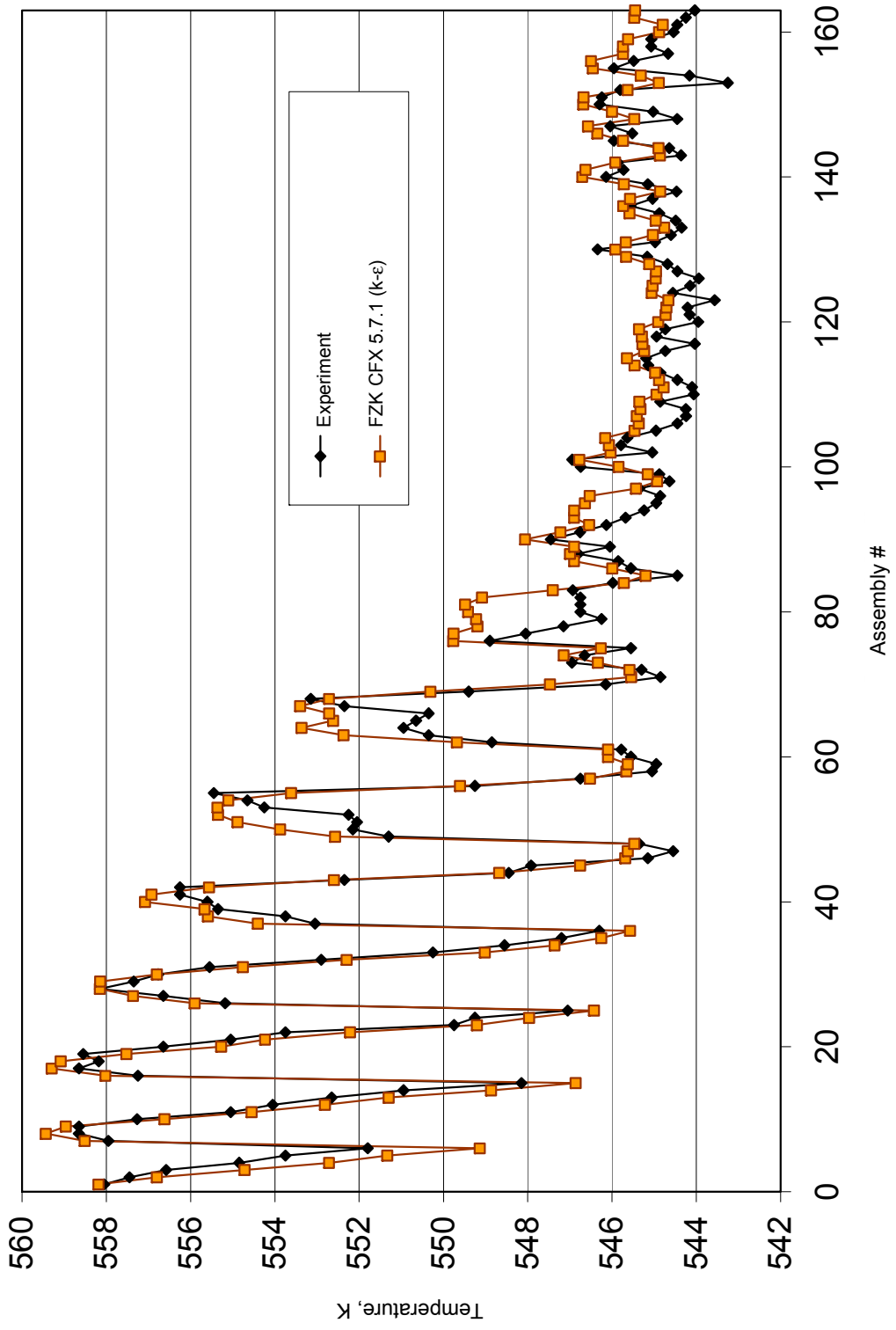

Figure 4.36: FZK CFX 5 results vs. plant data – assembly-by-assembly comparison of the core outlet temperatures

Figure 4.37: Assembly-by-assembly core inlet velocities in the initial and final states. The FZK results were obtained by CFX 5 k-ε with porous medium in the lower plenum.

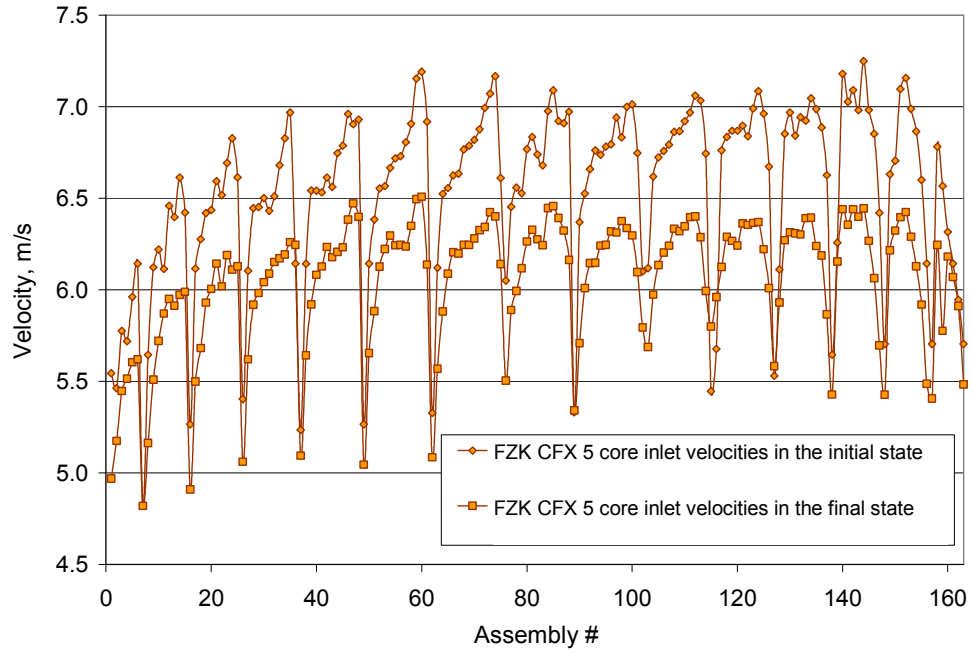

Figure 4.38: Assembly-by-assembly core inlet velocities in the final state. The FZK CFX 10 SST result was obtained with explicit modelling of the elliptical sieve plate.

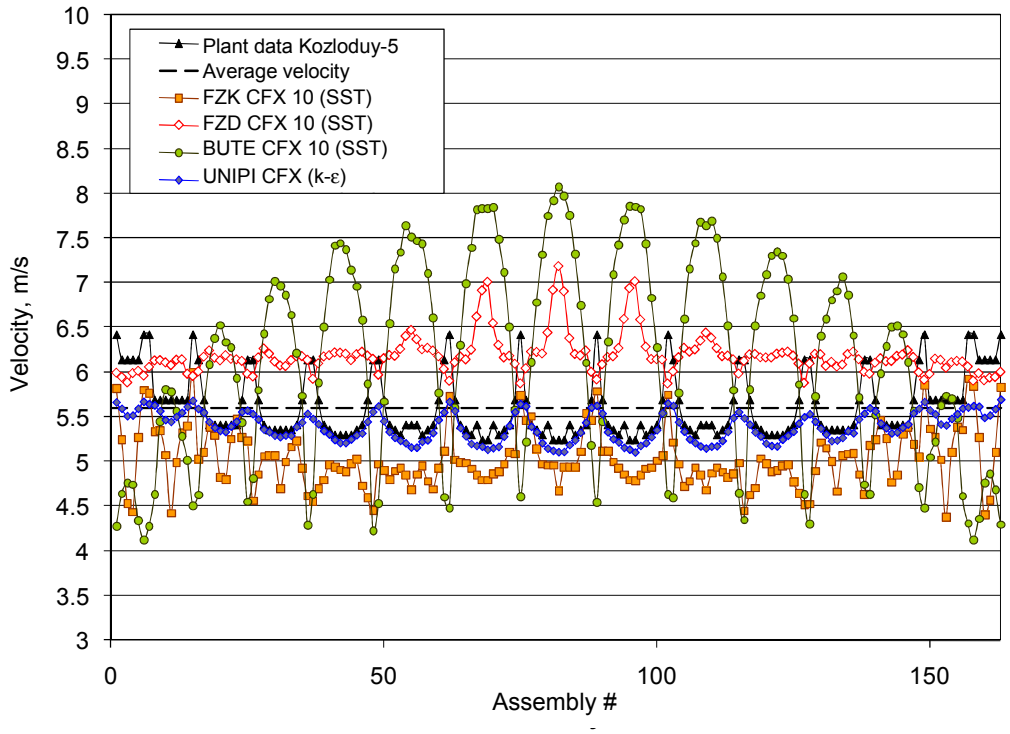

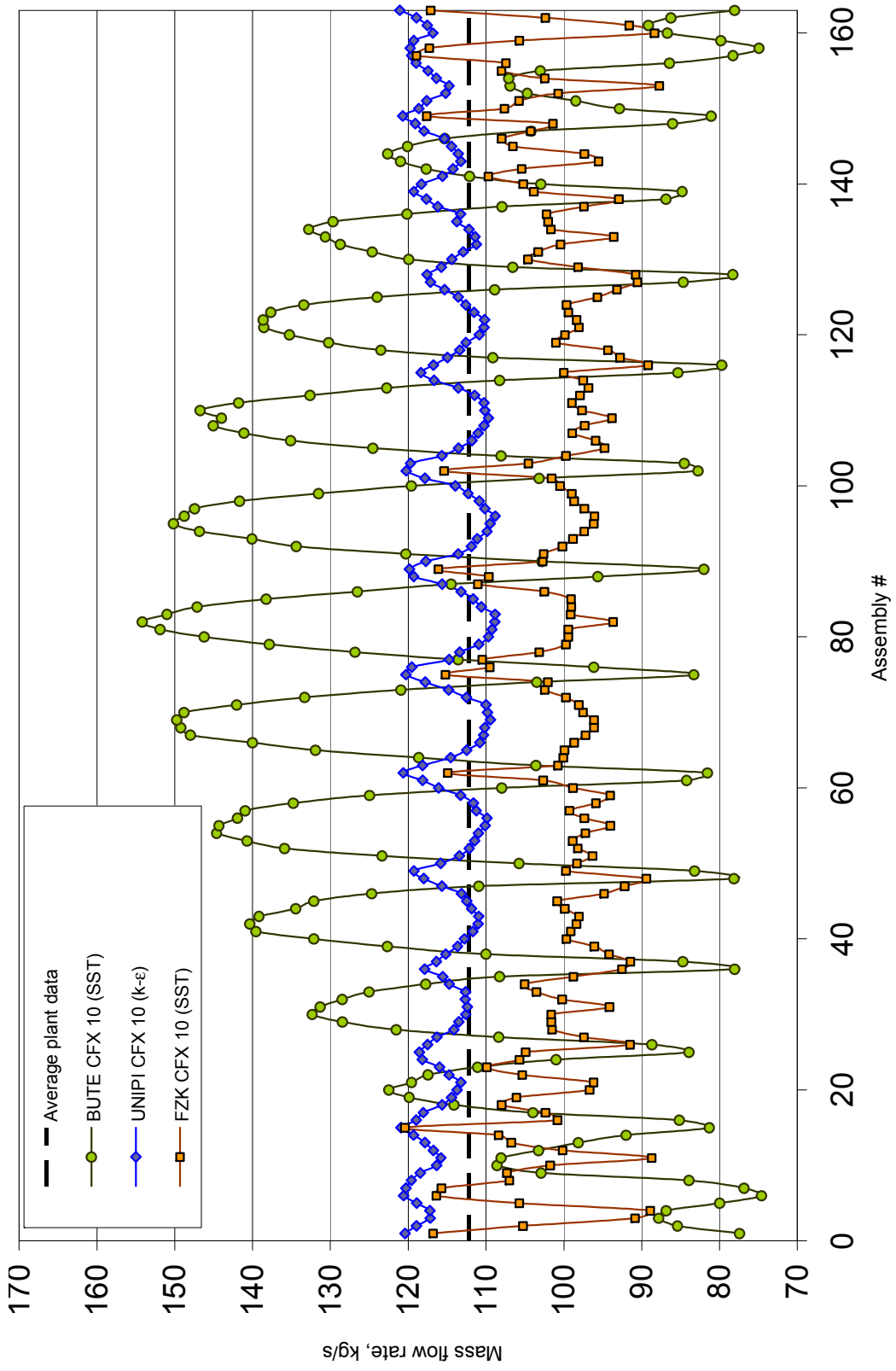

Figure 4.39: Assembly-by-assembly core inlet mass flow rates

Figure 4.40: Computed radial profile of the core inlet velocity in qualitative comparison with plant data from Kozloduy-5

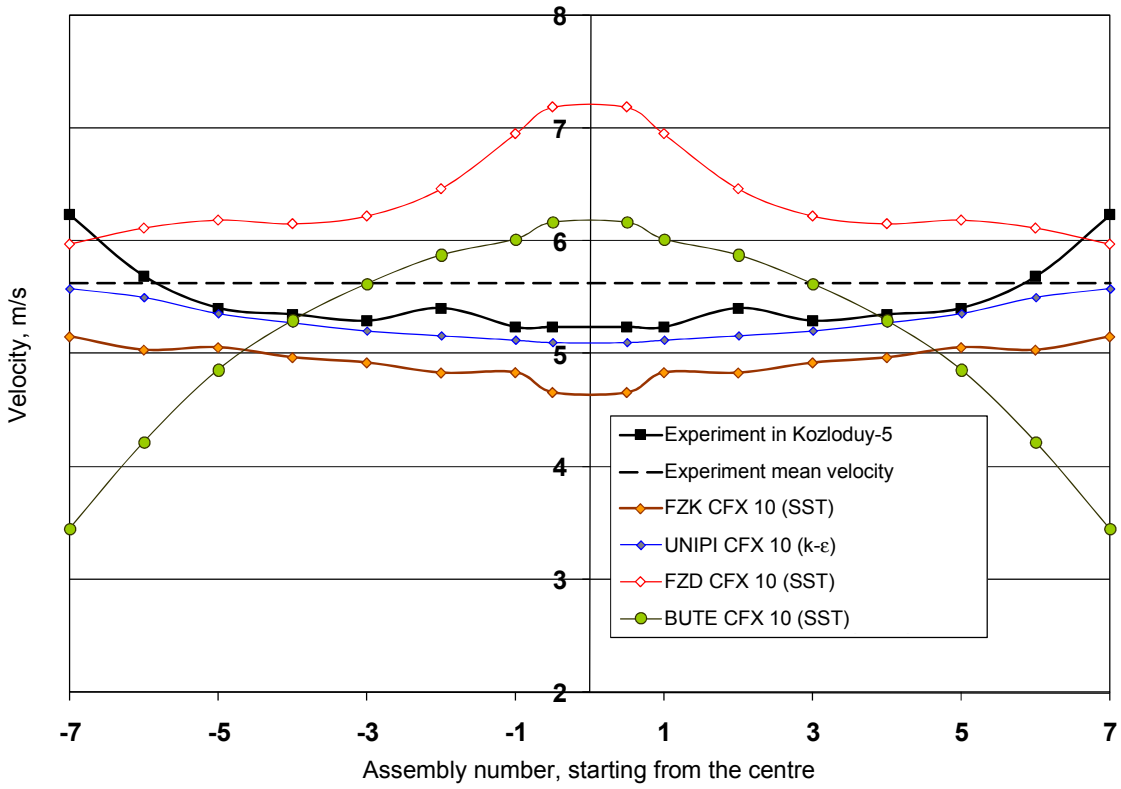

Chapter 5: Coarse mesh results

This chapter presents the comparative analysis of coarse mesh results for V1000CT-2 Exercise 1 obtained with system codes.

The basic reference problem is a vessel boundary condition problem. The domain of solution is the whole reactor vessel. The task is to calculate the integral parameters during the transient as well as the temperature and velocity distributions in the downcomer and at the core inlet in the final state, given the vessel boundary conditions and the pressure above the core. Code-to-experiment and code-to-code comparisons are considered.

Full plant simulation is an option. Measured time histories of integral parameters can be used for comparison, in addition to core inlet and outlet temperature distributions in the initial and final stabilised states.

As discussed in Chapters 3 and 4, plant-measured core outlet temperature distributions are available for comparison. However, the direct use of the core outlet temperature measurements would require modelling of the guide channels bypass flow and coolant mixing in each assembly head. In order to simplify the task and have a clear test of the mixing in the downcomer and the lower plenum, the estimated assembly inlet temperatures were used for comparison as for CFD (Chapter 4). Reconstructed full core distributions (163 assemblies) were also used for validation purposes.

A total of five solutions were submitted by six organisations, listed in Table 5.1. The submitted results were obtained using multi-1-D vessel models with cross-flow in CATHARE2 (INL, 2001) and ATHLET (Bajorek, 2007), and coarse-3-D vessel thermal-hydraulic models in TRACE (Nikonov, 2006) and RELAP3D (Frisani, 2006). The comparative analysis includes the initial and final state, and transient results.

Table 5.1: List of participants with coarse-mesh models

Organisation	Code	Model	Nodalisation
GRS/KI	ATHLET/BIPR8H	Multi-1-D	16 sectors in the vessel 7 radial rings
INRNE	CATHARE2	Multi-1-D	24 sectors in the vessel
KU	RELAP3D	Coarse 3-D	36 sectors in the DC and LP 7 radial rings
ORNL	RELAP3D	Coarse 3-D	6 sectors in the DC and LP 5 radial rings
PSU	TRACE	Coarse 3-D	6 sectors in the vessel 5 radial rings
UNIPI	RELAP3D	Coarse 3-D	20 sectors in the DC 60 sectors in the upper LP max. 8 radial rings in LP

5.1 Initial steady state

The integral parameters in the initial steady state are shown in Table 5.2. The results are in good agreement with the plant data except the loop flow rates in the ORNL results.

5.2 Final state

The integral parameters in the final steady state are shown in Table 5.3. The results are in good overall agreement with the plant data except for the loop flow rates in the ORNL results.

The vessel mixing is considered at several elevations along the flow path, two of them in the downcomer. The first is below the impinging jets of the cold legs and just above the expansion, at 5 800 mm from the inner vessel bottom. The second is in the lower downcomer, at 2 500 mm from the vessel bottom. The flow parameters are compared code-to-code in 24 points (8 points above each console plus 2 points at ±10 cm in azimuth direction). The next elevations are at the assembly inlets (163 assemblies) and at the reactor vessel outlet axes (4 nozzles).

Coolant mixing in the downcomer

Figures 5.1 and 5.2 present the computed azimuth temperature distributions at elevations of 5 800 mm and 2 500 mm respectively, in comparison with the FZD CFX 10 SST results. Generally good agreement is displayed. The RELAP3D 20-sector downcomer model of UNIPI gives results closest to those of CFD. The RELAP3D 36-sector model of KU predicts steeper gradients at the disturbed sector borders. The CATHARE2 24-sector multi-1-D model yields quite reasonable results which can be improved by further azimuth mesh refinement.

Figures 5.3 and 5.4 show the downcomer velocity distributions at 5 800 mm and 2 500 mm respectively. The results indicate certain differences in the pressure drops along the flow path.

Coolant mixing from the reactor inlet to the core inlet

For the purposes of this analysis, we compare:

- the ability of the models to represent the main features of the flow, such as the swirl in the downcomer and the lower plenum;
- the errors in the predicted assembly by assembly core inlet temperatures, in terms of the chosen metrics in Chapter 3.

The experimentally observed counter-clockwise angular turn of the loop flow (looking from the top) is presented in Figure 5.5. The calculated results are presented in Figures 5.6 through 5.16.

Figure 5.6 shows the INRNE-CATHARE result for the angular turn of loop #1 flow, computed by a 24-sector multi-1-D model with cross-flow. There is no radial subdivision in the core barrel. Acceptable agreement with the plant data is displayed. The model predicts angular turn of 23° for the loop #1 flow. Figure 5.7 shows the corresponding core inlet temperature distribution, obtained by means of an appropriate mapping scheme that transforms the channel parameters into assembly-by-assembly parameters. The results are in acceptable agreement with the plant data. The maximal in modulus deviation (for instrumented assemblies) is 3.41 K and the average in modulus deviation is 0.835 K (see Table 5.4). Numerical experiments with 12, 16 and 24-sector vessel models showed that the solution is sensitive to azimuth mesh refinement. At least 16-18 sectors are recommended for an acceptable resolution in the assembly-by-assembly inlet temperatures.

The GRS/KI-ATHLET results are presented in Figures 5.8 and 5.9. The vessel model is 16-sector multi-1-D with cross-flow and seven radial rings, one for each concentric row of fuel assemblies in the core. This is a coupled 3-D neutronics/thermal-hydraulic calculation using ATHLET/BIPR8KN with the BIPR8 cross-section library and full plant simulation. The computed turn of loop #1 flow is around 18°. The maximal in modulus deviation in core inlet temperatures is 4.70 K and the average in modulus deviation is 1.06 K (see Table 5.4). The results are in acceptable agreement with the plant data. A GRS/KI sensitivity study (Electrogorsk, 2006) using up to 48 sectors showed that resolution improves with angular mesh refinement. This improvement tends to saturation after 32 azimuth sectors.

Figure 5.10 illustrates the KU-RELAP3D result for the angular turn of loop #1 flow, computed by a 36-sector coarse 3-D model with seven radial rings in the LP and the core. The predicted angular flow turn is 18°. Figure 5.11 shows the corresponding core inlet temperature distribution. The maximal in modulus deviation is 5.61 K and the average in modulus deviation is 1.30 K (see Table 5.4). The results are in reasonable agreement with plant data.

Figure 5.12 shows the PSU-TRACE result for the angular turn of loop #1 flow, computed by a six-sector coarse 3-D model with five radial rings in the LP and the core. As the zone of minimal mixing is a whole 60° sector, the predicted angular flow turn is about 8° clockwise. Figure 5.13 shows the corresponding core inlet temperature distribution. The maximal in modulus deviation is 9.21 K and the average in modulus deviation is 1.62 K (see Table 5.4). This result illustrates the limitations of the models using less than 12 azimuth sectors. Such coarse meshes may represent acceptably well the loop-to-loop mixing and sector averaged temperatures but have insufficient resolution for the assembly-by-assembly inlet parameters.

Figure 5.14 shows the UNIPI-RELAP3D result for the angular turn of loop #1 flow, computed by a coarse 3-D 20-sector model of the downcomer and 60-sector model of the upper part of LP with eight radial rings. The predicted angular flow turn is about 20°. Figure 5.15 shows the corresponding core inlet temperature distribution. The results are in reasonable agreement with plant data. The maximal deviation is 8.81 K, somewhat larger than expected for this meshing. The average in modulus deviation is 1.35 K (see Table 5.4).

The comparison of all coarse-mesh computed core inlet temperature distributions is presented in Figure 5.16. Reasonable agreement with plant data is observed for all participants, in terms of the chosen metrics.

For a more informative comparison, the deviations of computed to plant-estimated core inlet temperatures in the final state are shown in Figures 5.17 through 5.39. The results are compared to each other and to the CEA-TRIO_U LES results. Good qualitative agreement of all coarse-mesh results is observed, with some model-dependent quantitative differences.

The comparison of coarse-mesh and TRIO_U solution deviations from the plant-estimated core inlet temperatures is shown in Figures 5.28, 5.30, 5.32, 5.34 and 5.36 (for 95 instrumented assemblies). The respective whole-core comparison for 163 assemblies is shown in Figures 5.29, 5.31, 5.33, 5.35, 5.37 and 5.39. The results are in acceptable agreement within the sector of minimal mixing. The maximal differences occur at the borders of the disturbed sector, depending on the predicted angular flow turn and the diffusion in the sector formation.

Figures 5.38 and 5.39 show a comparison between INRNE CATHARE2 and BUTE CFX 10 SST results, in terms of deviations from plant data. It is interesting to note that the results are qualitatively close to each other, which can be explained in part by the similar prediction of the disturbed sector formation.

The computed assembly inlet velocities are shown in Figure 5.40. The results show discrepancies, which seem to be related to somewhat different predicted pressure drops and different elevations, corresponding to the submitted data. Thus, the CATHARE calculated velocities are given at 1 800 mm and not at 1 630 mm from the vessel bottom, for modelling reasons. The assembly flow area at this elevation is 0.0256 m^2 and the corresponding average velocity is 5.60 m/s. The average velocity at the assembly inlets, shown in Figure 5.40, corresponds to elevation 1 630 mm just above the core support plate. The flow area at this elevation is 0.02545 m^2 (NEA, 2010a) and the average velocity is 5.634 m/s. The UNIPI RELAP3D velocities seem to correspond to the inlet of the heated part.

5.3 Transient

We compare results from full plant simulation by system codes and plant data.

Time histories of the hot leg temperatures are shown in Figures 5.41 through 5.44. The uncertainty of the measured data is given in Table 5.2. All code-to-experiment deviations are within the uncertainty range. Tables 5.5 through 5.8 illustrate the corresponding deviations and figures of merit.

The computed time histories of cold leg temperatures are shown in Figures 5.45 through 5.48. The results of all participants are reasonably close to the plant data, well within the uncertainty band. Tables 5.9 through 5.12 illustrate the corresponding deviations and figures of merit.

Figures 5.49 through 5.52 present the comparison of loop mass flow rates. The CATHARE2 and ATHLET/BIPR results agree well with plant data. The KU-RELAP3D result for loop #4 slightly exceeds the uncertainty range. The ORNL-RELAP3D computed loop flow rates are not shown because they are beyond the admissible uncertainty (due to improper initialisation, see Table 5.2).

Figure 5.53 shows the time history of pressure above the core. Figure 5.54 shows the time history of SG-1 pressure.

Generally good agreement with plant data and code-to-code is displayed, with the exception of loop flow rates in the ORNL results and pressure above the core in the KU simulation.

5.4 Discussion

Computationally efficient coarse-mesh vessel TH models were tested in flow mixing calculations. Code-to-experiment, code-to-CFD and coarse-mesh code-to-code comparisons were performed.

The detailed evaluation of the differences to plant data shows that the coarse-mesh vessel TH models can reasonably well reproduce the main flow features and the assembly inlet temperatures in asymmetric flow mixing transients, characterised by sector formation. For this type of coolant transient, coarse-3-D models do not perform noticeably better than multi-1-D.

The resolution improves with the mesh refinement. The solutions are sensitive to the azimuth meshing. The available results suggest that for an acceptable accuracy in core inlet distributions at least 16-18 azimuth sectors are necessary.

The deviations in assembly inlet temperatures are within 1-8 K which is significantly larger than the observed CFD error range.

Some of the discrepancies between different coarse-mesh results can be explained by the modelling differences summarised in Table 5.1 and the participants' provided calculation details given in Appendix D.

Table 5.2: Initial state results

Parameter	Plant data	INRNE CATHARE 2.5	GRS/KI ATHLET/BIPR8	KU RELAP3D	ORNL RELAP3D	PSU TRACE	Uncertainty
Core power, MW	281	281	295	281	281	–	±60
Pressure above the core, MPa	15.59	15.605	15.595	15.593	15.6	–	±0.3 MPa
Cold leg #1 temperature, K	541.75	541.75 (BC)	541.74	541.74	541.62	–	±1.5 K
Cold leg #2 temperature, K	541.85	541.85 (BC)	541.83	541.7	541.64	–	±1.5 K
Cold leg #3 temperature, K	541.75	541.75 (BC)	541.95	541.73	541.62	–	±1.5 K
Cold leg #4 temperature, K	541.75	541.75 (BC)	541.76	541.7	541.64	–	±1.5 K
Hot leg #1 temperature, K	545	544.65	544.85	544.73	544.8	–	±1.5 K
Hot leg #2 temperature, K	545.09	544.68	544.91	544.59	544.9	–	±1.5 K
Hot leg #3 temperature, K	545.09	544.71	545	544.7	544.8	–	±1.5 K
Hot leg #4 temperature, K	545	544.83	544.88	544.61	544.9	–	±1.5 K
Loop #1 flow rate, kg/s	4 737	4 737.0	4 738.4	4635.4	4 245	–	±110 kg/s
Loop #2 flow rate, kg/s	4 718	4 718.0	4 720.4	4 636.1	4 275	–	±110 kg/s
Loop #3 flow rate, kg/s	4 682	4 682.0	4 684.1	4 635.4	4 245	–	±110 kg/s
Loop #4 flow rate, kg/s	4 834	4 833.9	4 831.5	4 636.1	4 275	–	±110 kg/s
Core flow rate, kg/s	18 971	18 970.9	18 699.7	18 543	16 762	–	±490 kg/s
Reactor pressure drop, MPa	0.418	0.418	0.4132	0.407	0.409	–	±0.043 MPa
Pressure in SG 1, MPa	5.11		5.1344	5.131	–	–	±0.2 MPa
Pressure in SG 2, MPa	5.13		5.1344	5.131	–	–	±0.2 MPa
Pressure in SG 3, MPa	5.15		5.1344	5.131	–	–	±0.2 MPa
Pressure in SG 4, MPa	5.13		5.1344	5.131	–	–	±0.2 MPa
MSH pressure, MPa	5.07		5.13	5.129	5.12	–	±0.2 MPa

Table 5.3: Final state results for the integral parameters

Parameter	Plant data	INRNE CATHARE 2.5	GRS/KI ATHLET/BIPR8	KU RELAP3D	ORNL RELAP3D	PSU TRACE	Uncertainty
Core power, MW	286	286	283.34	288	281	286	±60
Pressure above the core, MPa	15.593	15.59	15.60	15.63	15.80	15.62	±0.3 MPa
Cold leg #1 temperature, K	555.35	555.35 (BC)	554.7	555.39	554.8	555.35	±1.5 K
Cold leg #2 temperature, K	543.05	543.05 (BC)	543.12	542.56	543.0	543.05	±1.5 K
Cold leg #3 temperature, K	542.15	542.15 (BC)	542.17	541.86	541.90	542.15	±1.5 K
Cold leg #4 temperature, K	542.35	542.35 (BC)	542.11	542.06	542.30	542.35	±1.5 K
Hot leg #1 temperature, K	554.85	555.24	554.48	555.13	554.60	554.4	±1.5 K
Hot leg #2 temperature, K	548.15	547.54	548.09	547.69	548.20	548.2	±1.5 K
Hot leg #3 temperature, K	545.75	545.48	545.55	545.16	545.50	545.8	±1.5 K
Hot leg #4 temperature, K	546.45	546.89	545.85	545.84	546.50	546.1	±1.5 K
Loop #1 flow rate, kg/s	4 566	4 567.5	4 590.7	4 641.31	4 070	4 566	±110 kg/s
Loop #2 flow rate, kg/s	4 676	4 676.2	4 711.6	4 639.29	4 279	4 676	±110 kg/s
Loop #3 flow rate, kg/s	4 669	4 668.2	4 688.2	4 481.89	4 265	4 669	±110 kg/s
Loop #4 flow rate, kg/s	4 819	4 818.2	4 833.8	4 632.87	4 288	4 819	±110 kg/s
Core flow rate, kg/s	18 730	18 730	18 552	18 395	16 752	18 577	±490 kg/s
Reactor pressure drop, MPa	0.419	0.411	0.410	0.404	0.406	N/A	±0.043 MPa
Pressure in SG 1, MPa	6.51		6.53	6.51	–	–	±0.2 MPa
Pressure in SG 2, MPa	5.14		5.14	5.14	–	–	±0.2 MPa
Pressure in SG 3, MPa	5.15		5.13	5.13	–	–	±0.2 MPa
Pressure in SG 4, MPa	5.14		5.14	5.13	–	–	±0.2 MPa
MSH pressure, MPa	5.07		5.13	5.13	5.12	–	±0.2 MPa

Figure 5.1: Downcomer temperature distribution at z = 5 800 mm

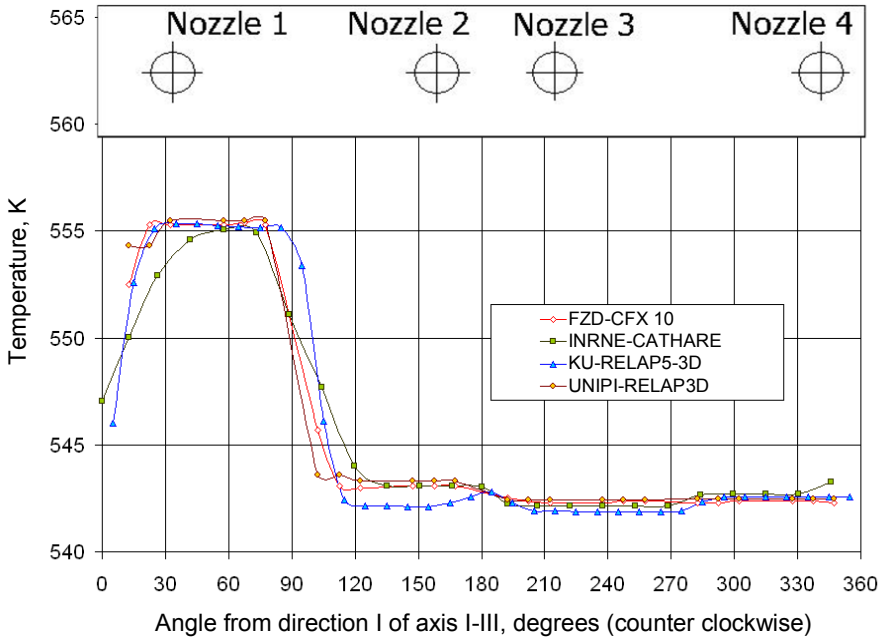

Figure 5.2: Downcomer temperature distribution at z = 2 500 mm

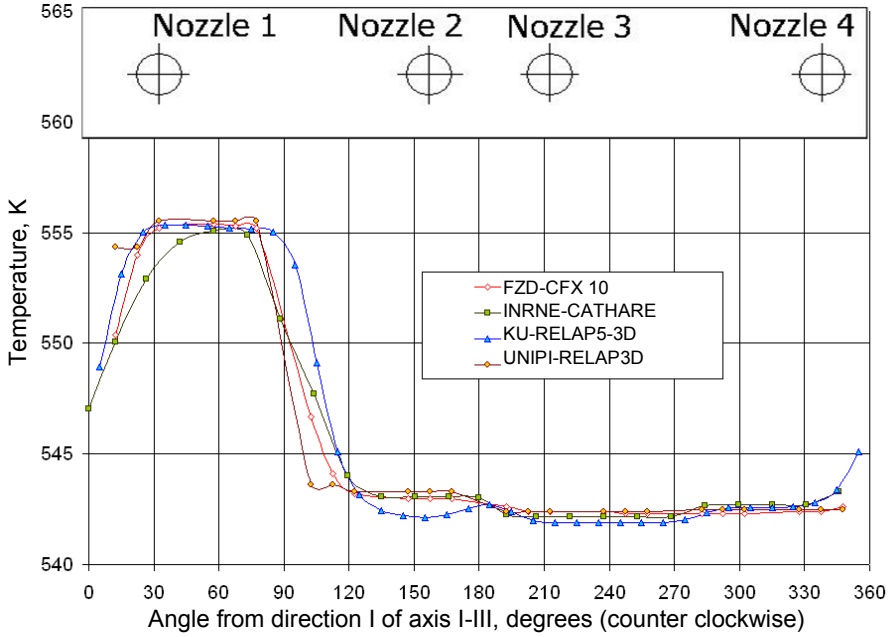

Figure 5.3: Downcomer velocity distribution at z = 5 800 mm

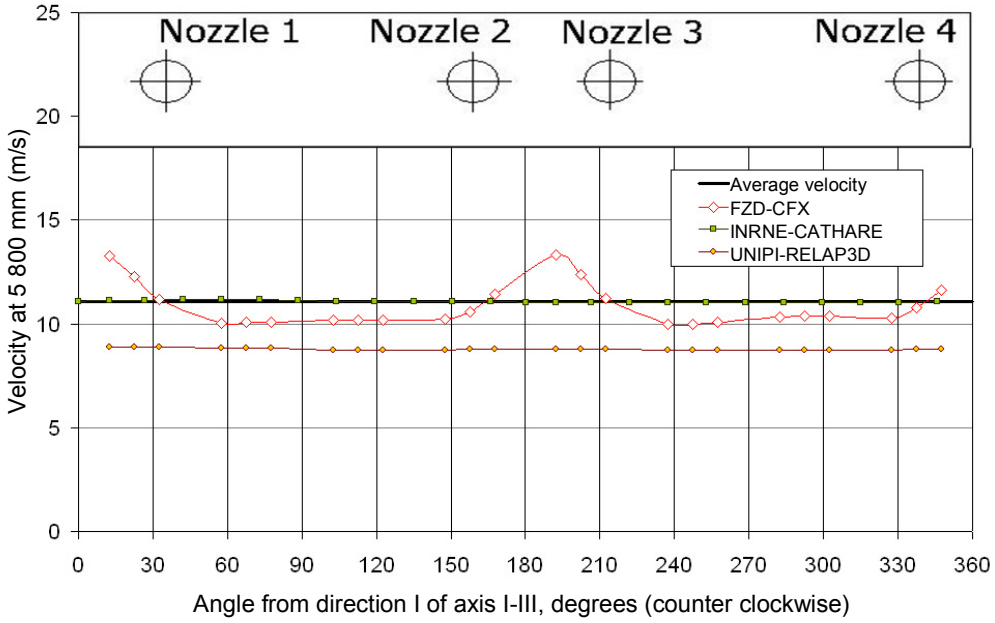

Figure 5.4: Downcomer velocity distribution at z = 2 500 mm

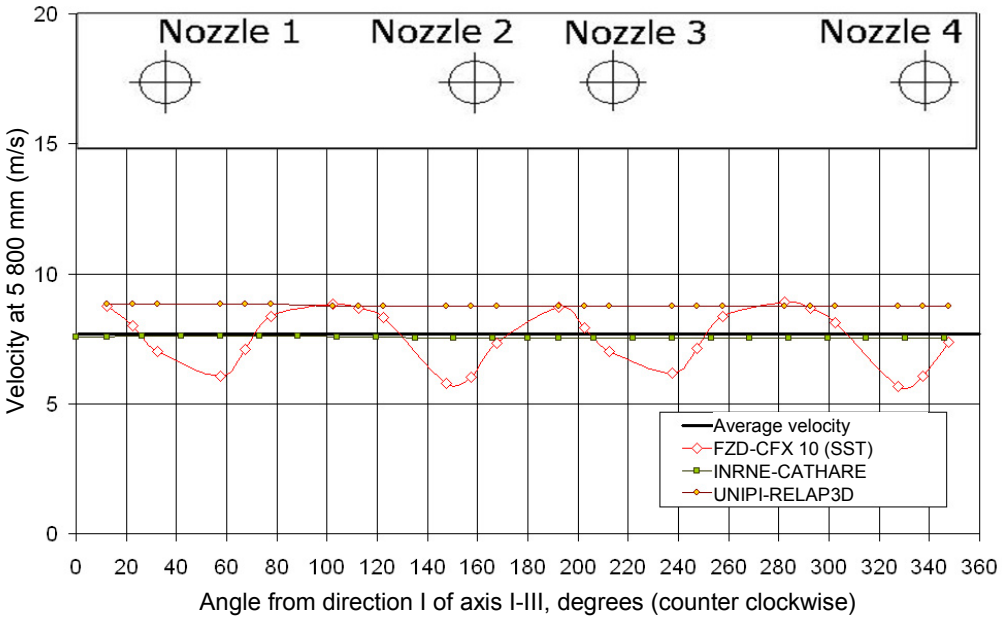

Figure 5.5: Plant-estimated data at the core inlet – angular turn of the loop #1 flow centre according to min $dT_k = T_{cold\ leg1} - T_{k,in\ core}$, k = 1,163

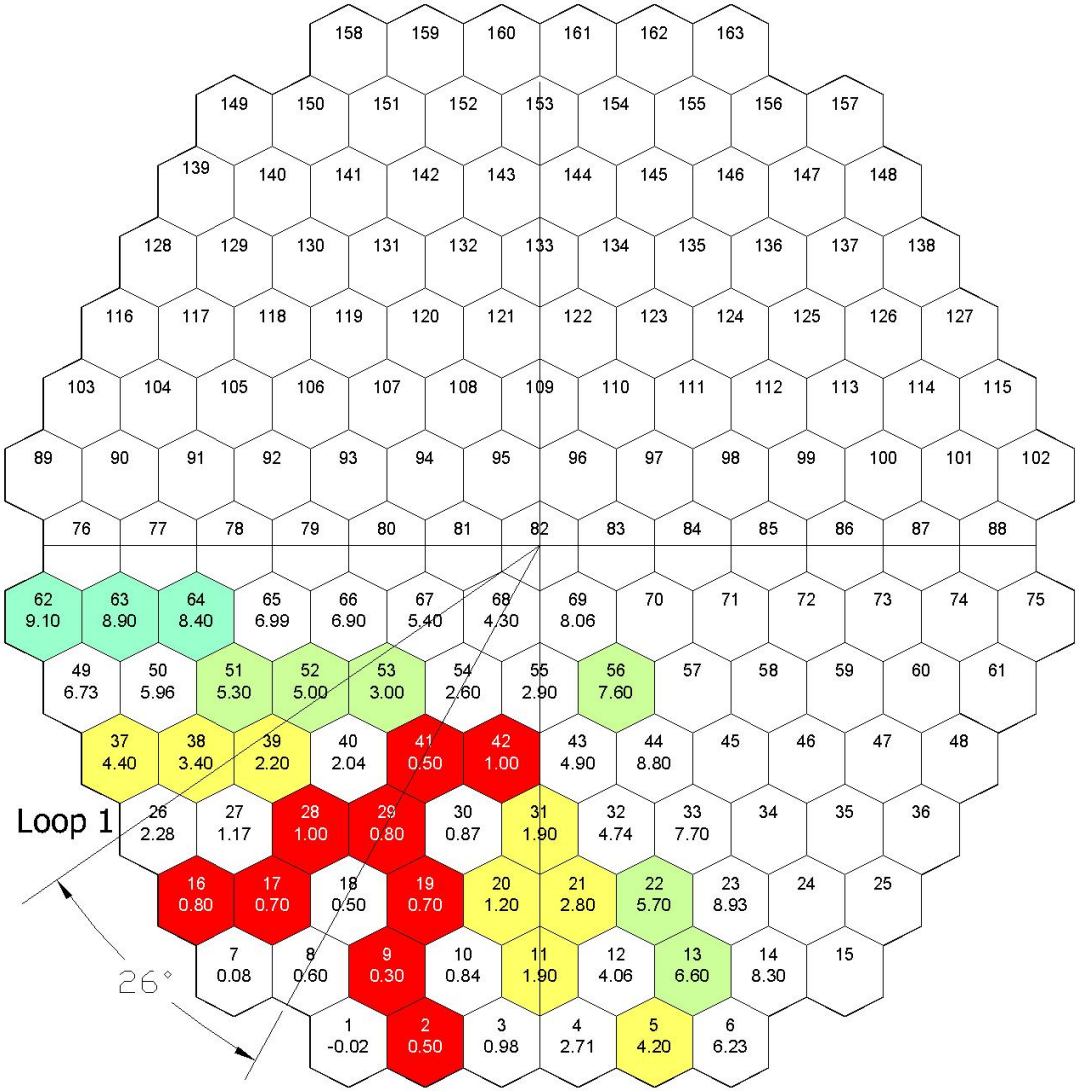

Figure 5.6: INRNE-CATHARE – angular turn of loop #1 flow centre

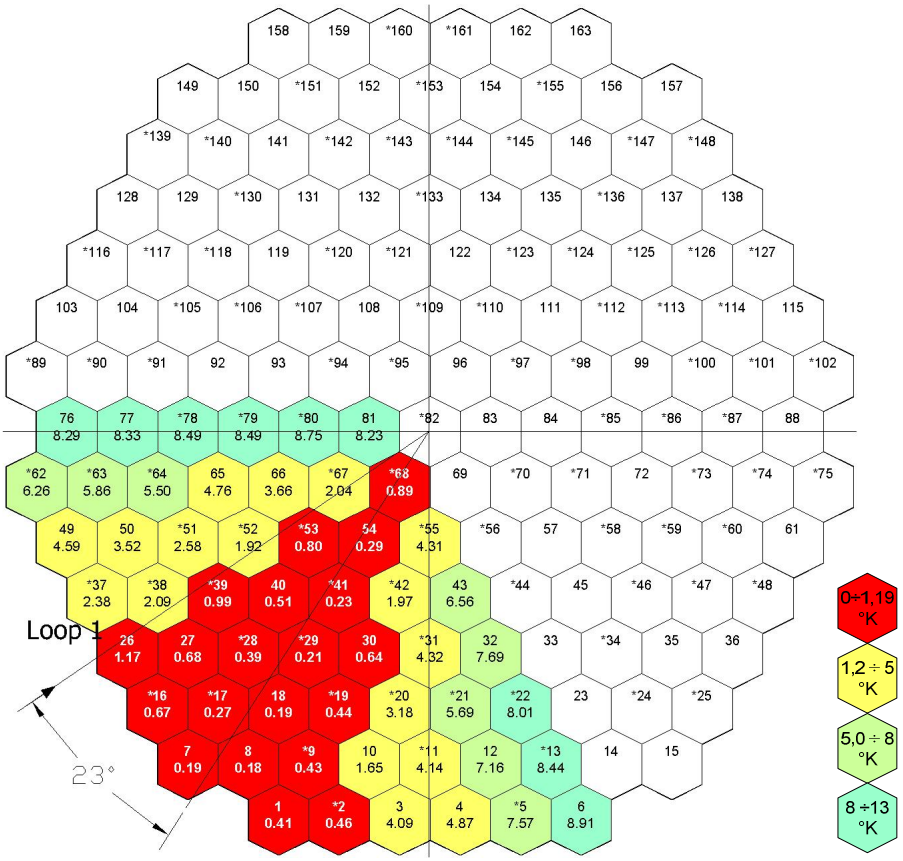

Figure 5.7: INRNE-CATHARE calculated core inlet temperatures in comparison with plant data

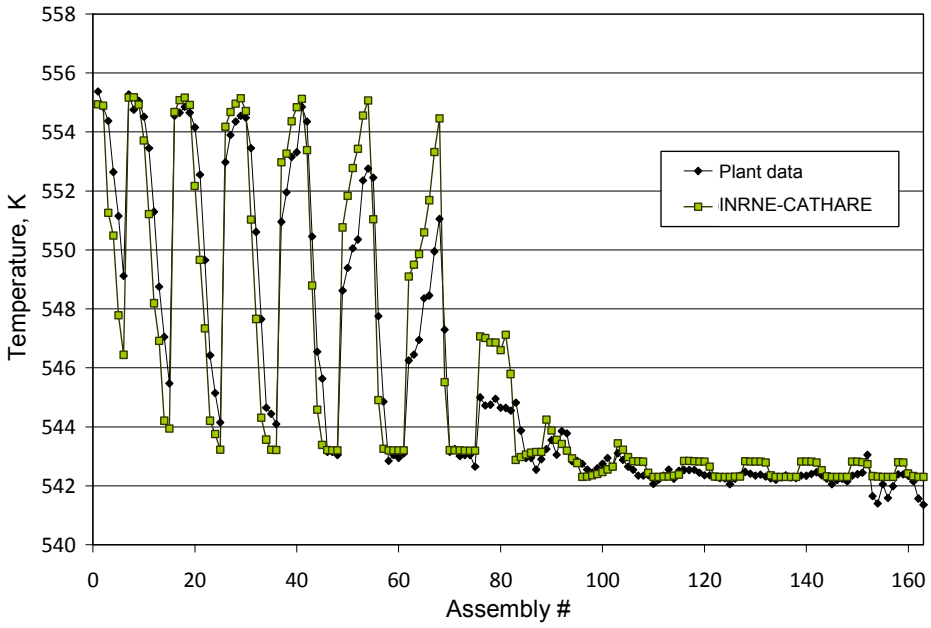

Figure 5.8: GRS/KI-ATHLET – angular turn of the loop #1 flow centre

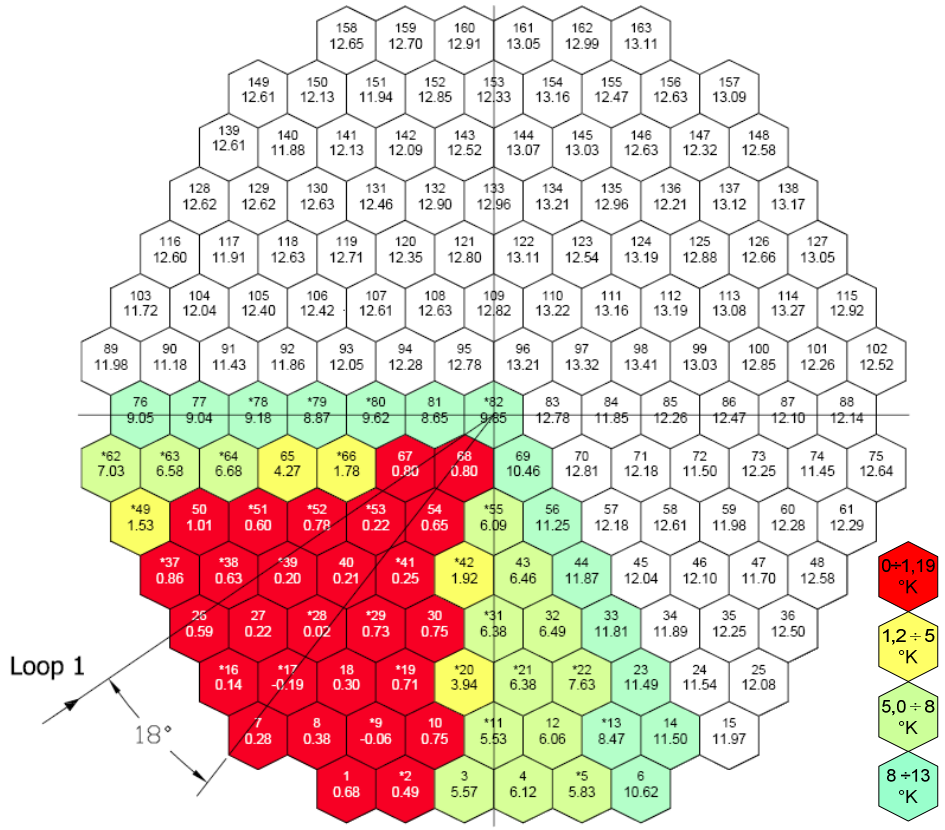

Figure 5.9: GRS/KI-ATHLET calculated core inlet temperatures in comparison with plant data

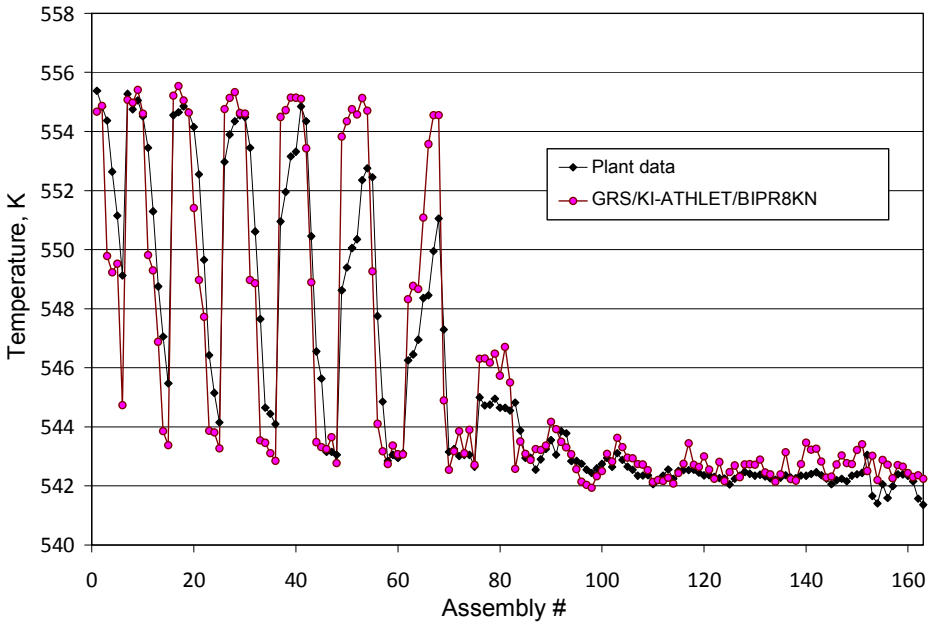

Figure 5.10: KU-RELAP3D – angular turn of the loop #1 flow centre

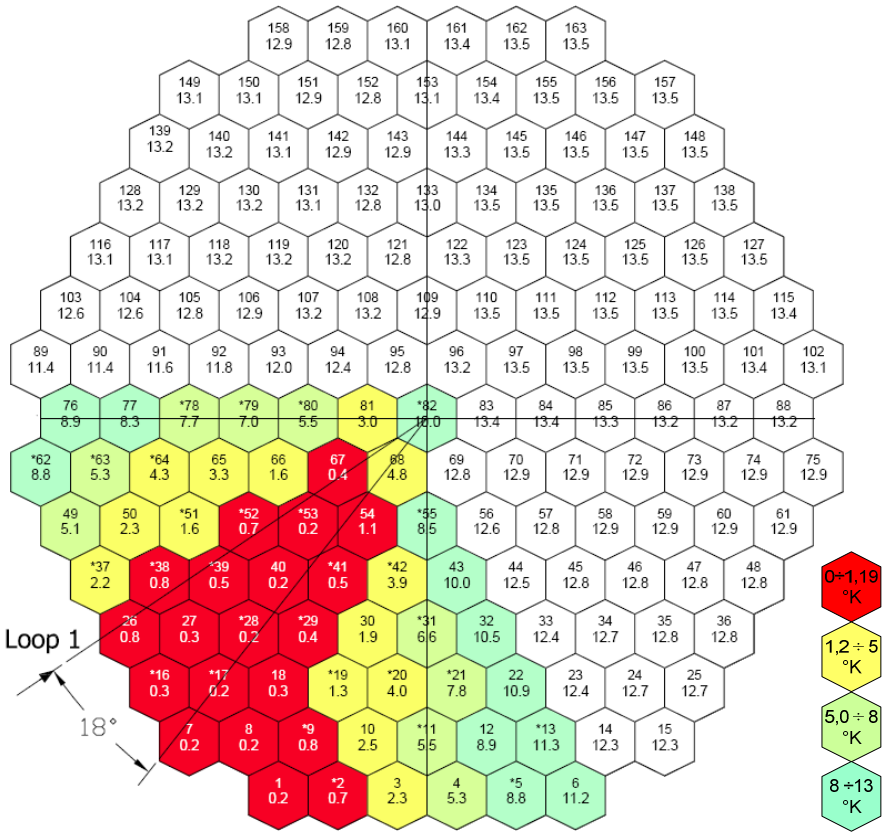

Figure 5.11: KU-RELAP3D calculated core inlet temperatures in comparison with plant data

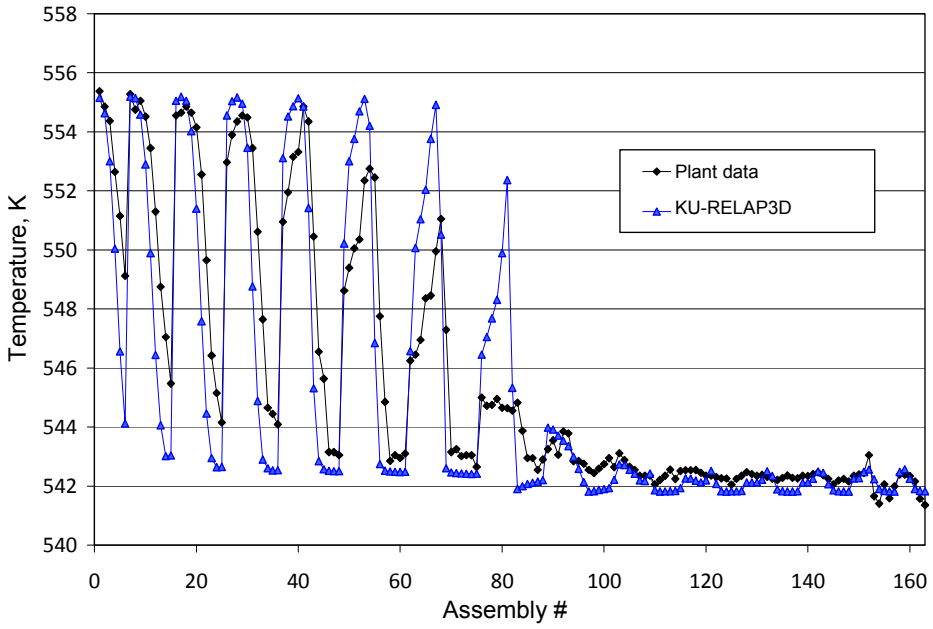

Figure 5.12: PSU-TRACE – angular turn of the loop #1 flow centre

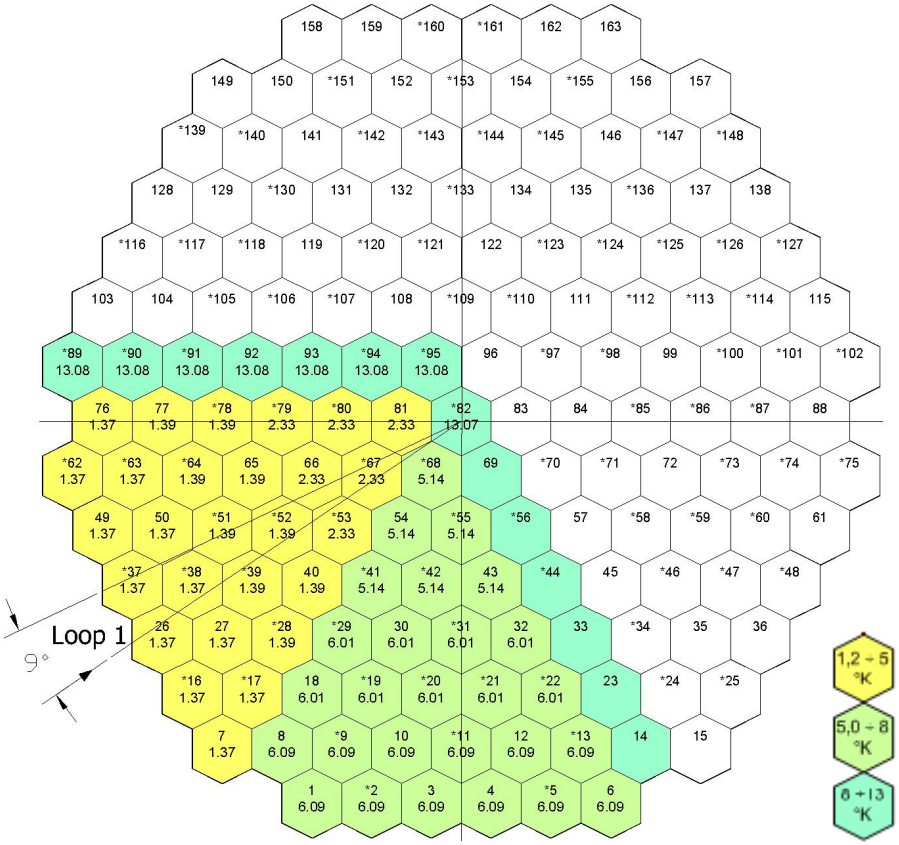

Figure 5.13: PSU-TRACE calculated core inlet temperatures in comparison with plant data

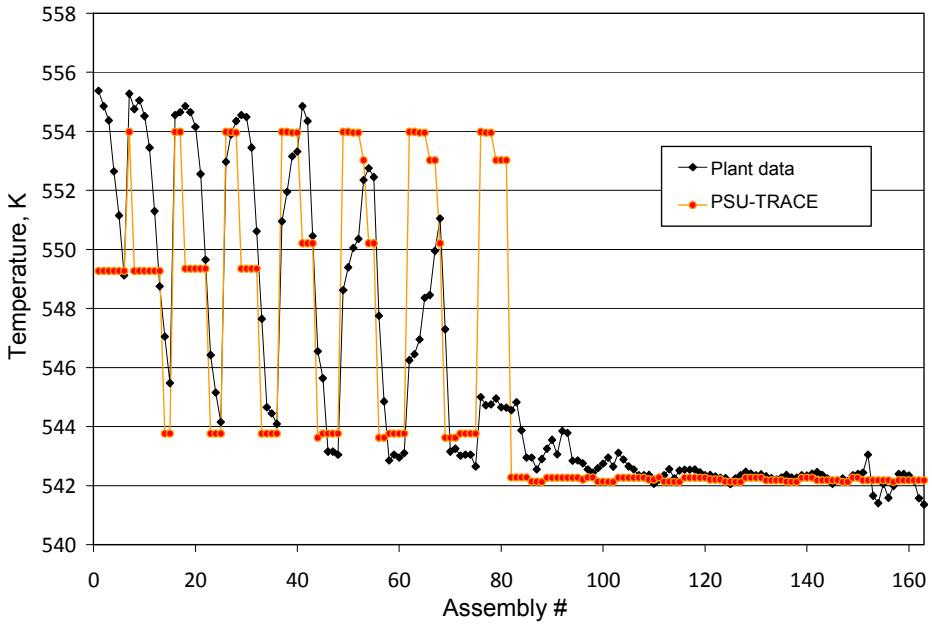

Figure 5.14: UNIPI-RELAP3D – angular turn of the loop #1 flow centre

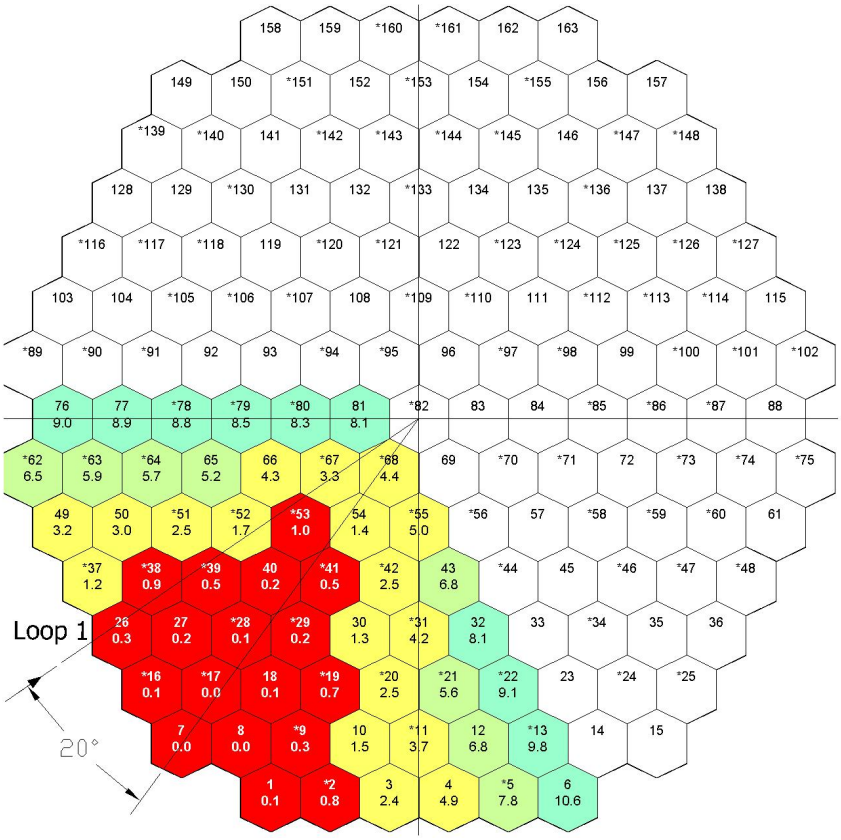

Figure 5.15: UNIPI-RELAP3D calculated core inlet temperatures in comparison with plant data

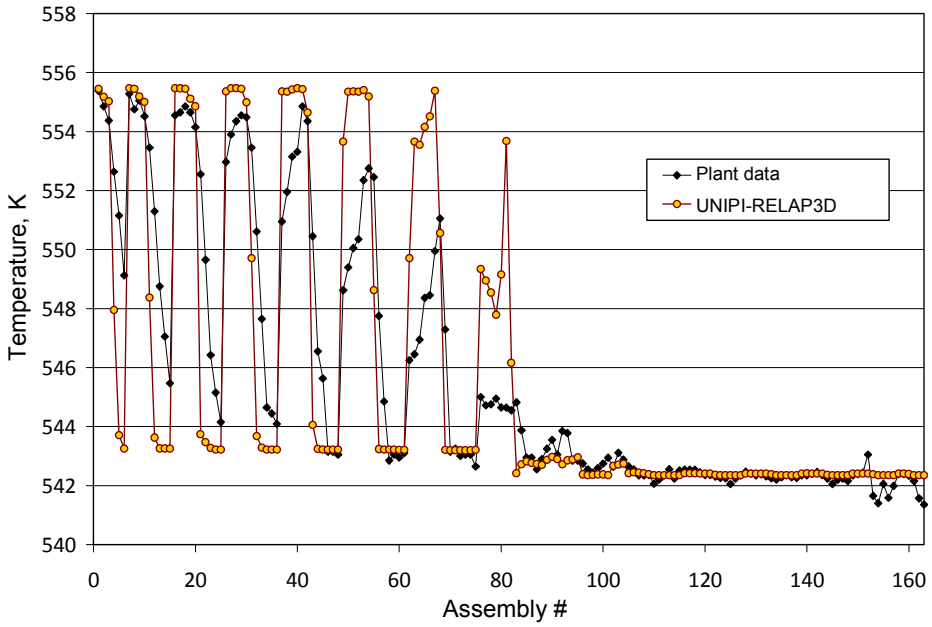

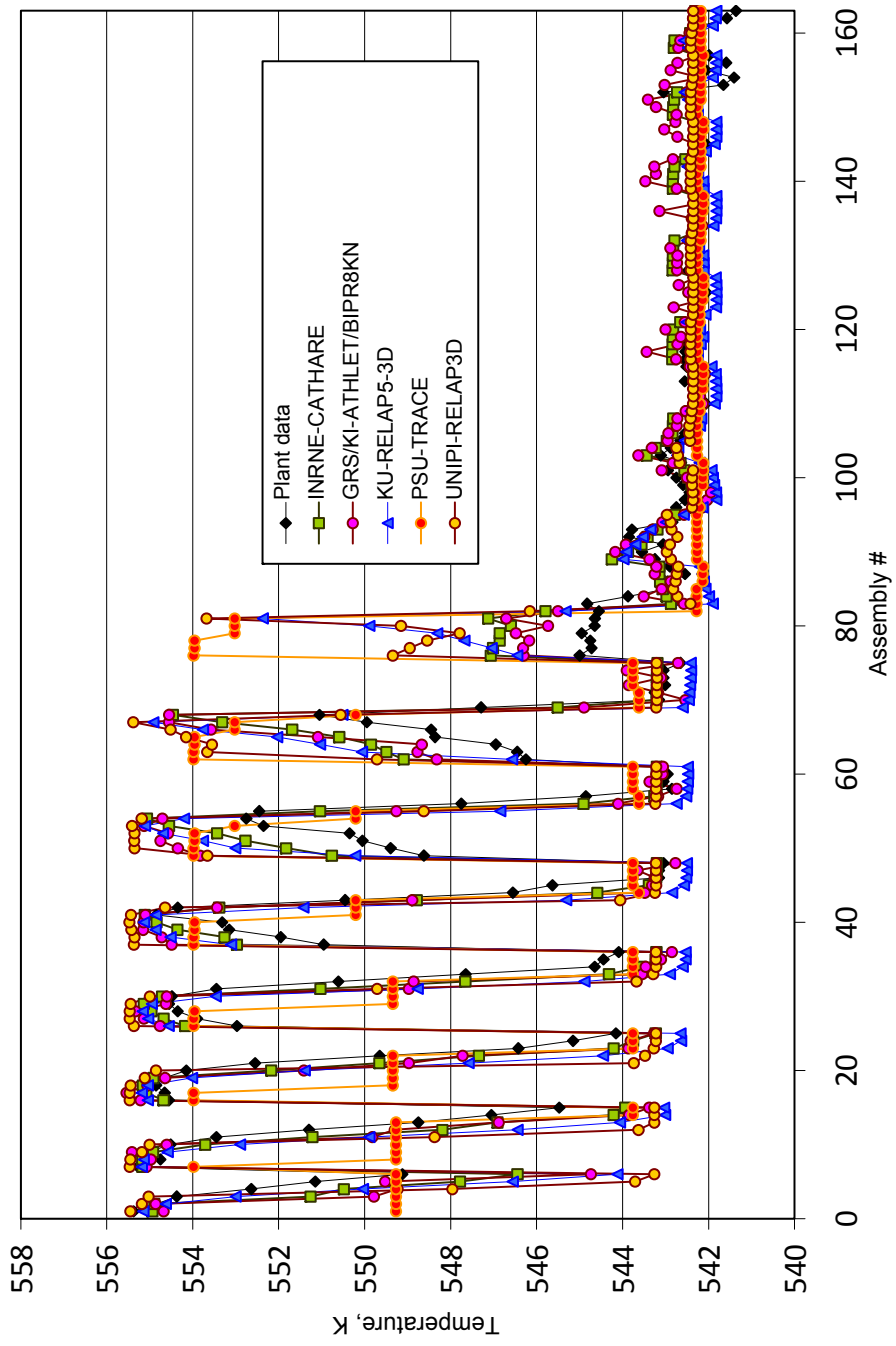

Figure 5.16: Assembly-by-assembly comparison of the core inlet coolant temperatures

Figure 5.17: Deviations of the computed to plant-estimated assembly inlet temperatures

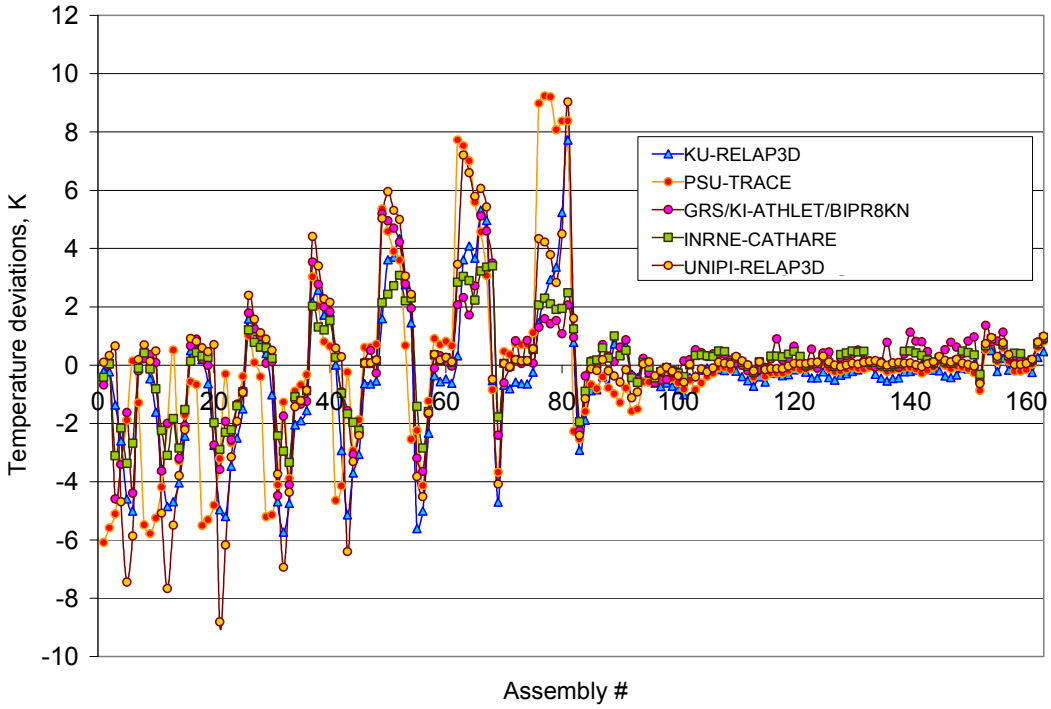

Table 5.4: Maximum and average deviations in the assembly inlet temperatures

95 instrumented assemblies	RELAP3D KU	TRACE PSU	ATHLET/BIPR8KN GRS-KI	RELAP3D UNIPI	CATHARE INRNE
Mean error (ME)	0.299	0.052	-0.252	-0.151	-0.219
Average in modulus error ME_{ABS}	1.304	1.616	1.043	1.348	0.835
Maximal in modulus error	5.61	9.21	4.70	8.81	3.41
Mean square error (MSE)	4.218	7.604	2.549	6.134	1.682

163 assemblies	RELAP3D KU	TRACE PSU	ATHLET/BIPR8KN GRS-KI	RELAP3D UNIPI	CATHARE INRNE
Mean error (ME)	0.399	0.175	-0.126		-0.091
Average in modulus error ME_{ABS}	1.404	1.737	1.136		0.936
Maximal in modulus error	7.72	9.24	5.20		3.41
Mean square error (MSE)	4.735	8.221	2.936		1.872

Figure 5.18: Temperature deviations from plant-estimated data at the core inlet – GRS/KI-ATHLET/BIPR8 and INRNE-CATHARE results (95 assemblies)

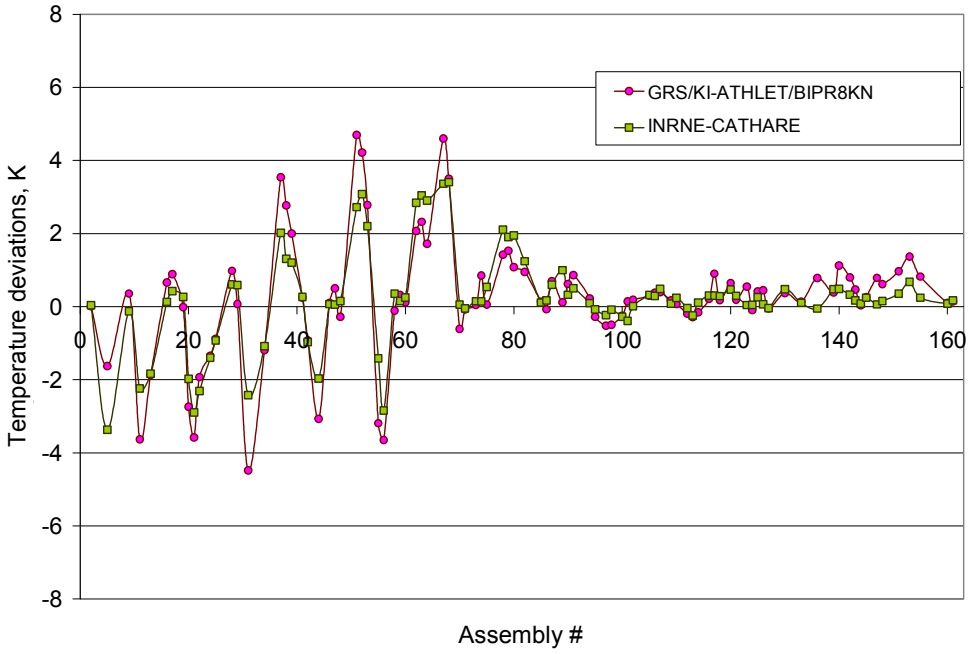

Figure 5.19: Temperature deviations from plant-estimated data at the core inlet – GRS/KI-ATHLET/BIPR8 and INRNE-CATHARE results (163 assemblies)

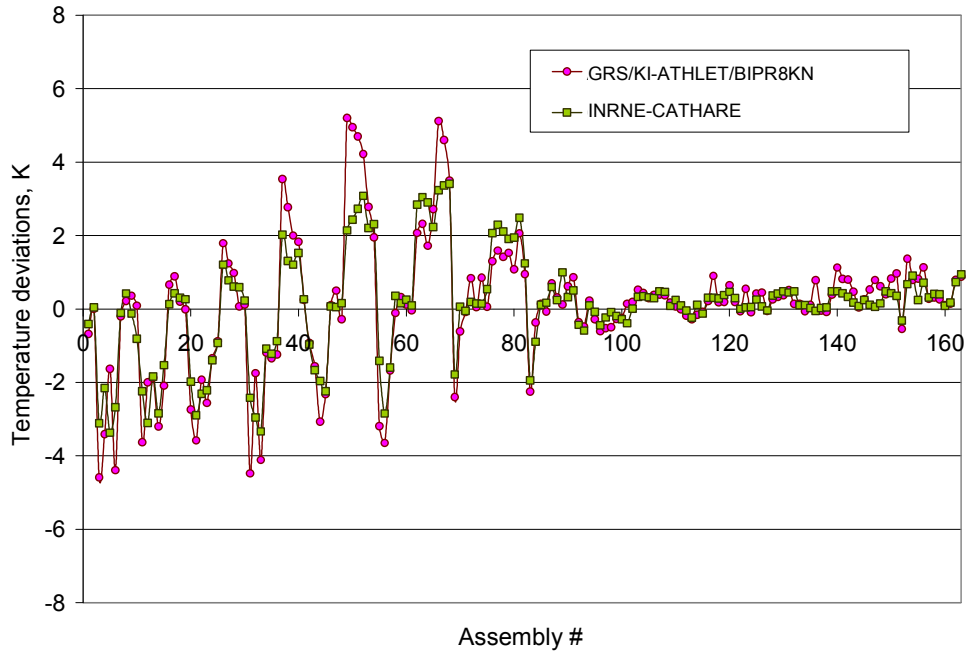

Figure 5.20: Temperature deviations from plant-estimated data at the core inlet – KU-RELAP3D and UNIPI-RELAP3D results (95 assemblies)

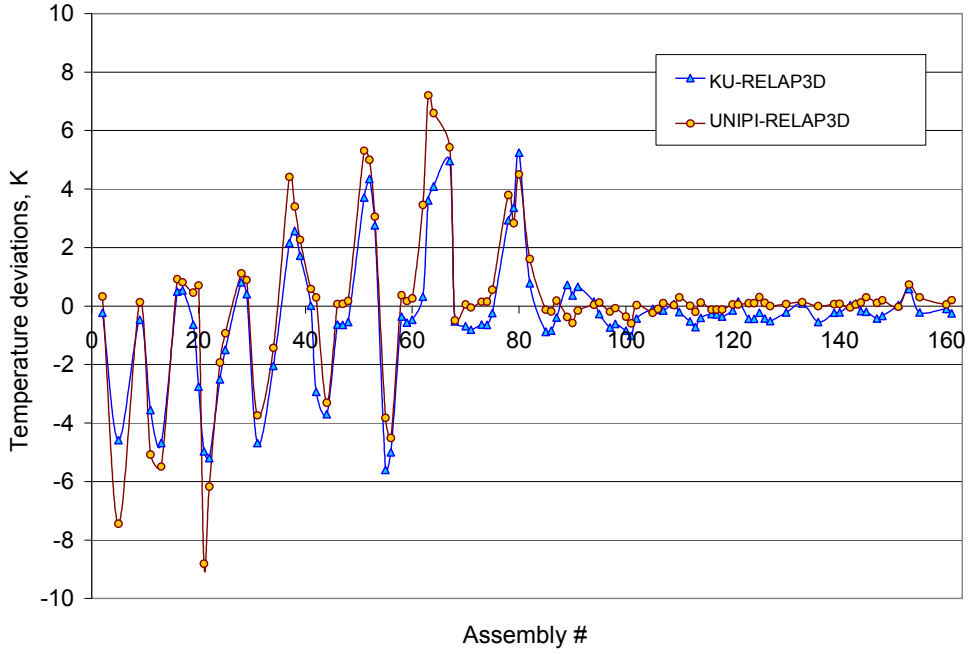

Figure 5.21: Temperature deviations from plant-estimated data at the core inlet – KU-RELAP3D and UNIPI-RELAP3D results (163 assemblies)

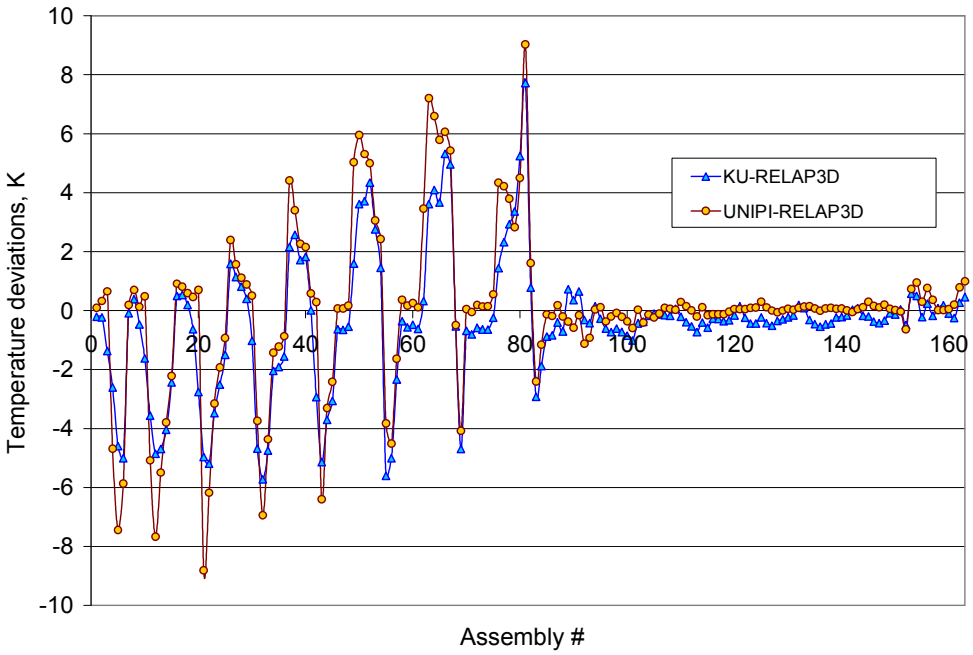

Figure 5.22: Temperature deviations from plant-estimated data at the core inlet – KU-RELAP3D and INRNE-CATHARE results (95 assemblies)

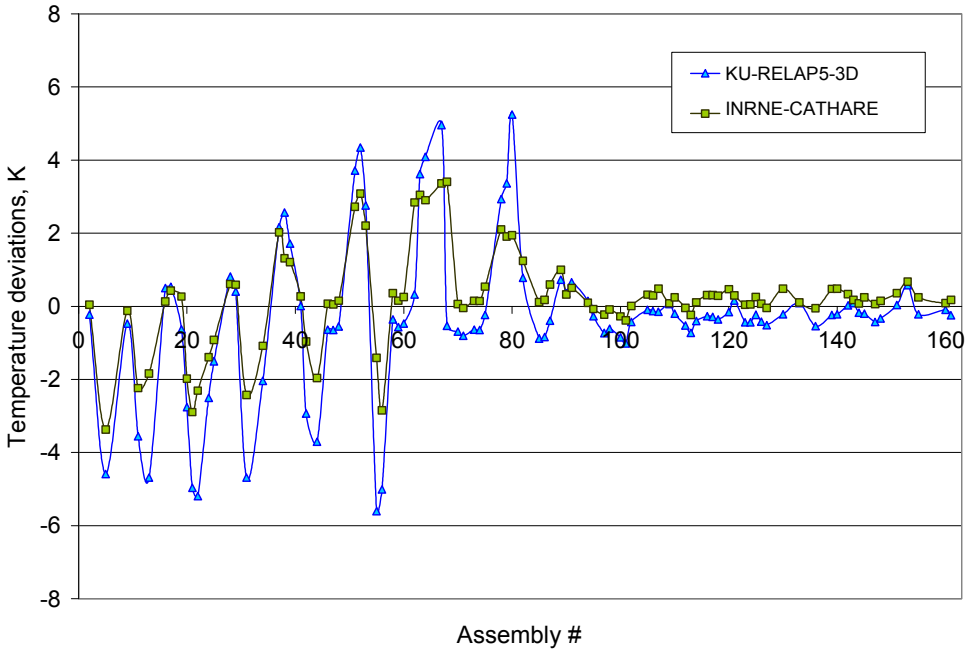

Figure 5.23: Temperature deviations from plant-estimated data at the core inlet – KU-RELAP3D and INRNE-CATHARE results (163 assemblies)

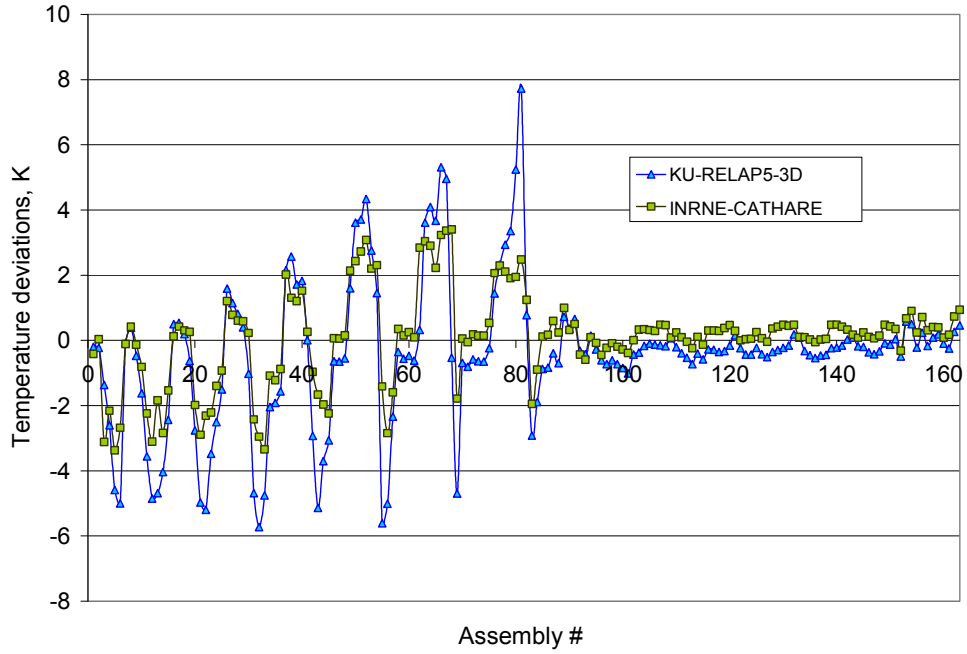

Figure 5.24: Temperature deviations from plant-estimated data at the core inlet – PSU-TRACE and INRNE-CATHARE results (95 assemblies)

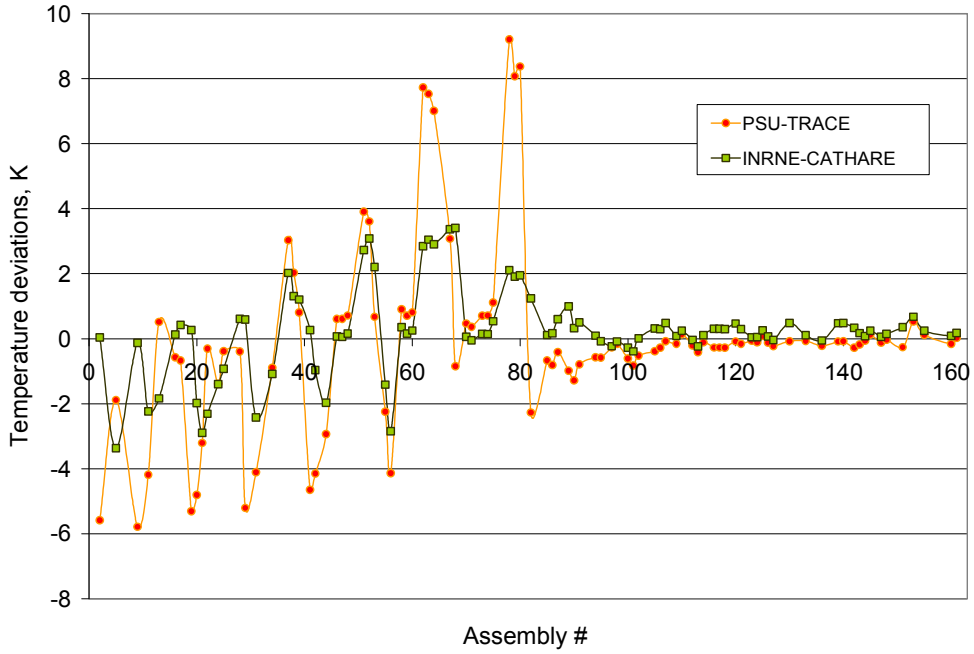

Figure 5.25: Temperature deviations from plant-estimated data at the core inlet – PSU-TRACE and INRNE-CATHARE results (163 assemblies)

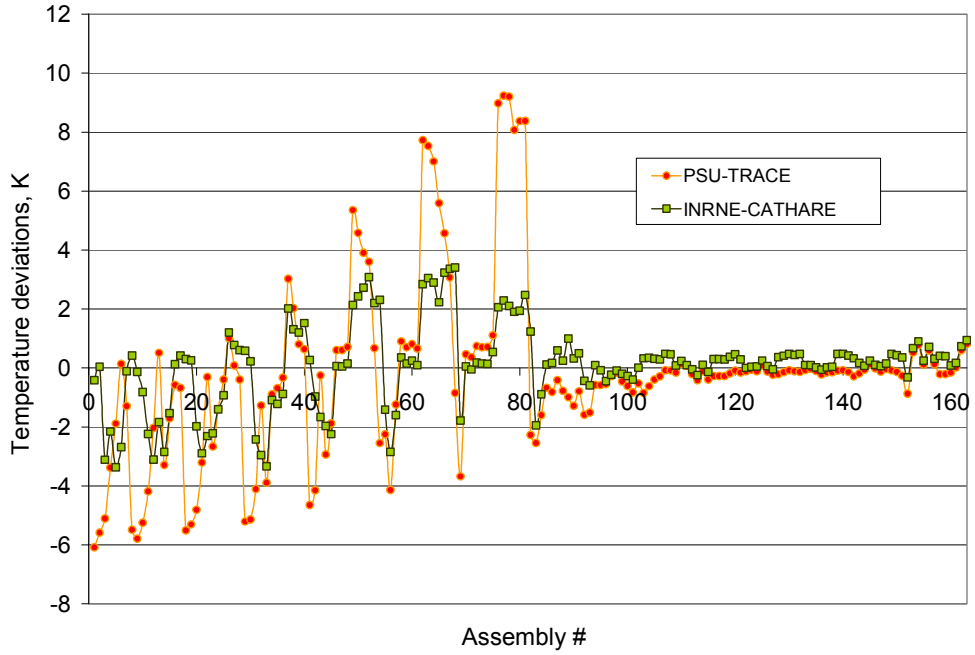

Figure 5.26: Temperature deviations from plant-estimated data at the core inlet – INRNE-CATHARE and UNIPI-RELAP3D results (95 assemblies)

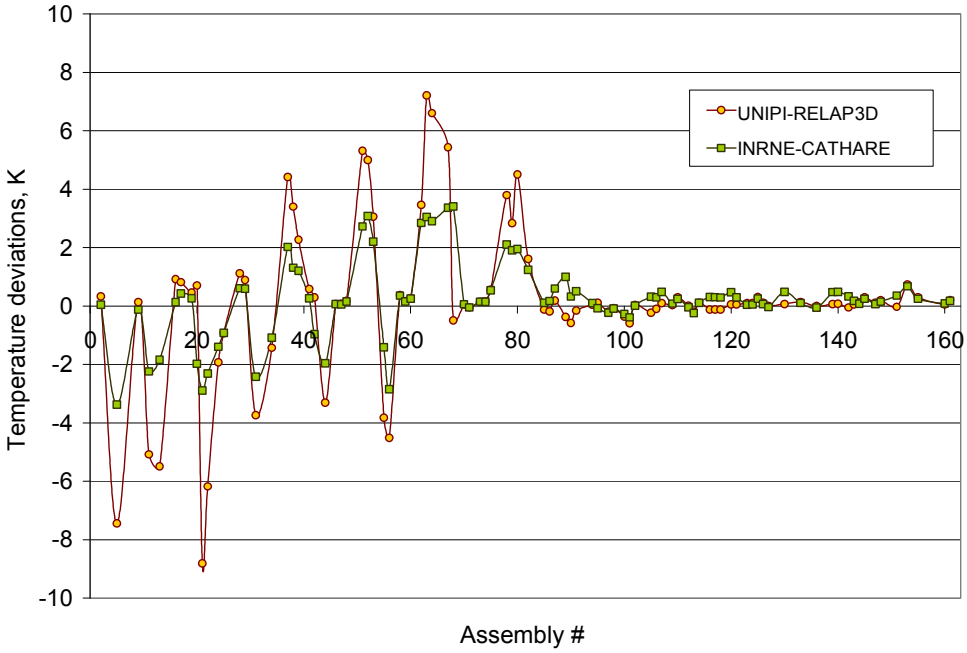

Figure 5.27: Temperature deviations from plant-estimated data at the core inlet – INRNE-CATHARE and UNIPI-RELAP3D results (163 assemblies)

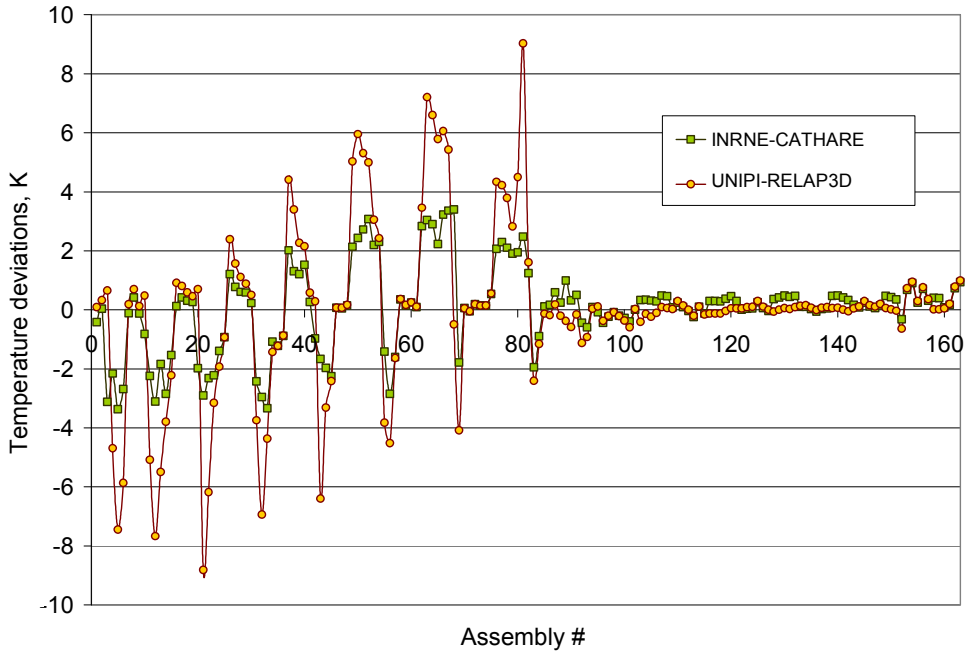

Figure 5.28: Temperature deviations from plant-estimated data at the core inlet – KU-RELAP3D and CEA-TRIO_U results (95 assemblies)

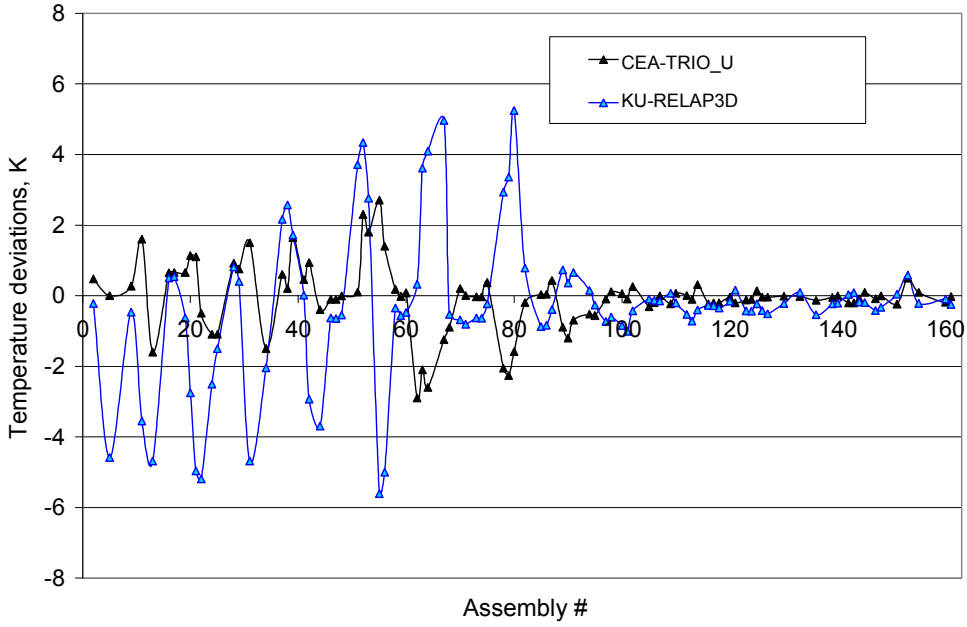

Figure 5.29: Temperature deviations from plant-estimated data at the core inlet – KU-RELAP3D and CEA-TRIO_U results (163 assemblies)

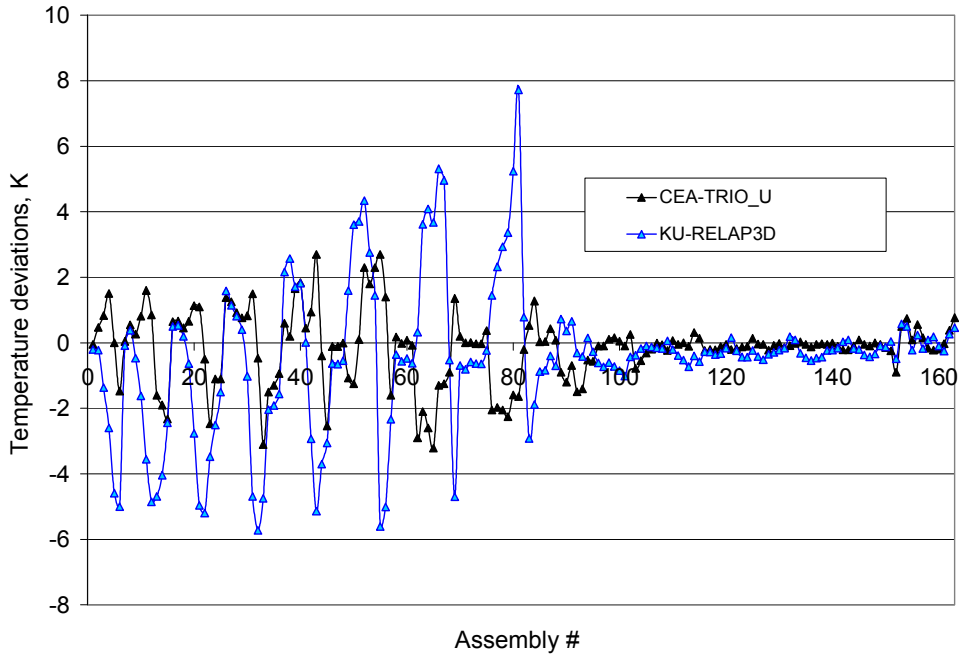

Figure 5.30: Temperature deviations from plant-estimated data at the core inlet – GRS/KI-ATHLET/BIPR8 and CEA-TRIO_U results (95 assemblies)

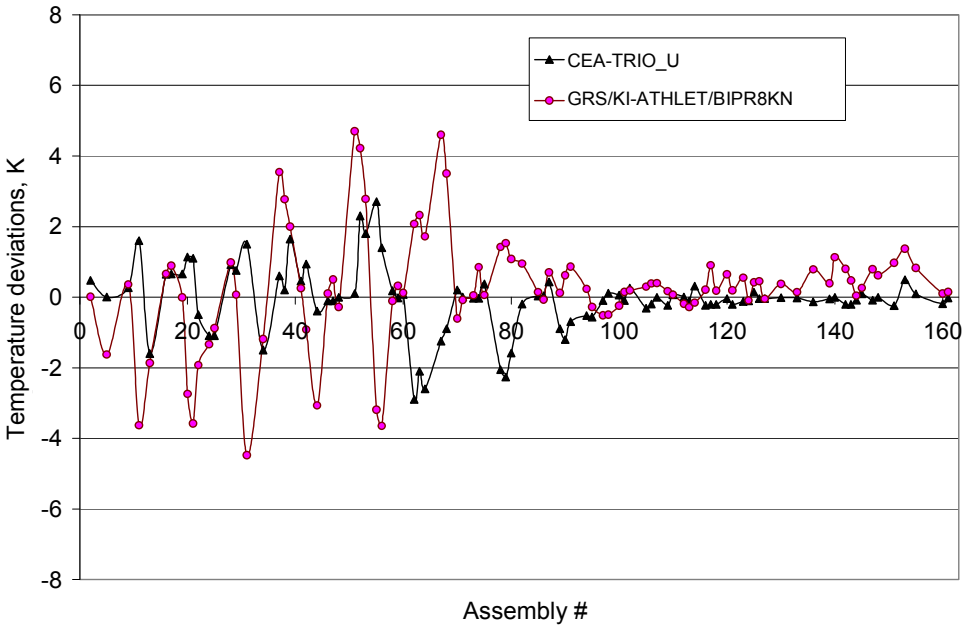

Figure 5.31: Temperature deviations from plant-estimated data at the core inlet – GRS/KI-ATHLET/BIPR8 and CEA-TRIO_U results (163 assemblies)

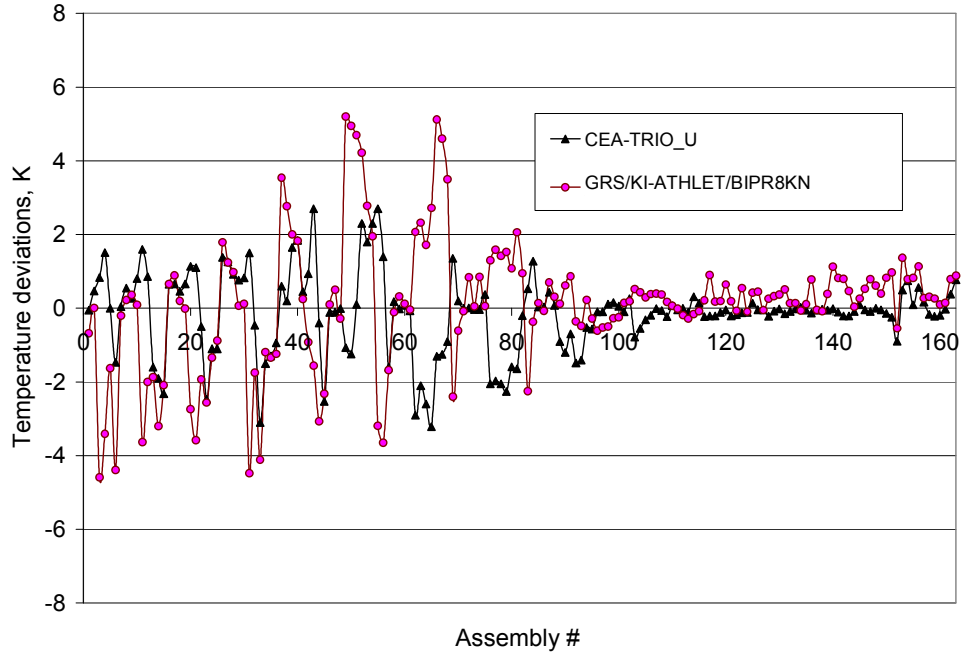

Figure 5.32: Temperature deviations from plant-estimated data at the core inlet – PSU-TRACE and CEA-TRIO_U results (95 assemblies)

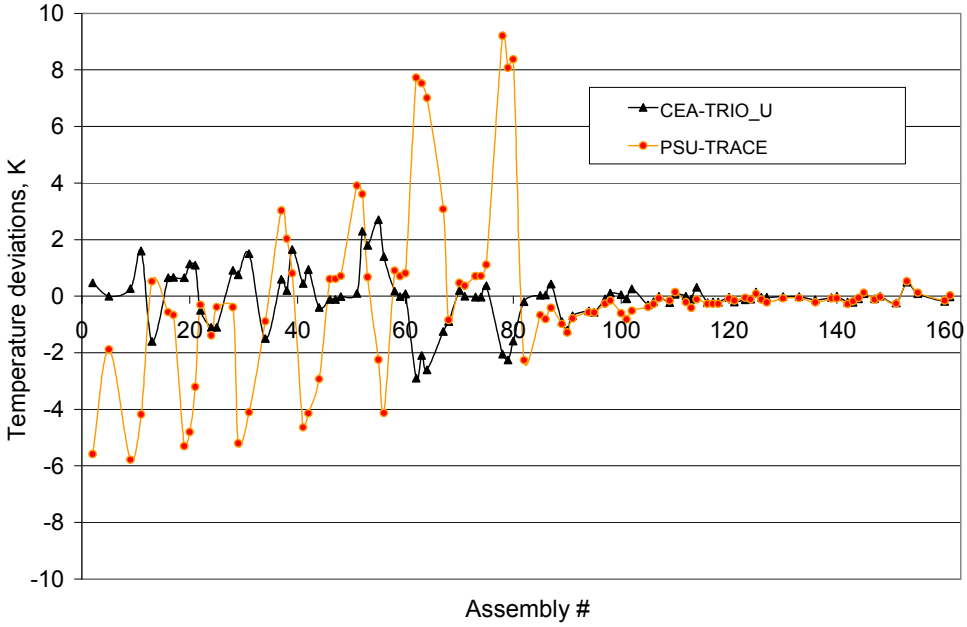

Figure 5.33: Temperature deviations from plant-estimated data at the core inlet – PSU-TRACE and CEA-TRIO_U results (163 assemblies)

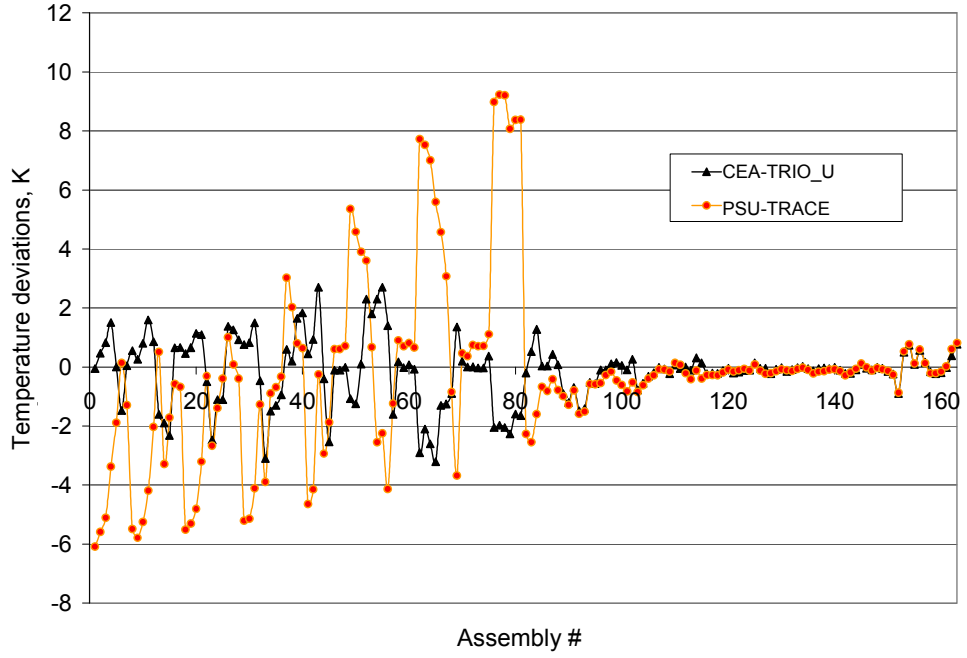

Figure 5.34: Temperature deviations from plant-estimated data at the core inlet – INRNE-CATHARE and CEA-TRIO_U results (95 assemblies)

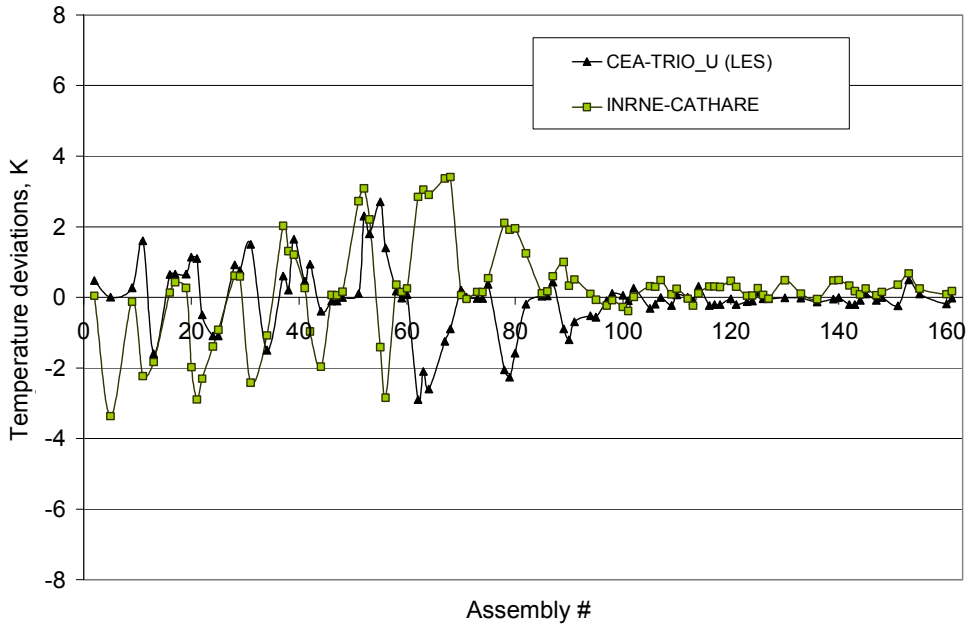

Figure 5.35: Temperature deviations from plant-estimated data at the core inlet – INRNE-CATHARE and CEA-TRIO_U results (163 assemblies)

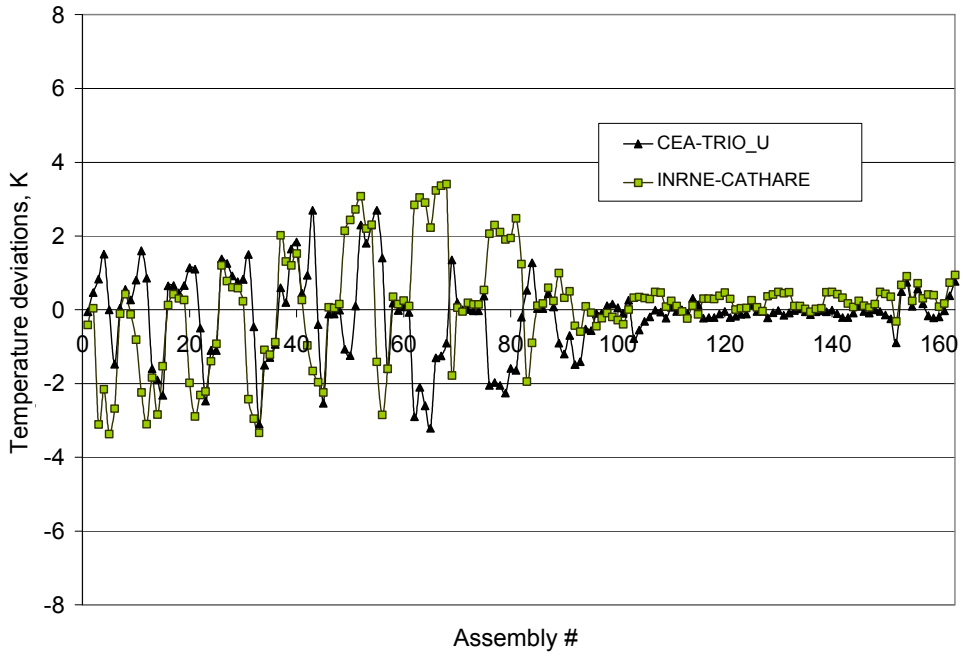

Figure 5.36: Temperature deviations from plant-estimated data at the core inlet – UNIPI-RELAP3D and CEA-TRIO_U results (95 assemblies)

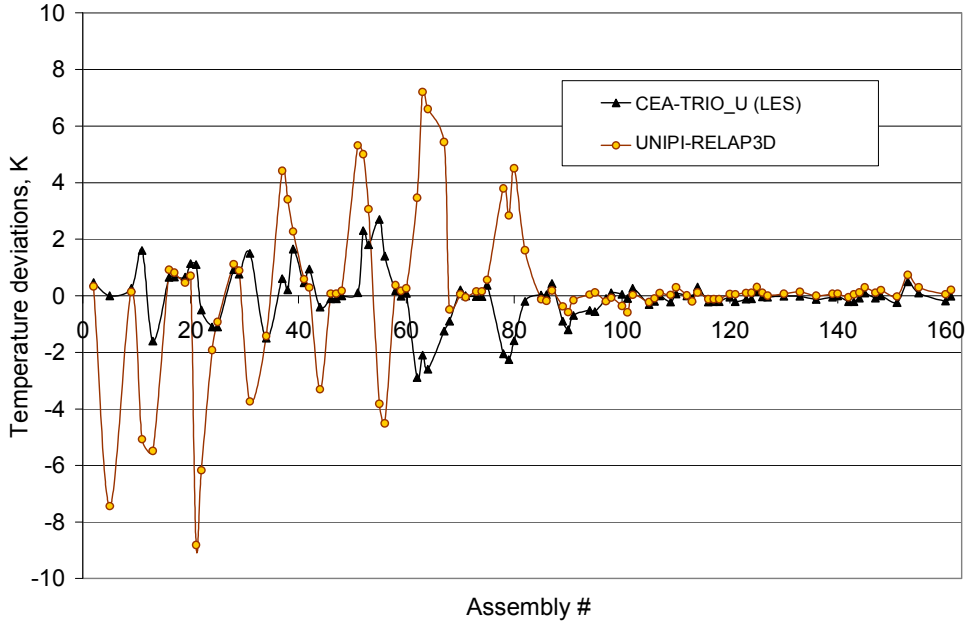

Figure 5.37: Temperature deviations from plant-estimated data at the core inlet – UNIPI-RELAP3D and CEA-TRIO_U results (163 assemblies)

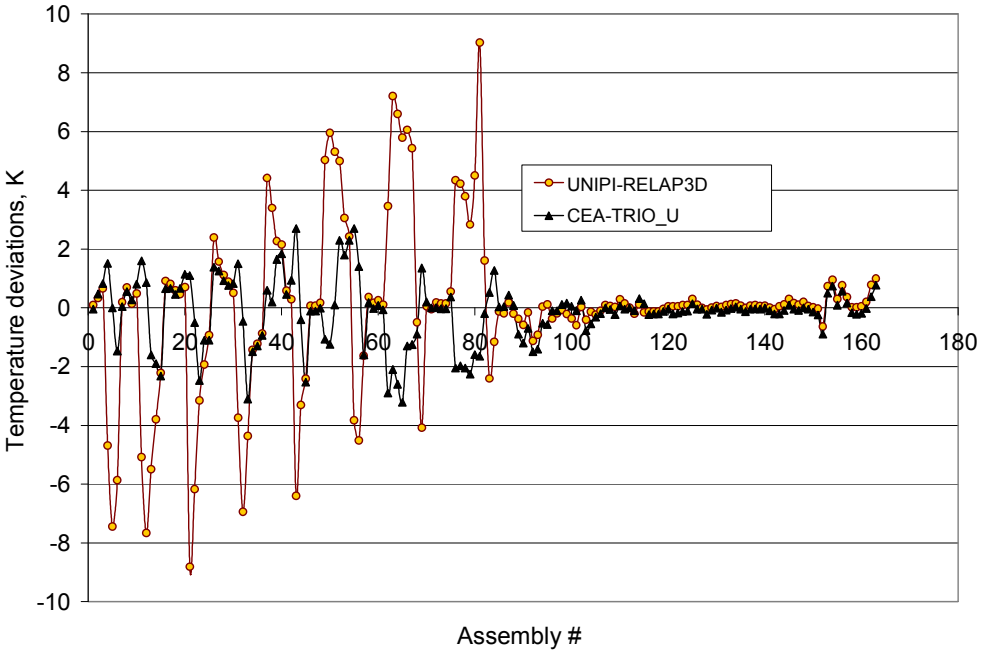

Figure 5.38: Temperature deviations from plant-estimated data at the core inlet – INRNE-CATHARE and BUTE CFX 10 SST results (95 assemblies)

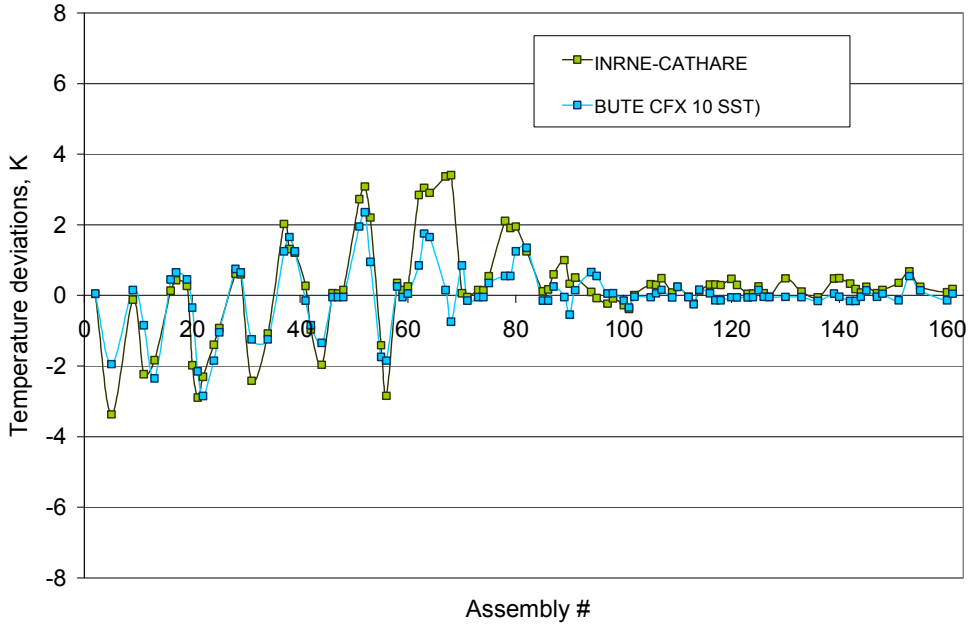

Figure 5.39: Temperature deviations from plant-estimated data at the core inlet – INRNE-CATHARE and BUTE CFX 10 SST results (163 assemblies)

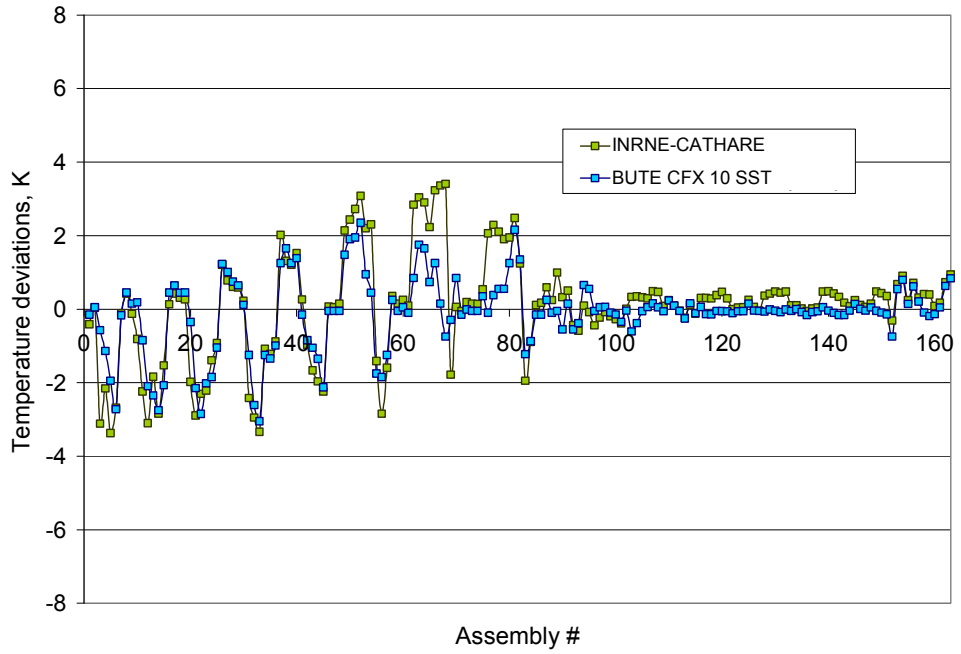

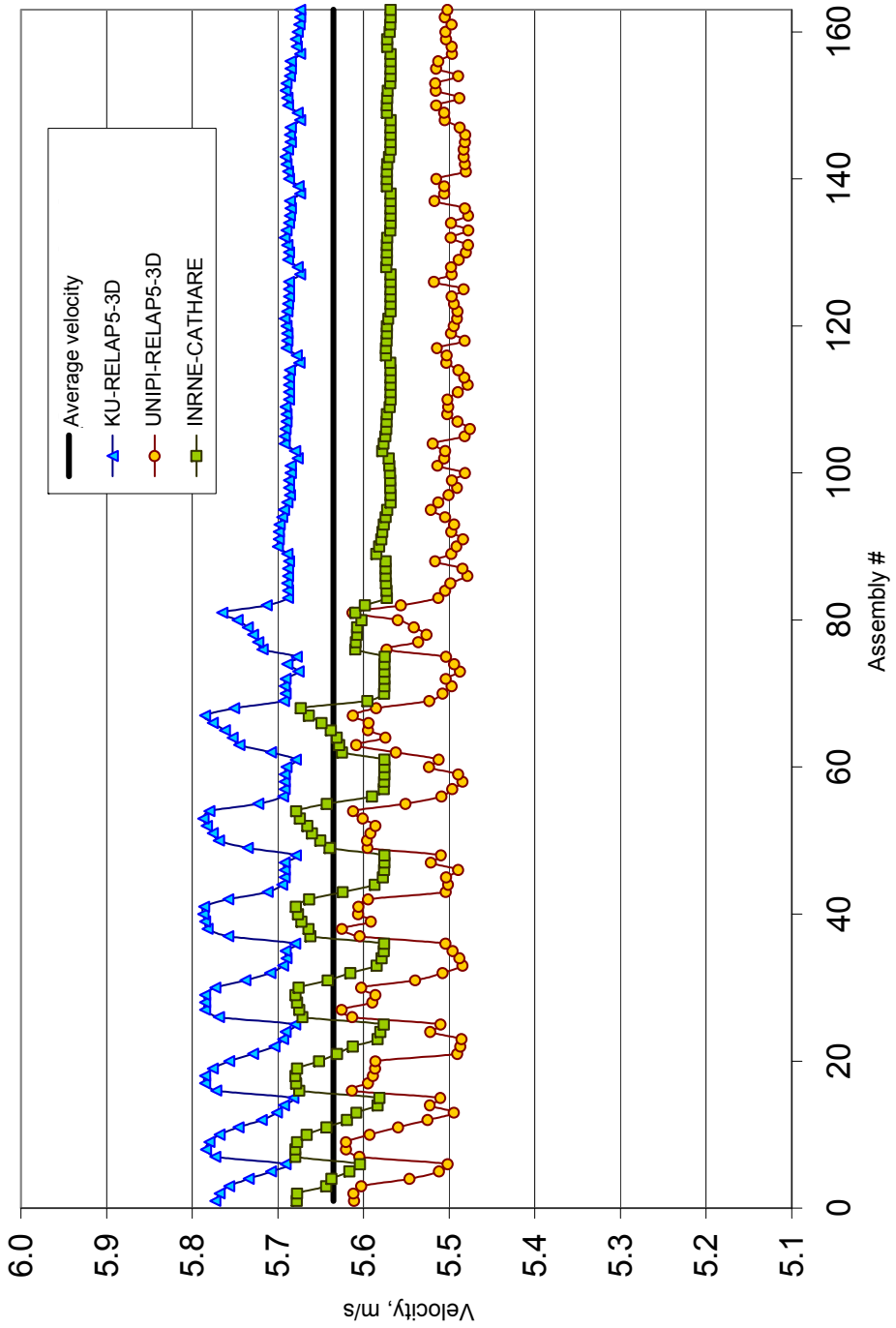

Figure 5.40: Assembly-by-assembly core inlet velocities

Figure 5.41: Time history of hot leg 1 temperature

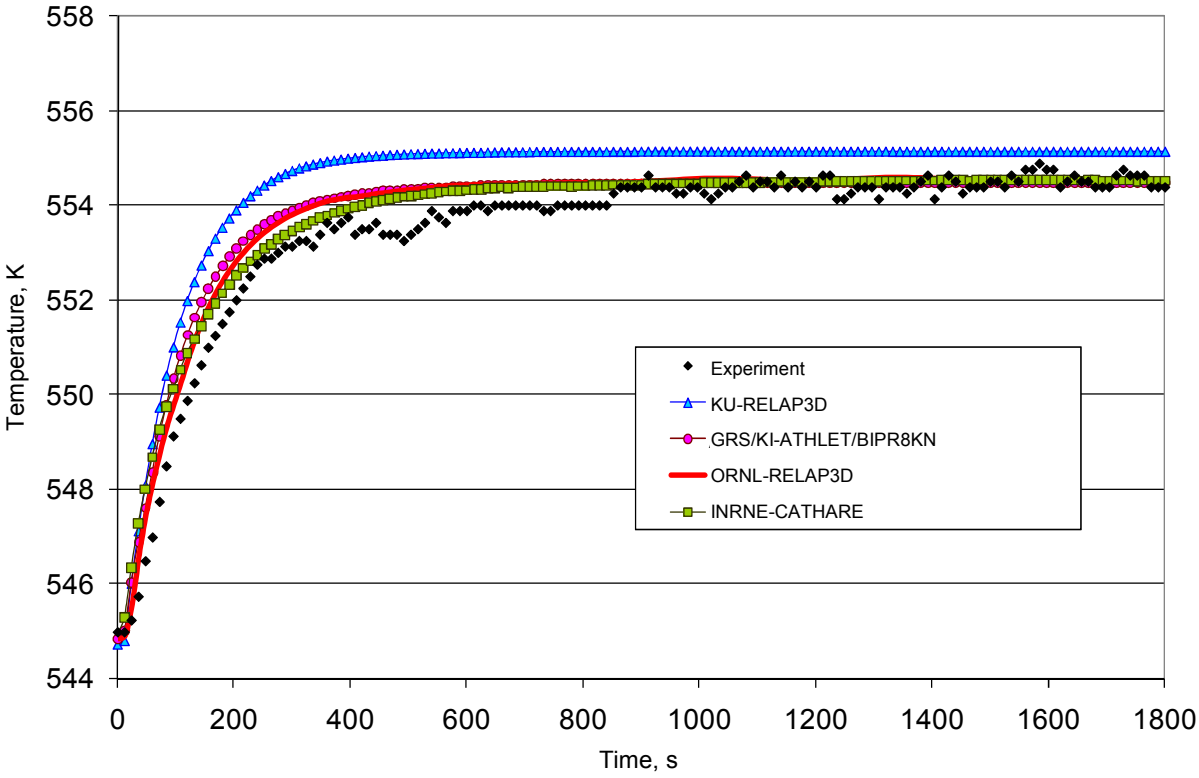

Table 5.5: Hot leg 1 temperature deviations and FOM

Participant	ME	VE	MSE	FOM_{ME}	FOM_{VE}	FOM_{MSE}
INRNE	-0.29465	0.13024	0.21620	0.77241	0.88476	0.82223
GRS/KI	-0.36404	0.19655	0.32778	0.73312	0.83573	0.75314
KU	-1.04475	0.24204	1.33195	0.48906	0.80513	0.42883
ORNL	-0.43532	0.09652	0.28527	0.69671	0.991197	0.77805

Figure 5.42: Time history of hot leg 2 temperature

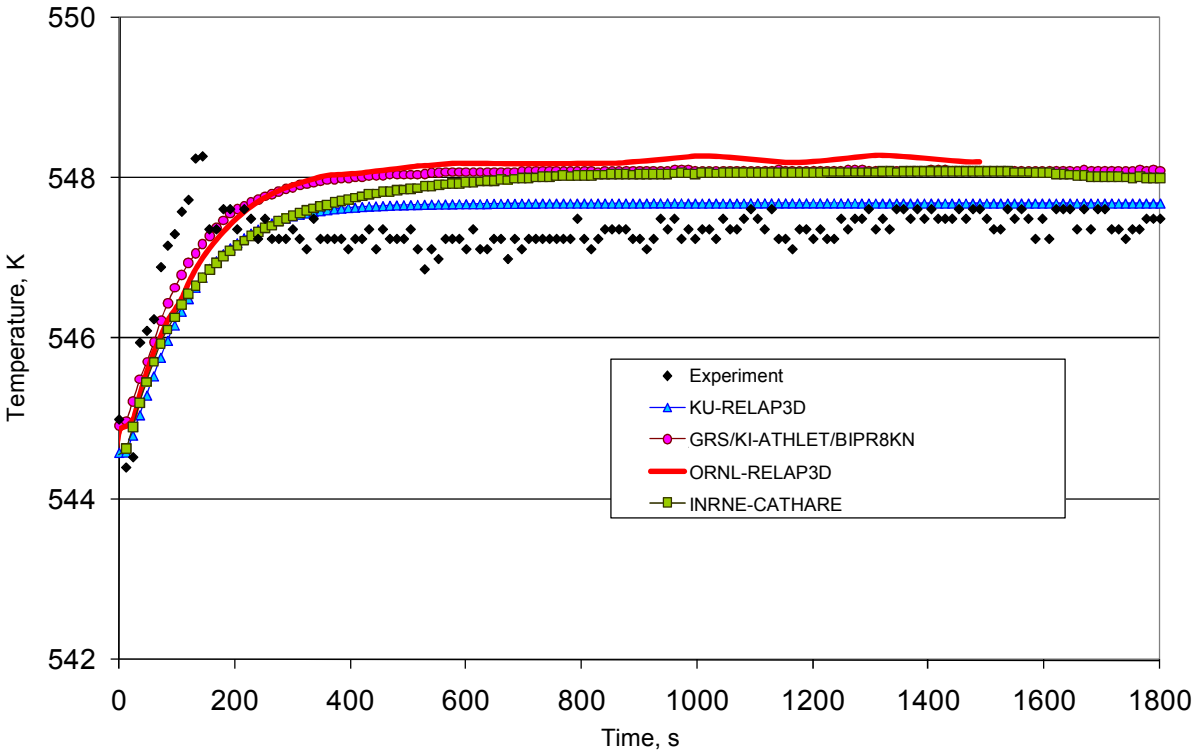

Table 5.6: Hot leg 2 temperature deviations and FOM

Participant	ME	VE	MSE	FOM_{ME}	FOM_{VE}	FOM_{MSE}
INRNE	-0.44919	0.25127	0.45137	0.69004	0.79919	0.68900
GRS/KI	-0.57255	0.17005	0.49674	0.63591	0.85466	0.66812
KU	-0.17592	0.17822	0.20799	0.85040	0.84873	0.82782
ORNL	-0.63813	0.28525	0.69023	0.61045	0.77806	0.59163

Figure 5.43: Time history of hot leg 3 temperature

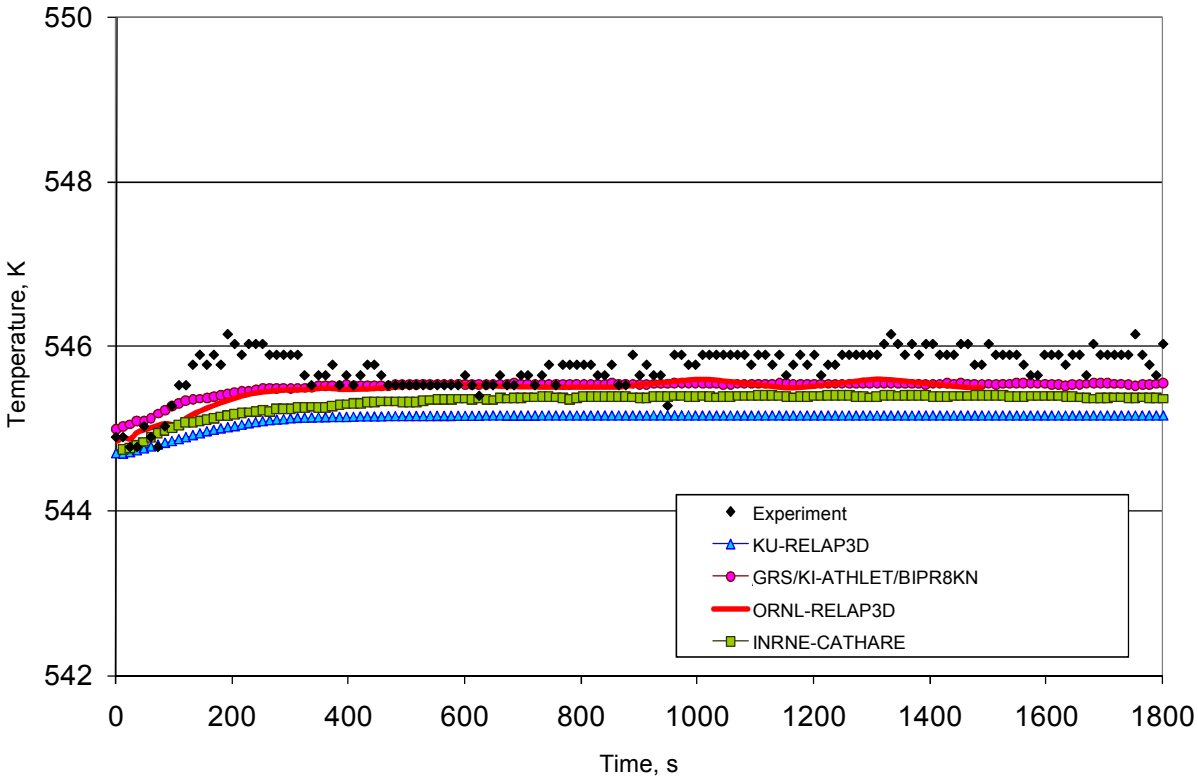

Table 5.7: Hot leg 3 temperature deviations and FOM

Participant	ME	VE	MSE	FOM_{ME}	FOM_{VE}	FOM_{MSE}
INRNE	0.41896	0.04182	0.21706	0.70474	0.95986	0.82165
GRS/KI	0.22477	0.04302	0.09326	0.81648	0.95875	0.91470
KU	0.61653	0.04569	0.42550	0.61861	0.95631	0.70151
ORNL	0.24953	0.04249	0.10442	0.80030	0.95924	0.90545

Figure 5 44: Time history of hot leg 4 temperature

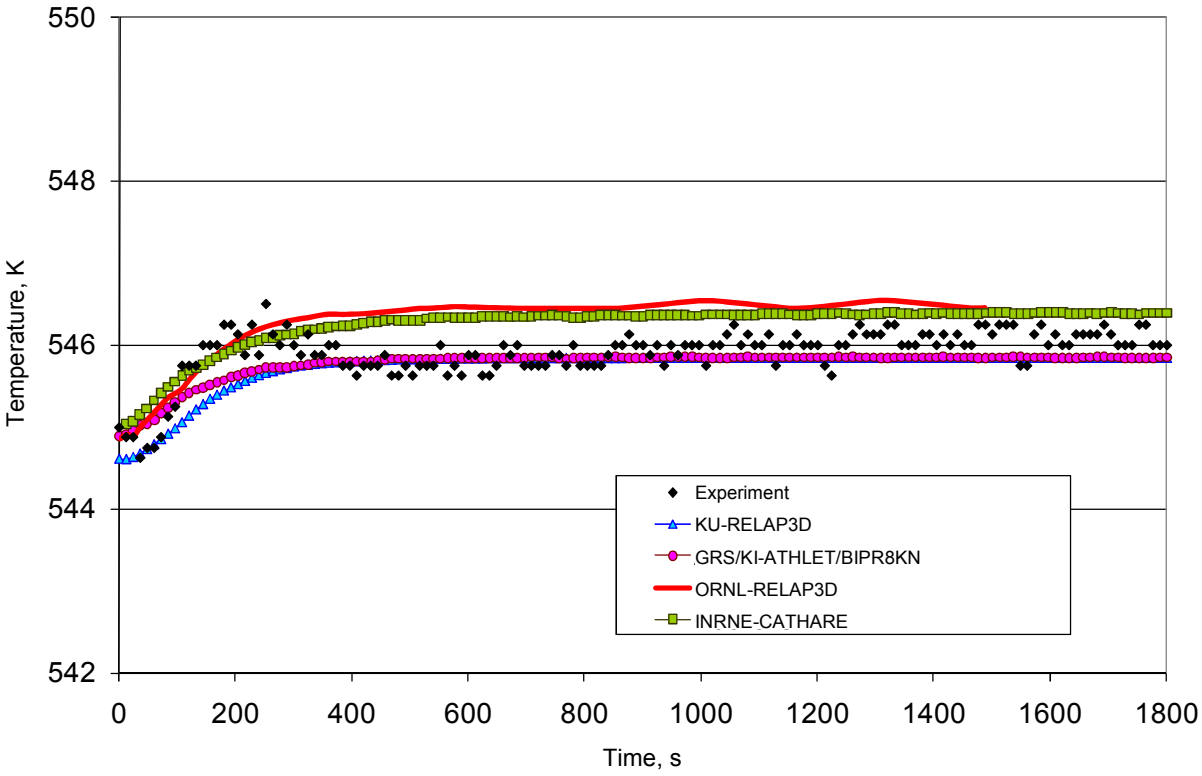

Table 5.8: Hot leg 4 temperature deviations and FOM

Participant	ME	VE	MSE	FOM_{ME}	FOM_{VE}	FOM_{MSE}
INRNE	-0.33706	0.05302	0.16628	0.74791	0.94965	0.85743
GRS/KI	0.13821	0.04594	0.06473	0.87857	0.95608	0.93920
KU	0.17791	0.05021	0.08153	0.84896	0.95219	0.92462
ORNL	-0.43770	0.07208	0.26310	0.69555	0.93276	0.79170

Figure 5.45: Time history of cold leg 1 temperature

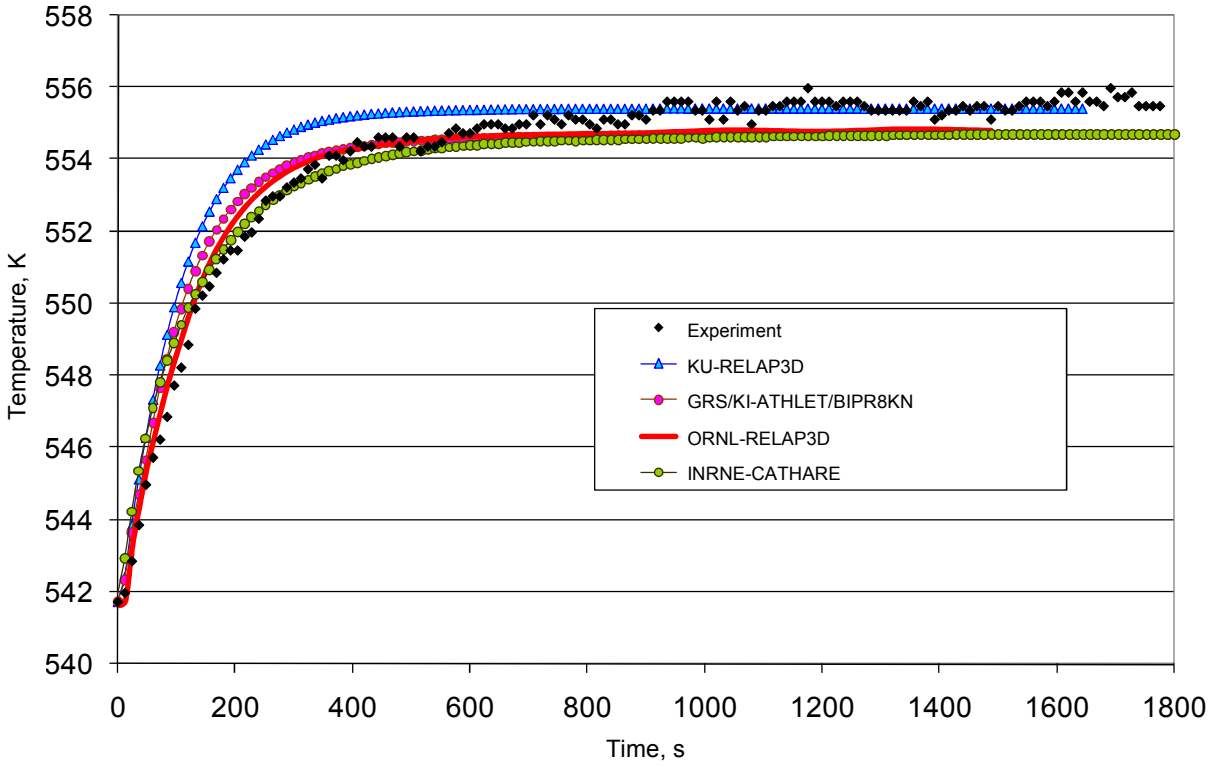

Table 5.9: Cold leg 1 temperatures and FOM

Participant	ME	VE	MSE	FOM_{ME}	FOM_{VE}	FOM_{MSE}
INRNE	0.42203	0.36482	0.54048	0.70322	0.73270	0.64915
GRS/KI	0.28060	0.51489	0.59017	0.78088	0.66012	0.62886
KU	-0.46099	0.55692	0.76569	0.68447	0.64229	0.56635
ORNL	0.21303	0.25604	0.29942	0.82438	0.79615	0.76957

Figure 5.46: Time history of cold leg 2 temperature

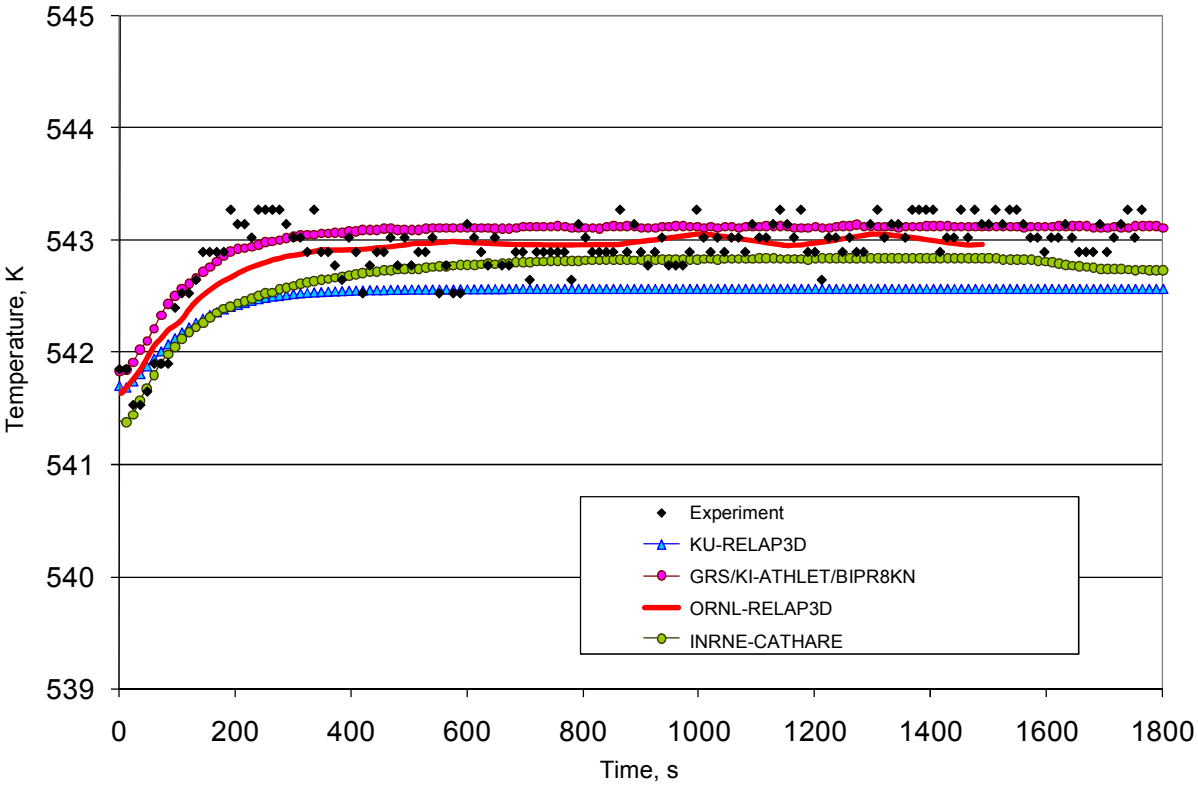

Table 5.10: Cold leg 2 temperatures and FOM

Participant	ME	VE	MSE	FOM_{ME}	FOM_{VE}	FOM_{MSE}
INRNE	0.23376	0.04870	0.10302	0.81053	0.95356	0.90661
GRS/KI	-0.10405	0.04128	0.05182	0.90575	0.96036	0.95073
KU	0.42044	0.05012	0.22655	0.70401	0.95227	0.81529
ORNL	0.03023	0.04826	0.04878	0.97065	0.95396	0.95349

Figure 5.47: Time history of cold leg 3 temperature

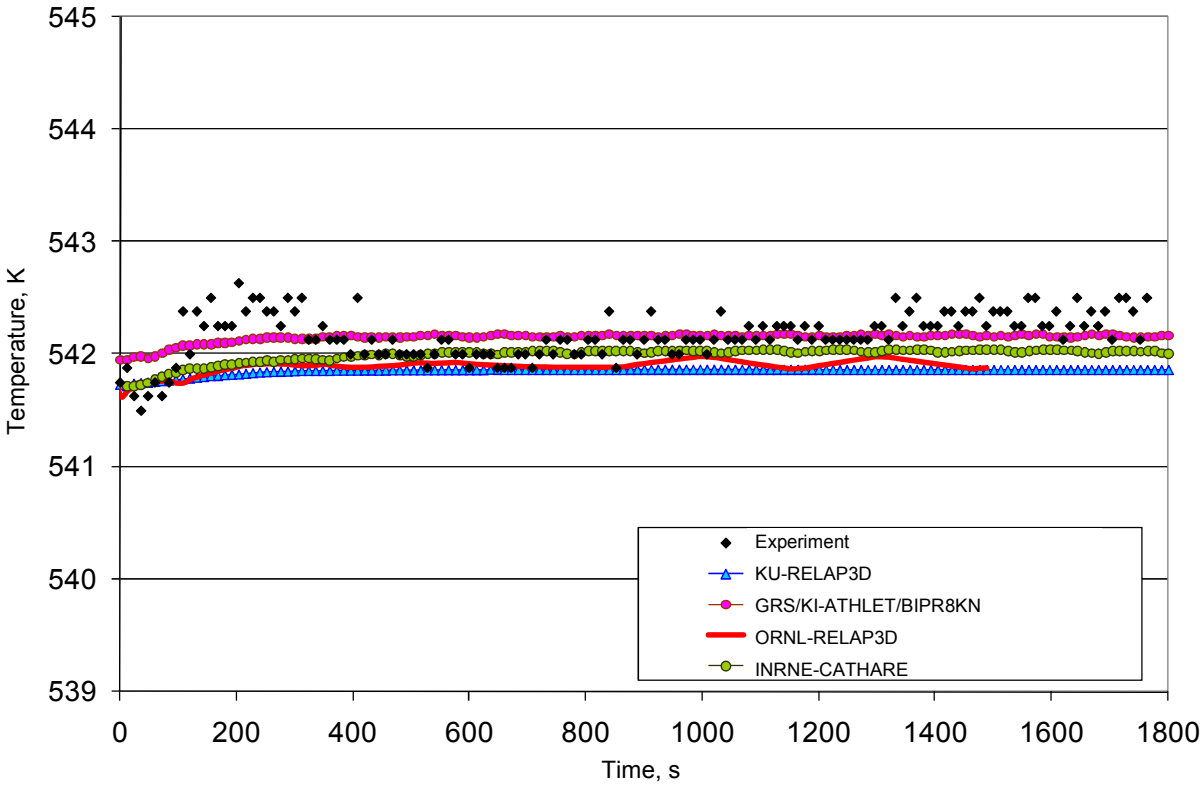

Table 5.11: Cold leg 3 temperatures and FOM

Participant	ME	VE	MSE	FOM_{ME}	FOM_{VE}	FOM_{MSE}
INRNE	0.17915	0.03702	0.06887	0.84807	0.96430	0.93557
GRS/KI	0.01845	0.03716	0.03725	0.98189	0.96417	0.96409
KU	0.31720	0.03941	0.13976	0.75918	0.96209	0.87738
ORNL	0.24734	0.03662	0.09751	0.80170	0.96468	0.91115

Figure 5.48: Time history of cold leg 4 temperature

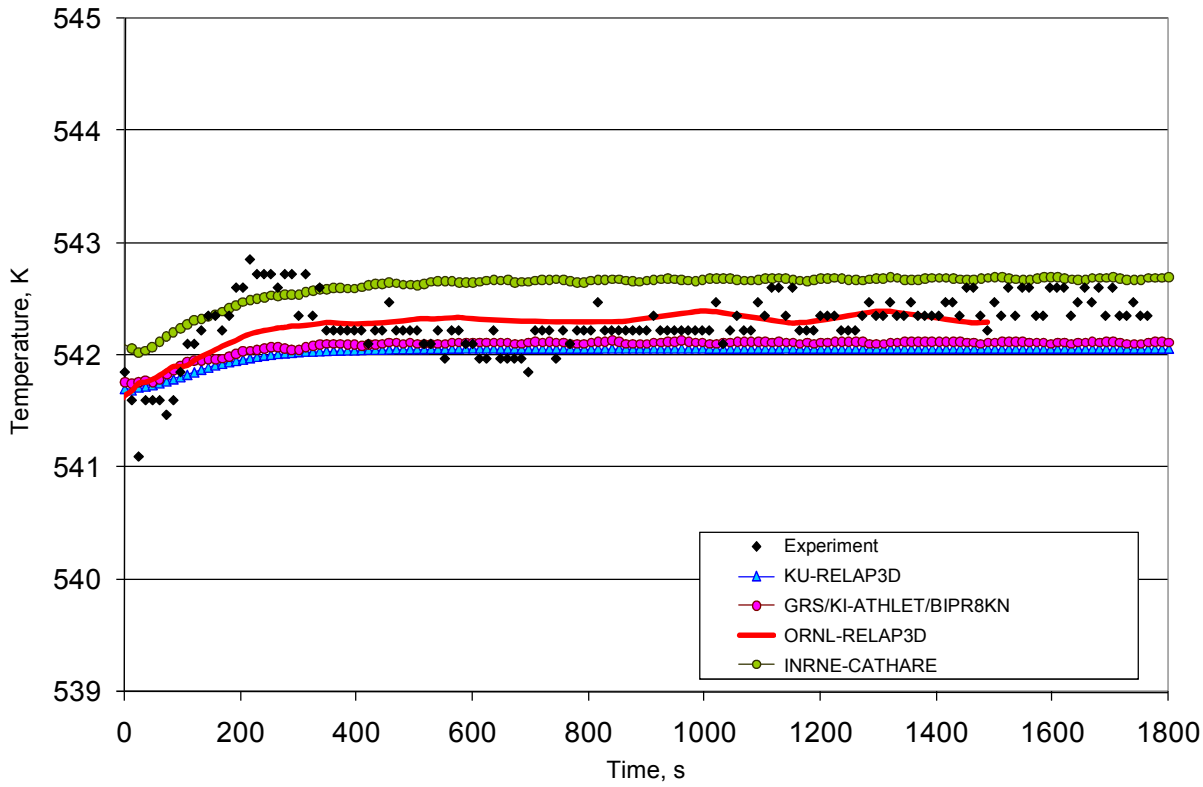

Table 5.12: Cold leg 4 temperatures and FOM

Participant	ME	VE	MSE	FOM_{ME}	FOM_{VE}	FOM_{MSE}
INRNE	-0.32591	0.04855	0.15444	0.75420	0.95370	0.86622
GRS/KI	0.20068	0.05083	0.09075	0.83286	0.95163	0.91680
KU	0.25563	0.05136	0.11636	0.79641	0.95115	0.89577
ORNL	-0.01069	0.05134	0.05060	0.98943	0.95117	0.95184

Figure 5.49: Time history of mass flow rate in loop 1

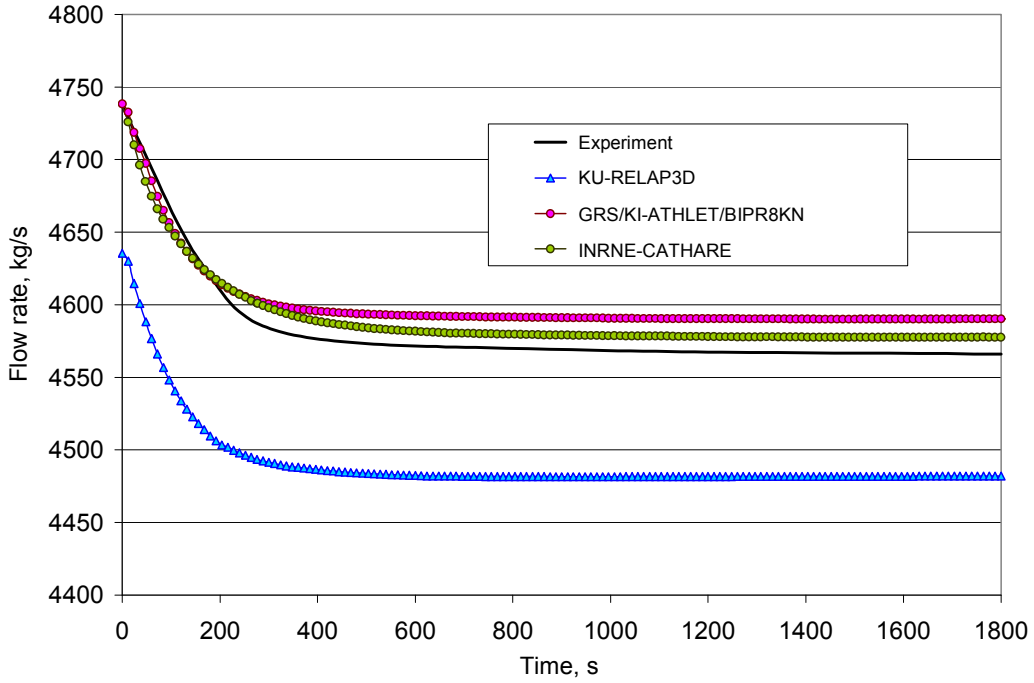

Figure 5.50: Time history of mass flow rate in loop 2

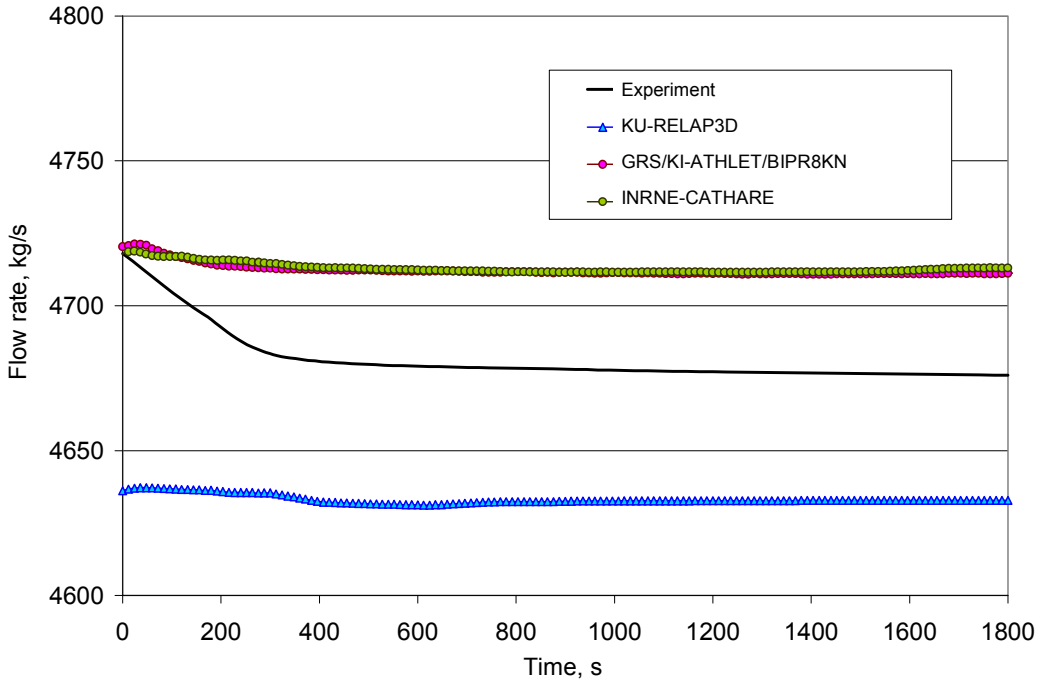

Figure 5.51: Time history of mass flow rate in loop 3

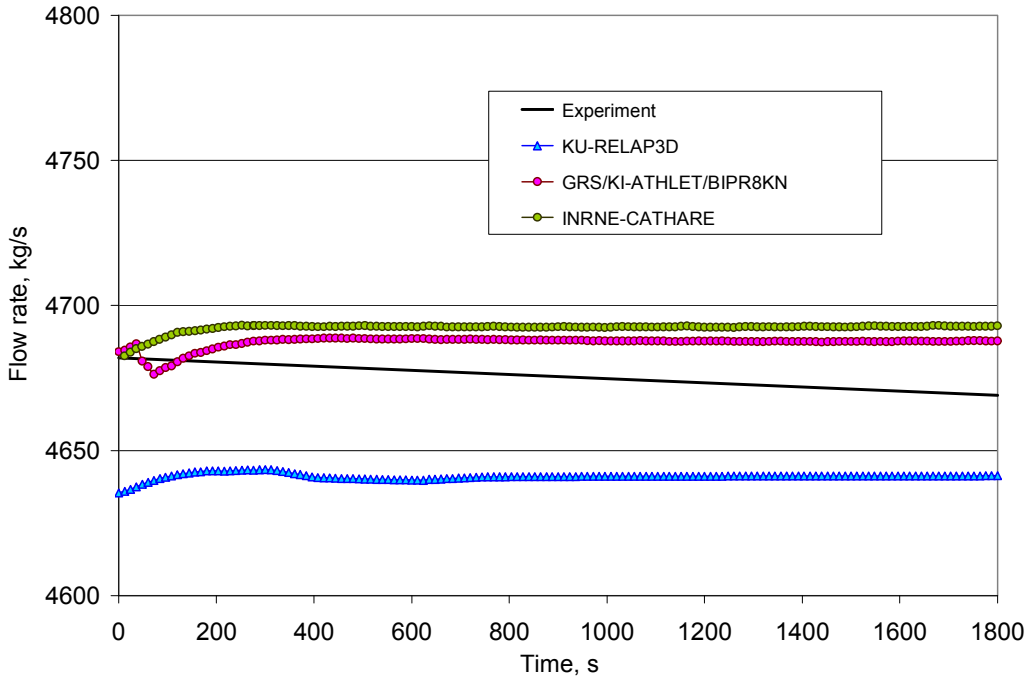

Figure 5.52: Time history of mass flow rate in loop 4

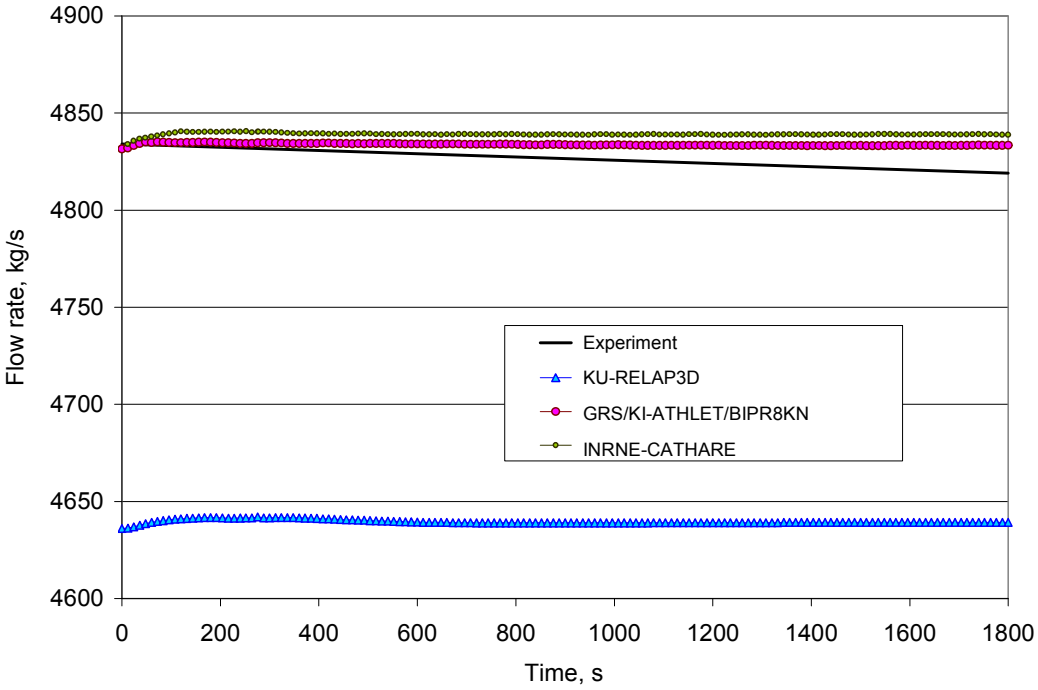

Figure 5.53: Pressure above the core (plant data used by ORNL)

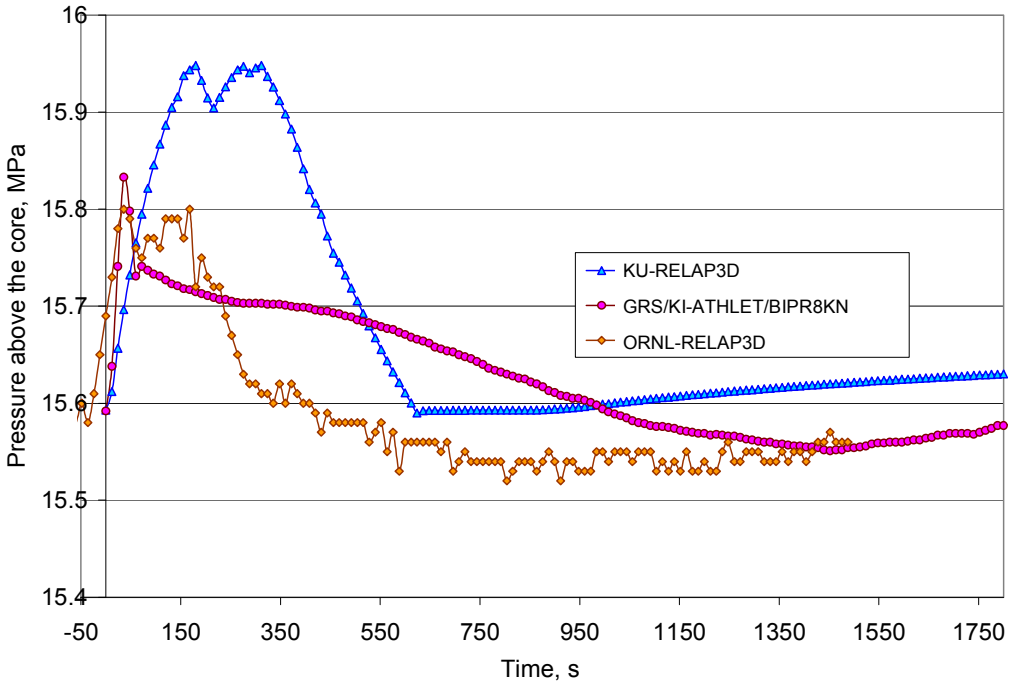

Figure 5.54: Time history of SG1 pressure

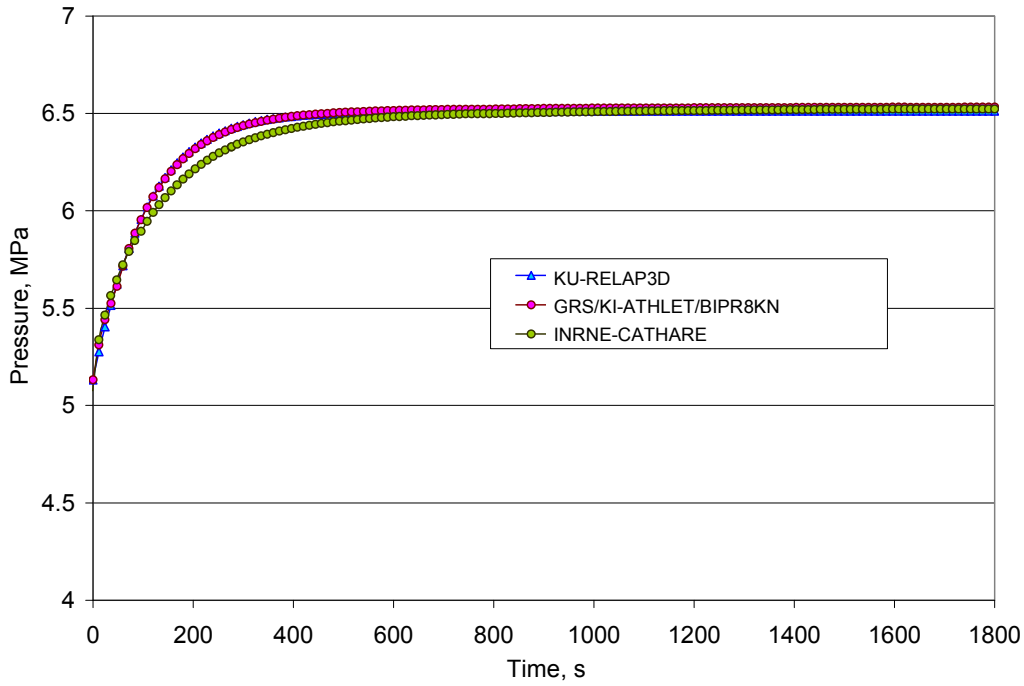

Chapter 6: Summary and conclusions

The V1000CT-2 benchmark was designed to provide a validation framework for the new generation best-estimate codes using coupled 3-D neutron kinetics and system thermal-hydraulics models. A specific objective was to assess the performance of single-phase vessel mixing models (CFD and coarse-mesh) and to test coarse-mesh models in coupled core-vessel and core-plant MSLB simulations.

Based on previous experience, a step-by-step procedure was applied, which allows a consistent and comprehensive testing. The participants validated and analysed their thermal-hydraulic models against plant data and code-to-code in Exercise 1, on different scales:

- separate effects (mixing in the downcomer and lower plenum);
- vessel component;
- plant system.

The validated mixing models have been used in Exercise 2 (coupled core-vessel MSLB simulation), and Exercise 3 (coupled core-plant MSLB simulation) to assess the applicability of best-estimate codes to safety analysis of VVER-1000 reactivity transients.

A detailed evaluation of the CFD results of Exercise 1 was presented in Chapter 4 of this report. The results show that:

- There is reasonable agreement for each parameter, with some exceptions for the core inlet velocity. This agreement was achieved under the following conditions: use of the actual and not the conceptual design geometry of the reactor vessel + appropriate treatment of turbulence + compliance with the Best Practice Guidelines.
- CFD simulations predict qualitatively well the flow rotation in the lower plenum but the sector formation is predicted with more diffusion than in the measurements.
- The maximum error of CFD for temperature prediction at the core inlet is in the range 1-4 K and the average in modulus error is below 1 K, which can be acceptable for industrial applications.
- The observed differences depend on the modelling assumptions, summarised in Table 4.1 and Appendix C, and on the degree of compliance with the BPG. The TRIO_U LES results show best agreement in the angular turn of the loop flow. The BUTE CFX SST simulation is the best in terms of maximum and average in modulus temperature deviations at the core inlet. The UNIPI CFX 10 k-ε predicted core inlet radial velocity profile is the closest to that expected.
- The qualitative difference between the computed and plant estimated core inlet velocity distribution requires additional analysis. Further improvement of the core inlet velocity distribution is possible by explicit modelling of the elliptical sieve plate, as well as modelling of the fuel assemblies and using appropriate boundary conditions.
- CFD codes still have limitations but the development work for single phase mixing is on the right track. The quality of the results depends on the experience of the user and the level of compliance with the Best Practice Guidelines.

The coarse-mesh solutions of the mixing problem show that:

- The disturbed sector formation and the angular turn of loop #1 flow are in reasonable agreement with plant data. The angular turn is somewhat underestimated and the diffusion at the disturbed sector borders is larger than in the experiment.

- The predicted downcomer temperature distributions are in generally good agreement with the CFD results and with each other.
- The maximal deviations in assembly inlet temperatures are within 1-8 K, which is significantly larger than the observed CFD error range.
- The resolution improves with mesh refinement. The solutions are sensitive to azimuth meshing. The available results show that at least 16-18 azimuth sectors are necessary for acceptable accuracy in the core inlet distributions.
- For this type of coolant transient, coarse 3-D models do not perform noticeably better than multi-1-D with cross-flow governed by the local pressure drops.

Some of the discrepancies between different coarse-mesh results can be explained by the modelling differences summarised in Table 5.1 and the participant's provided calculation details given in Appendix D.

Based on this comparison it can be concluded that the considered vessel mixing models in system codes are applicable to the analysis of asymmetric coolant transients characterised by sector formation, such as MSLB.

The CFD and coarse-mesh results of this exercise enable the participants to improve and verify their vessel thermal-hydraulics models, and are important for the correct assessment of the performance of coupled codes in the other two exercises of the benchmark.

The lessons learned from this benchmark will have significant impact on the future coupled code analysis of reactivity transients.

References

ANSYS (2010a), ANSYS CFX web page, accessed 19 May 2010, *www.ansys.com/products/fluid-dynamics/cfx*.

ANSYS (2010b), FLUENT web page, accessed 19 May 2010, *www.FLUENT.com*.

Bajorek, S., *et al.* (2007), *TRACE Theory Manual*, Volume 2, US NRC.

Bieder, U., *et al.* (2004), "Preparation of the Thermal-hydraulic Benchmark V1000CT-2", *2nd Workshop on the OECD V1000CT Benchmark*, Sofia, 5-6 April.

Bieder, U., *et al.* (2005), "Calculation of Coolant Mixing in a VVER-1000", *11th Int. Conf. on Nuclear Reactor Thermal-Hydraulics (NURETH-11)*, Avignon, France, 2-6 October, Paper 201.

Bieder, U., *et al.* (2007), "Simulation of Mixing Effects in a VVER-1000 Reactor", *Nuclear Engineering and Design*, 237, 1718-1728.

Boettcher, M. (2008a), "Detailed CFX-5 Study of the Coolant Mixing Within the Reactor Pressure Vessel of a VVER-1000 Reactor during a Non-symmetrical Heat-up Test", *Nuclear Engineering and Design*, 238, 445-452.

Boettcher, M. (2008b), "Whole Vessel ANSYS CFX Calculation of the V1000CT-2 Vessel Mixing Benchmark", *Proc. XCFD4NRS*, Grenoble, September.

Commissariat à l'énergie atomique (CEA) (2005), *www.triou.cea.fr*.

CEA (2007), *CATHARE 2.5 User's Manual*, CEA Grenoble.

Electrogorsk (2006), *REMIX Code*, Electrogorsk, Russia.

Frisani, A., C. Parisi, F. D'Auria (2006), "The Use of RELAP5-3D Code in the OECD/NEA VVER-1000 CT-1 and CT-2 Benchmark", *RELAP5-3D Users Seminar*, West Yellowstone, USA, 16-18 August.

GRS mbH (2006), *ATHLET Code Manuals*, GRS mbH, Germany.

Hoehne, T. (2007a), "CFD Simulation of Thermal Hydraulic Benchmark V1000CT–2 Using ANSYS CFX", *Proc. ICONE15*, Japan, Paper 10259; *J. Fluid Science and Technology*, JSME (2008).

Hoehne, T. (2007b), "CFX-5 Calculated Transient Core Inlet TH Parameters for the OECD VVER-1000 MSLB Benchmark", Invited contribution to the V1000CT-2 benchmark.

Idaho National Laboratory (INL) (2001), *RELAP5-3D Code Manuals*, INEEL-EXT-98-00834, Revision 1.3a, February.

Mahaffy, J., *et al.* (2007), "Best Practice Guidelines for the Use of CFD in Nuclear Reactor Safety Applications", NEA/CSNI/R(2007)5, OECD/NEA, Paris.

Menter, F., *et al.* (2002), "CFD Best Practice Guidelines for CFD Code Validation for Reactor Safety Applications", ECORA FIKS-CT-2001-00154.

Moretti, F., *et al.* (2006), "Application of CFX-10 to the Investigation of RPV Coolant Mixing in VVER Reactors", *ICONE14-89840, Proceedings of 14th International Conference on Nuclear Engineering*, 17-20 July, Miami, Florida, USA.

Nikonov, S., *et al.* (2006), "Optimal Nodalization Schemes of VVER-1000 Reactor Pressure Vessel for the Coupled Code ATHLET-BIPR8KN", *Proc. 16th AER Symposium on VVER Reactor Physics and Safety*, Bratislava, 25-29 September.

Nuclear Energy Agency (NEA) (1999), *Pressurised Water Reactor Main Steam Line Break (MSLB) Benchmark, Volume I: Final Specifications*, OECD/NEA, Paris, *www.nea.fr/science/docs/1999/nsc-doc99-8.pdf*.

NEA (2010a), *VVER-1000 Coolant Transient Benchmark: Phase 2 (V1000CT-2), Final Specifications of the VVER-1000 Vessel Mixing Problem*, NEA/NSC/DOC(2007)22, OECD/NEA, Paris.

NEA (2010b), *VVER-1000 Coolant Transient Benchmark: Phase 2 (V1000CT-2), Final Specifications of the VVER-1000 MSLB Problem*, NEA/NSC/DOC(2006)6, OECD/NEA, Paris.

Popov, E., *et al.* (2007), "Simulation of the Flow Rotation and Mixing in the Downcomer of a VVER-1000 Reactor", *Nuclear Technology*, ANS, Vol. 158, No. 3, pp. 358-365.

Topalov, Ts., D. Popov (2004), "Overview of the Mixing Tests Performed in the Kozloduy VVER-1000", *2nd Workshop on the OECD V1000CT Benchmark*, Sofia, 5-6 April.

Yamaji, B., A. Aszodi (2006), "CFD Analysis of Coolant Mixing in VVER-1000 Pressure Vessel", *Proc. 16th AER Symposium on VVER Reactor Physics and Safety*, Bratislava, 25-29 September.

Appendix A: Description of CFD codes

CFX 10 (FZK, FZD, BUTE, UNIPI)

ANSYS CFX software (ANSYS, 2010a) delivers powerful computational fluid dynamics (CFD) technology for simulations of all levels of complexity.

As one of the many computer-aided engineering (CAE) tools within the ANSYS Workbench platform, ANSYS CFX takes advantage of data and information common to many simulations. This begins with common geometry; users can link to existing native computer-aided design (CAD) packages as well as create and/or modify CAD models in an intuitive solid modelling environment. Complementing the common geometry model is a suite of meshing tools, designed to ensure easy generation of the most appropriate mesh for the given application. ANSYS CFX tools then guide the user through the set-up of operating conditions, selection of materials and definition of models.

The ANSYS CFX solver uses the most modern solution technology with a coupled algebraic multi-grid solver and extremely efficient parallelisation to help ensure that solutions are ready for analysis quickly and reliably. Solution analysis with the ANSYS CFX post-processor then gives users the power to extract any desired quantitative data from the solution; it also provides a comprehensive set of flow visualisation options. Animations of flow simulations are easily generated, and 3-D images can be directly created and shared with any colleagues or clients using the freely-distributed 3-D viewer from ANSYS CFX.

The next-generation physics pre-processor, ANSYS CFX-Pre, allows multiple meshes to be imported, allowing each section of complex geometries to use the most appropriate mesh. ANSYS CFX includes the following features:

- an advanced coupled solver which is both reliable and robust;
- full integration of problem definition, analysis and results presentation;
- an intuitive and interactive set-up process, using menus and advanced graphics.

ANSYS CFX is capable of modelling:

- steady-state and transient flows;
- laminar and turbulent flows;
- subsonic, transonic and supersonic flows;
- heat transfer and thermal radiation;
- buoyancy;
- non-Newtonian flows;
- transport of non-reacting scalar components;
- multi-phase flows;
- combustion;
- flows in multiple frames of reference;
- particle tracking.

ANSYS interaction

The coupling of CFX and ANSYS software continues to improve in both user workflow and simulation capabilities. This release introduces a full two-way Fluid Structure Interaction capability coupling the ANSYS and CFX solvers, and the ability to run ANSYS CFX within the Workbench engineering simulation environment is extended to a number of Unix platforms.

Transient analysis

Analysis of fully transient situations continues to be a growing trend in CFD simulation, and ANSYS CFX introduces both new transient physical models (such as Transient Particle Tracking and Kinetic Theory for Fluidised Beds), as well as algorithmic and transient efficiency improvements (Adaptive Timestepping and Extrapolated Initial Solutions).

Some of the new features of ANSYS CFX 10 are described below.

ANSYS FSI coupling

ANSYS CFX now has full two-way transient coupling with the ANSYS multi-physics solver to allow the simulation of Fluid Structure Interaction. The ANSYS and ANSYS CFX solvers run simultaneously with force, displacement and/or thermal data shared implicitly at each time step. The communication between the solvers uses a native ANSYS CFX IPC library, and the solvers can be run on the same or different computers, in serial or parallel.

Porosity

To complement the various momentum porous loss models available in CFX-5.7 and earlier, ANSYS CFX has added a true volume porosity model. This porous domain model uses a unique “double node” approach at the porous interface, to ensure sharp capture of the pressure and velocity discontinuities that occur at that location. The interface treatment conserves total pressure and supports significantly greater pressure losses than the previous sub-domain based models in previous versions of ANSYS CFX.

Turbulence modelling

A significant capability in ANSYS CFX is the first-ever commercial release of a predictive laminar to turbulent transition capability, the Menter-Langtry model. The transition model in ANSYS CFX has been highly validated and can be used to determine the location and extent of transition in both aerospace and turbomachinery applications. The model requires no special provisions for geometry or grid topology. For expert users, ANSYS CFX also provides user control of turbulent wall functions, including heat transfer.

Transient improvements

Computing resources needed for a transient calculation can be optimised through the use of Timestep Adaption and Extrapolated Initial Guess for transient calculations in ANSYS CFX. Timestep Adaption allows the solver to automatically adjust the physical time step in a transient solution based on user-specified criteria including target number of coefficient loops or Courant number. The Extrapolated Initial Guess extends the solution from previous time steps as the initial guess for the current time step, providing a better starting condition and minimising the required number of coefficient loops to reach time step convergence. Key numerical transient improvements have also been made, which make it possible to achieve second-order transient calculation with one iteration per time step for time steps in the explicit range.

TRIO_U (CEA)

Trio_U (CEA, 2005) is a CFD code developed by CEA Grenoble, which is especially designed for industrial large eddy simulations (LES) on structured and non-structured grids of several tens of

millions of nodes. The platform-independent code is based on an object-oriented, intrinsically parallel approach and is coded in C++. The flexible code structure allows the user to choose a suitable discretisation method and to combine various appropriate physical models. Several convection and time marching schemes as well as a wide range of boundary conditions are available. This flexibility is implemented without a significant reduction of the overall performance of the code.

Discretisation

In Trio_U, the conservation equations are discretised on structured and unstructured grids. For structured grids, the classical "marker and cell" finite volume (FV) method on a staggered grid is used. For unstructured grids, a hybrid finite volume-based finite element (FV/FE) method is applied. This method consists in determining for a continuous problem a discrete solution in the space of the finite element by maintaining the balance notation of finite volumes. The space discretisation is performed with triangles in 2-D cases and with tetrahedral cells in 3-D cases. The main vector unknowns (velocity) and scalar unknowns (temperature, k, ε, and concentration) are located in the centre of the faces of an element (triangle or tetrahedron) whereas the pressure is discretised in both the centre and the vertices of the element. This staggered mesh arrangement is called VEFPreP1B. The unknown continuous variable is expressed as a combination of a base of form functions that is assigned to each element and that depends on the nodal values. For the Navier-Stokes equations, the discretisation can be characterised as P1-non-conforming for the velocity and P0-P1 for the pressure (P1-NC/P0–P1).

- P1-NC: The unknown variable is calculated at the midpoints of the element faces, and is assumed to be a linear function of the co-ordinates (its gradient is constant); it is discontinuous at the interfaces, but the continuity of the fluxes is respected.
- P0-P1: One unknown is calculated in the centre of an element and is assumed to be constant over the entire control volume. This variable is discontinuous at the interfaces. The other unknowns are calculated for the vertices of the element, and are assumed linear in the control volume. These variables are continuous at the interfaces.

This discretisation method yields a strong velocity/pressure coupling, a condition which is indispensable for LES calculations. The reason is that in LES calculations, in general, the non-linear convection term is compensated by the pressure gradient and not by the linear diffusion term as in RANS calculations.

Turbulence modelling: Large eddy simulation

The large-eddy simulation approach (LES) proposes an intermediate alternative to averaged approach RANS and direct simulation DNS. Unlike the RANS approach, LES gives access to fluctuating quantities without requiring the resolution of all spatio-temporal scales, as for DNS; the effect of small non-resolved scales ("filtered" scales) on the resolved ones has to be modelled. Since modelling is based on the assumption of isotropy for the smallest resolved scales (Smagorinsky model, WALE, structure-function ...), this should require the use of very refined meshes.

In industrial applications and despite the use of multi-million element meshes, this last criterion cannot be fulfilled near walls where flows are locally strongly anisotropic. As a consequence, at the walls, where turbulence is produced and small coherent structures called streaks are generated, the mesh cells are much larger than these structures. The "universal" character of LES models being inappropriate to correctly resolve the flow in the near-wall region under such conditions, a specific wall-modelling has to be employed to reproduce the local effect of the wall turbulence on the rest of the flow.

At the smallest scale, a two-phase flow is made of phases separated by moving interfaces. The direct numerical simulation of such flows consists in simulating all the scales in time and space of the flow. In particular, all the inclusions (bubbles or droplets) of the flow are accounted for individually. In contrast to the numerical simulation of single-phase flows, the main difficulty deals with the numerical tracking of the moving interfaces. Several numerical methods are dedicated to such a numerical tracking. Among them, two are more particularly studied and developed within the Trio_U project: the diffuse-interface method and the "front tracking" method. Whatever the method, the goal is to have a method that is accurate and efficient in the sense that it must allow to simulate complex flows with several inclusions.

Parallelism

An object-oriented, parallel data structure was developed which is especially designed in order to hide the parallelism to the user. As a consequence, new physical methods and numerical schemes that are introduced in the code will no longer lead to new developments for their parallelisation. The calculation domain is distributed in a load-balanced way among the available processors. The parallel efficiency is of the order of 80%, tested on various clusters with a weak scaling method on up to 256 processors.

FLUENT (ORNL-PSU)

FLUENT (ANSYS, 2010b) is a computational fluid dynamics (CFD) software produced by Fluent Inc., which has been a subsidiary of ANSYS, Inc., Canonsburg, Pennsylvania, USA, since 2006. Since FLUENT has been very popular in industry and academia, there is a good chance that you will encounter and use it. FLUENT's numerical solver is based on the finite volume method (FVM).

FLUENT uses unstructured grid technology, meaning the grid can consist of elements in a variety of shapes such as quadrilaterals and triangles for 2-D simulations and hexahedra, tetrahedra, polyhedra, prisms and pyramids for 3-D simulations. Sophisticated numerics and robust solvers ensure FLUENT's accurate results. Mature parallel processing capabilities, available on NT, Linux and Unix platforms can be used on multiple processors of a single machine or multiple machines on a network.

In FLUENT, the dynamic mesh capability meets the needs of challenging applications, including in-cylinder flows, valves and store separation. Several different mesh rebuilding schemes can be used for different moving parts within the same simulation as needed. Only the initial mesh and a description of the boundary movement are required. A built-in six-degrees-of-freedom solver is also available for applications with unconstrained motion, including store separation, missile launch and tank sloshing. Dynamic meshing is compatible with a host of other models including FLUENT's suite of spray break-up and combustion models and multi-phase models including those for free surface prediction and compressible flow.

FLUENT offers an unparalleled breadth of turbulence models such as several versions of the time-honoured k-epsilon model, the k-omega model and the Reynolds stress model (RSM). Recent increases in computer power, coupled with decreases in cost, have made the large eddy simulation (LES) model and the more economical detached eddy simulation (DES) model very attractive choices for industrial simulations. For acoustics, FLUENT can compute the noise resulting from unsteady pressure fluctuations in several ways. Transient LES predictions for surface pressure can be converted to a frequency spectrum using the built-in Fast Fourier Transform (FFT) tool. The Ffowcs-Williams & Hawkings acoustics analogy can be used to model the propagation of acoustics sources for various objects, ranging from exposed bluff bodies to rotating fan blades. Broadband noise source models allow acoustic sources to be estimated based on the results of steady-state simulations.

Heat transfer accompanies many fluid flow phenomena and FLUENT offers a comprehensive suite of options for convection, conduction and radiation. Several radiation models are available, including the P1 and Rosseland models for optically thick, participating media, and the view-factor based surface-to-surface model for non-participating media. The discrete ordinates (DO) model is also available and suitable for any medium, including glass. Other capabilities closely associated with heat transfer include models for cavitation, compressible liquids, heat exchangers, shell conduction, real gas and wet stream.

FLUENT makes use of the Eulerian multi-phase model with its separate sets of fluid equations for interpenetrating fluids or phases, as well as offering a more economical mixture model. Both models can also handle granular flows. Several other multi-phase models are also standard in FLUENT. For some multi-phase applications such as spray dryers, liquid fuel sprays and coal furnaces the discrete phase model (DPM) can be used. The volume of fluid model is available for free surface flows, such as ocean waves, where the prediction of the interface is of interest. The cavitation model has proven useful for modelling hydrofoils, pumps and fuel injectors.

REMIX (EREC)

REMIX v.1.0 (Electrogorsk, 2006) is a CFD code under development in the Electrogorsk Research and Engineering Center (EREC), Russia.

Appendix B: Description of system codes

CATHARE2 (INRNE)

CATHARE2 (CEA, 2007) is a best-estimate code for thermal-hydraulic reactor safety studies covering the domain of large breaks, small breaks and transients. It was developed in CEA Grenoble in the framework of a CEA, EDF, AREVA and IRSN joint effort. Successive versions are released to users. The current version V2.5 includes a 3-D coarse-mesh module. This summary presents CATHARE2 V2.5, used to solve the benchmark problem. The main characteristics of the code are:

- A modular structure with the possibility to represent any reactor and test facility by assembling modules and sub-modules.
- The two-fluid model which is used in all main modules.
- Time discretisation is fully implicit for the 1-D module, and the space discretisation uses the staggered mesh and the donor cell principle.
- The constitutive relations are established mainly on the basis of an extensive experimental support programme.
- Each version is carefully assessed following a two-step procedure: qualification of the closure relations on a large separate effect test matrix, and verification of the overall code behaviour on an integral test matrix.

Every module is able to describe the mechanical and thermal non-equilibrium, which may be encountered in various components of PWR circuits. Advanced modelling of breaks is possible. CATHARE is used for several types of PWR including western designs and VVER. The experimental programme carried out for assessment includes separate effect tests, component tests and integral tests. The qualification matrix includes experiments relative to VVER such as GP horizontal SG, CCFL and re-flooding. All the existing integral test facilities with horizontal steam generators (PACTEL, PMK and PSB) were used for the assessment. The code has been tested in multi-1-D calculations of VVER-1000 plant experiments, including the OECD benchmarks on coolant mixing tests and main coolant pump start-up.

ATHLET/BIPR (GRS/KI)

The thermal-hydraulic computer code ATHLET (Analysis of Thermal-hydraulics of Leaks and Transients) is being developed by the Gesellschaft für Anlagen- und Reaktorsicherheit (GRS, 2006) for the analysis of anticipated and abnormal plant transients, small and intermediate leaks as well as large breaks in light water reactors. The aim of the code development is to cover the whole spectrum of design basis and beyond design basis accidents (without core degradation) for PWR and BWR with only one code. The main code features are: advanced thermal-hydraulics, modular code architecture, separation between physical models and numerical methods, pre- and post-processing tools and portability.

Code development is accompanied by a systematic and comprehensive validation programme. A large number of integral experiments and separate effect tests, including the major International Standard Problems, have been calculated by GRS and by independent organisations. The range of applicability has been extended to the Russian reactor types VVER and RBMK in co-operation with foreign partner organisations.

ATHLET is being applied by numerous institutions in Germany and abroad; its development and validation are sponsored by the German Federal Ministry of Economics and Labour (BMWA).

RELAP5-3D (KU, ORNL, UNIPI)

The RELAP5-3D code (INL, 2001) was developed at the Idaho National Engineering and Environmental Laboratory under the sponsorship of the US Nuclear Regulatory Commission, the US Department of Energy and a consortium of several countries and domestic organisations that were members of the International Code Assessment and Applications Program for best-estimate transient simulation of light water reactor coolant systems during postulated accidents. The code models the coupled behaviour of the reactor coolant system and the core for loss-of-coolant accidents and operational transients.

RELAP5-3D, the latest in the series of RELAP5 codes, is a highly generic code that, in addition to calculating the behaviour of a reactor coolant system during a transient, can be used for simulation of a wide variety of hydraulic and thermal transients in both nuclear and non-nuclear systems. The most prominent attribute that distinguishes the RELAP5-3D code from the previous versions is the fully integrated, multi-dimensional thermal-hydraulic and kinetic modelling capability. This removes any restrictions on the applicability of the code to the full range of postulated reactor accidents.

The RELAP5-3D hydrodynamic model is a transient, two-fluid model for the flow of a two-phase vapour/gas-liquid mixture that can contain non-condensable components in the vapour/gas phase and/or a soluble component in the liquid phase. Both one-dimensional and multi-dimensional hydrodynamic models are included in the code. The RELAP5-3D hydrodynamic model contains several options for invoking simpler hydrodynamic models. These include homogeneous flow, thermal equilibrium and frictionless flow models. These options can be used independently or in combination. The two-fluid equations of motion that are used as the basis for the RELAP5-3D hydrodynamic model are formulated in terms of volume and time-averaged parameters of the flow. Phenomena that depend upon transverse gradients, *i.e.* friction and heat transfer, are formulated in terms of the bulk properties using empirical transfer coefficient formulations. In situations where transverse gradients cannot be represented within the framework of empirical transfer coefficients, *i.e.* sub-cooled boiling, additional models specially developed for the particular situation are employed.

RELAP5-3D heat structure models permit the calculation of the heat transferred across solid boundaries of hydrodynamic volumes. Modelling capabilities of heat structures are general and include fuel pins or plates with nuclear or electrical heating, heat transfer across steam generator tubes, and heat transfer from pipe and vessel walls. Temperatures and heat transfer rates are computed from the one-dimensional form of the transient heat conduction equation for non-re-flood and from the two-dimensional form of the transient heat conduction equation for re-flood. For one-dimensional heat conduction, heat structures are represented using rectangular, cylindrical or spherical geometry. Surface multipliers are used to convert the unit surface of the one-dimensional calculation to the actual surface of the heat structure. Temperature-dependent thermal conductivities and volumetric heat capacities are provided in tabular or functional form either from built-in or user-supplied data. Finite differences are used to advance the heat conduction solutions. Each mesh interval may contain different mesh spacing, a different material or both. The spatial dependence of the internal heat source may vary over each mesh interval. The time dependence of the heat source can be obtained from reactor kinetics, one of several tables of power versus time or a control system variable. Boundary conditions include symmetry or insulated conditions, a correlation package, tables of surface temperature versus time, heat transfer rate versus time, and heat transfer coefficient versus time or surface temperature. The heat transfer correlation package can be used for heat structure surfaces, connected to hydrodynamic volumes, and contains correlations for convective, nucleate boiling, transition boiling and film boiling heat transfer from the wall to fluid and reverse transfer from fluid to wall, including condensation. A two-dimensional conduction scheme is used in the re-flood model for cylindrical or rectangular heat structures.

The RELAP5-3D gap conductance model defines an effective gap conductivity based on a simplified deformation model. The model employs three assumptions as follows: *i)* the fuel-to-cladding radiation heat transfer, which only contributes significantly to the gap conductivity under the conditions of cladding ballooning, is neglected unless the cladding deformation model is activated; *ii)* minimum gap size is limited such that the maximum effective gap conductivity is about the same order as that of metals; *iii)* the direct contact of the fuel pellet and the cladding is not explicitly considered.

There are two options for the computation of the reactor power in the RELAP5-3D code. The first option is the point reactor kinetics model developed at the INEEL. The second is a multi-dimensional neutron kinetics model developed at North Carolina State University.

The reactor point kinetics model is the simplest model that can be used to compute the transient behaviour of the neutron fission power in a nuclear reactor. The power is computed employing the space-independent or point kinetics approximation, which assumes that power can be separated into space and time functions. This approximation is adequate for cases in which the space distribution remains nearly constant. The point reactor kinetics model computes both the immediate (prompt and delayed neutrons) fission power and the power from decay of fission products. Decay power is generated as the fission products undergo radioactive decay. The user can select the decay power model based on the approximate implementation of the 1973 ANS Proposed Standard, the exact implementation of the 1979 ANSI/ANS Standard or the exact implementation of the 1994 ANSI/ANS Standard. Either separable or tabular models can be selected for reactivity feedback in point reactor kinetics.

The multi-dimensional neutron kinetics model was developed to allow the user to model reactor transients where the spatial distribution of the neutron flux changes with time. The neutron kinetics model uses the few-group neutron diffusion equations. Two or four energy groups can be utilised, with all groups being thermal groups (*i.e.* upscatter exits) if desired. Core geometries modelled include Cartesian and hexagonal. Three-, two- and one-dimensional models can be used. Various core symmetry options are available, including quarter, half and full core for Cartesian geometry and one-sixth, one-third and full core for hexagonal geometry. Zero flux, non-re-entrant current, reflective and cyclic boundary conditions are treated. The few-group neutron diffusion equations are spatially discretised with the Nodal Expansion Method (NEM). Quartic or quadratic polynomial expansions for the transverse integrated fluxes are employed for Cartesian or hexagonal geometries, respectively. Transverse leakage terms are represented by a quadratic polynomial or constant for Cartesian or hexagonal geometry, respectively. Discontinuity factors (DF) are utilised to correct for homogenisation errors. Transient problems utilise a user-specified number of delayed neutron precursor groups. The neutron kinetics subroutines require as input the neutron cross-sections in the computational nodes of the kinetics mesh. A neutron cross-section model has been implemented that allows the neutron cross-sections to be parameterised as functions heat structure temperatures, fluid void fraction or fluid density, poison concentration and fluid temperatures. A flexible coupling scheme between the neutron kinetics mesh and the thermal-hydraulics mesh has been developed to minimise the input data needed to specify the neutron cross-sections in terms of thermal-hydraulic variables. A control rod model has been implemented so that the effect of the initial position and subsequent movement of the control rods during transients may be taken into account in the computation of the neutron cross-sections.

TRACE (PSU)

The code TRACE (TRAC/RELAP Advanced Computational Engine) (Bajorek, 2007) combines capabilities of RAMONA, RELAP5, TRAC-B and TRAC-P codes and was developed by the Los Alamos National Laboratory (LANL), the Information Systems Laboratory (ISL), and the Penn State University (PSU) for best-estimate analysis of light water reactors and Generation IV systems. To meet these challenges TRACE uses many new features like multi-dimensional flow modelling and 2-D heat conduction. TRACE is able to use different coolant types like H_2O, D_2O, He, Na and PbBi as well. The partial differential equations that describe two-phase flow and heat transfer are solved in TRACE using finite difference numerical methods.

Appendix C: Participant-provided computation details – CFD codes

BUTE (CFX 10.0)

Organisation name?

Institute of Nuclear Techniques, Budapest University of Technology and Economics (BUTE), Hungary.

Code used?

CFX 10.0.

Have you used plant specific geometry for the reactor vessel and internals?

Yes. CAD geometry is as provided by U. Bieder, CEA (2004) which is plant specific (actual angular co-ordinates of nozzle axes, elevations and gap between the vessel bottom and the elliptical sieve).

Discretisation?

Unstructured, tetrahedral, 3 266 140 elements, generated using ICEM CFD.

Turbulence model?

Shear Stress Transport (SST).

Advection scheme?

Upwind. High resolution scheme gives clearly worse results.

Other assumptions, if any?

Extended domain of solution to include part of the core, see Yamaji (2006).

Have you performed mesh refinement analysis? If yes, what are your conclusions?

No, such a study is underway.

Have you compared the performance of different turbulence models? If yes, what are your conclusions?

Yes, k-e model gives worse results compared with SST.

CEA (TRIO_U)

Organisation name?

Comissariat à l'Énergie Atomique, France.

Code?

TRIO_U.

Have you used plant specific geometry for the reactor vessel and internals?

Yes. A sensitivity study showed that this is a necessary condition for correct prediction of the observed angular turn of the loop flows.

Discretisation?

Unstructured, 10 000 000 control volumes.

Turbulence model?

Large Eddy Simulation (LES).

Advection scheme?

High resolution.

Other assumptions, if any?

Extended domain of solution to include part of the core.

Have you performed mesh refinement analysis? If yes, what are your conclusions?

Yes. Unstructured mesh with the above number of cells is found adequate.

Have you compared the performance of different turbulence models? If yes, what are your conclusions?

No.

EREC (REMIX v. 1.0)

Organisation name?

Electrogorsk Research and Engineering Center, (EREC), Russia.

Code?

REMIX v. 1.0.

Have you used plant specific geometry for the reactor vessel and internals?

Yes.

Discretisation?

Unstructured mesh with hexahedral cells, body-fitted, 311 394 cells, 332 940 vertices. The domain of solution consists of the following regions: four inlet pipes, downcomer, elliptic bottom (equivalent porosity 0.2 in vertical direction and 0 in lateral directions), lower plenum (porosity 0.8), and core up to 3 m elevation (porosity 0.526).

Turbulence model?

k-epsilon model with wall functions, lateral turbulent diffusion was suppressed in porous regions (perforated elliptical bottom, support columns in the lower plenum, core inlet).

Advection scheme?

Upwind.

Other assumptions, if any?

N/A

Have you performed mesh refinement analysis? If yes, what are your conclusions?

No.

Have you compared the performance of different turbulence models? If yes, what are your conclusions?

No.

FZD (ANSYS CFX 10)

Organisation name?

Forschung Zentrum Dresden, Germany.

Code?

ANSYS CFX 10.

Have you used plant specific geometry for the reactor vessel and internals?

Yes.

Discretisation?

Unstructured, 4 700 000 cells.

Turbulence model?

Shear Stress Transport (SST).

Advection scheme?

Upwind.

Other assumptions, if any?

Have you performed mesh refinement analysis? If yes, what are your conclusions?

Yes.

Have you compared the performance of different turbulence models? If yes, what are your conclusions?

Yes, SST, DES and LES in CFX 10. Best performance in terms of mixing scalar was achieved with DES, see Hoehne (2007a).

FZK (CFX 5.7.1)

Organisation name?

Forschung Zentrum Karlsruhe, Germany.

Code?

CFX 5.7.1.

Have you used plant specific geometry for the reactor vessel and internals?

Yes, CAD geometry data as prepared by Bieder/CEA and grid of the downcomer/lower plenum by Bieder/CEA.

Discretisation?

The whole reactor vessel was modelled with 14 000 000 cells, of which 2.6 Mio in the downcomer and lower plenum; core 800 000; upper plenum 9.6 Mio. The core was modelled with structured mesh (hexagonal cells), everything else with unstructured/hybrid mesh (inlets, downcomer and lower plenum – tetra cells).

Turbulence model?

k-ε and SST.

Advection scheme?

Upwind.

Other assumptions, if any?

Domain of solution is the whole reactor vessel. Two modelling options were tested: *i)* k-ε model and porous pressure loss over the elliptical plate, *ii)* SST and explicit modelling of the elliptical plate.

Have you performed mesh refinement analysis? If yes, what are your conclusions?

Yes.

Have you compared the performance of different turbulence models? If yes, what are your conclusions?

Yes. SST and explicit modelling of the elliptical sieve plate gave a realistic core inlet velocity distribution.

PSU/ORNL (FLUENT)

Organisation name?

Pennsylvania State University/Oak Ridge National Laboratory, USA.

Code?

FLUENT.

Have you used plant specific geometry for the reactor vessel and internals (CAD geometry file provided by CEA)?

Yes.

Have you used the plant specific pressure line in the RPV from the specifications, or conceptual design data?

Yes, plant specific.

Discretisation?

Unstructured mesh, cells count 541 000, generated with GAMBIT.

Have you performed mesh refinement analysis? If yes, what are your conclusions?

No.

Turbulence model?

SKE.

Have you compared the performance of different turbulence models? If yes, what are your conclusions?

No, SKE model performs sufficiently well.

Advection scheme?

First order upwind.

Other assumptions, if any?

Constant pressure boundary condition was imposed at the core inlet. Two porous pressure losses in the lower plenum were used to simulate the elliptical perforated plate and the assembly inlets.

UNIPI (ANSYS CFX 10.0)

Organisation name?

University of Pisa, Italy.

Code?

ANSYS CFX 10.0.

Have you used plant specific geometry for the reactor vessel and internals?

Yes.

Hardware?

8 CPU on a Linux-cluster based on AMD Opteron.

Discretisation?

The mesh is generated with ANSYS ICEM 10.0. Tetrahedra, without prism layers: 928 000 nodes; 4 188 511 cells. Several sub-domains connected with GGI interfaces [see Figure C.2 and Moretti (2006)].

Buoyancy modelling?

None.

Heat transfer modelling?

Thermal energy equation.

Boundary conditions?

See table.

Inlet 1	555.35 K	10.57 m/s	Medium turbulence intensity and viscosity ratio
Inlet 2	543.05 K	10.54 m/s	
Inlet 3	542.15 K	10.51 m/s	
Inlet 4	542.35 K	10.85 m/s	
Outlet (above the core inlet)	"Opening"; relative pressure 0 Pa		
Walls	No-slip; smooth; adiabatic		

Turbulence model?

κ-ε model, with "scalable" wall functions.

Additional pressure losses?

- On columns region (Figure C.1): "isotropic loss model", with resistance loss coefficient = 180 m^{-1}.
- On perforated shell region (Figure C.1): "directional loss model", with resistance loss coefficient = 180 m^{-1}, along z.

NOTE: The holes on the perforated shell are not explicitly modelled; they are accounted for by the "porous medium" approach, with the additional pressure losses defined above. Moreover, the two resistance coefficients were obtained by a "tuning" process so as to achieve the experimental LP-FA pressure drop given in the benchmark specifications. Obviously, the choice to define the two coefficients equal to each other is arbitrary.

Advection scheme?

Upwind.

Solver (transient vs. steady state)?

Steady state.

Convergence?

RMS residuals below 4×10^{-6}; close to asymptotic region monitor points stabilised; negligible imbalances.

Have you performed mesh refinement analysis? If yes, what are your conclusions?

Yes.

Have you compared the performance of different turbulence models? If yes, what are your conclusions?

No.

Other assumptions, if any?

Use of additional pressure losses in the "porous regions" defined in the LP. This may have played a role in yielding better results in terms of velocity distribution.

Figure C.1: Domain of solution

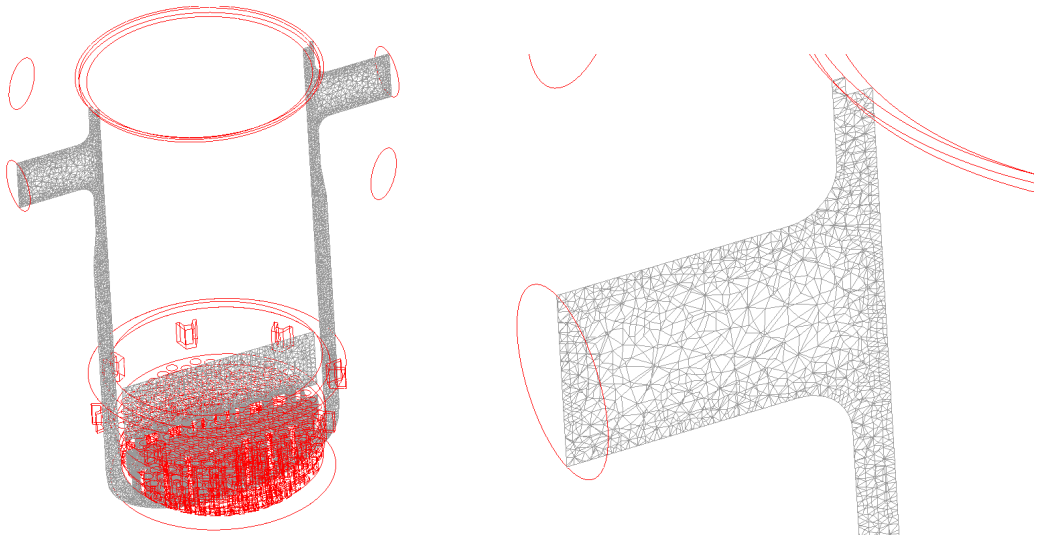

Figure C.2: Sub-domains of solution

Blue – inlet boundaries, green – outlet boundary, red – columns region, cyan – perforated shell region

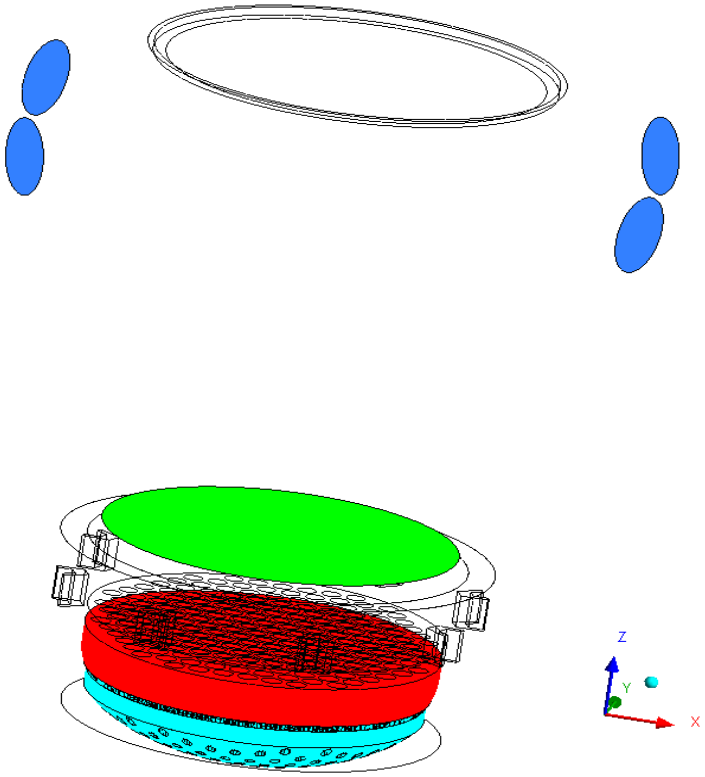

Appendix D: Participant-provided computation details – System codes

GRS/KI (ATHLET)

I. Vessel thermal-hydraulic model

1. *Type of model?*

   Multi-1-D.

2. *Vessel thermal-hydraulic nodalisation. How are the channels/T-H cells chosen?*

   The vessel model is with 16 azimuth sectors and 7 radial rings. See Nikonov (2006) for details.

3. *How is the vessel mixing modelled?*

   The vessel mixing is modelled through cross-flow between the parallel channels, governed by local pressure drops. Cross-flow is modelled with horizontal junctions.

4. *How are the inlet ring and downcomer modelled?*

   The downcomer is modelled with 16 downcomers with cross-flow at several elevations.

5. *How is the lower plenum modelled?*

   There are 3 axial layers and 179 parallel channels at the core inlet.

6. *How are the upper plenum and upper head modelled?*

   The upper plenum is modelled by 3 axial layers $\times$ 16 volumes each and 16 volumes in the outlet ring.

II. Core thermal-hydraulic model

1. *How many thermal-hydraulic channels/cells do you have in the core?*

   Channels: 163, bypass channels: 16.

2. *What is the number of axial nodes?*

   Ten (10) nodes in the heated core.

III. General

1. *Are you using vessel boundary conditions?*

   No, it is a full plant simulation.

2. *User assumptions?*

KU (RELAP5-3D)

I. Vessel thermal-hydraulic model

1. *Type of model?*

   Coarse 3-D.

2. *Vessel thermal-hydraulic nodalisation. How are the channels/T-H cells chosen?*

   Azimuth sectors: 36, radial nodes (rings): 3, in the vessel.

3. *How is the vessel mixing modelled?*

   Coarse 3-D simulation without turbulence.

4. *How are the inlet ring and downcomer modelled?*

   There are 36 azimuth sectors and 1 radial node. There are 2 axial nodes in the inlet ring and 10 in the downcomer. The safety injection nozzles in the inlet ring are taken into account.

5. *How is the lower plenum modelled?*

   The lower plenum is modelled with 36 azimuth nodes, 2 radial nodes and 2 axial layers.

6. *How are the upper plenum and upper head modelled?*

   The upper plenum is modelled with 36 azimuth nodes and 3 radial nodes.

II. Core thermal-hydraulic model

1. *How many thermal-hydraulic channels/cells do you have in the core?*

   The core was modelled with 169 thermal-hydraulic channels. Six of them are bypass channels and 163 are fuel assemblies.

2. *What is the number of axial nodes?*

   Ten (10).

III. General

1. *Are you using vessel boundary conditions?*

   No, it is a full plant simulation.

2. *User assumptions?*

   N/A

INRNE (CATHARE 2.5)

I. Vessel thermal-hydraulic model

1. *Type of model?*

   Multi-1-D.

2. *Vessel thermal-hydraulic nodalisation. How are the channels/T-H cells chosen?*

   The vessel model is 24-sector multi-1-D with cross-flow (from the vessel inlet to the core outlet) and 12-sector model in the upper plenum.

3. *How is the vessel mixing modelled?*

   The vessel mixing is modelled through cross-flow between the parallel channels, governed by local pressure drops. Cross-flow is modelled with horizontal junctions and vertical (diagonal) junctions connecting donor cells at a given elevation to receptor cells in the neighbouring sectors, at a higher elevation. Vertical junctions were used to a limited extent, with small flow area and in the lower and upper plenums only.

4. *How are the inlet ring and downcomer modelled?*

   The inlet ring is modelled with 24 volume elements corresponding to 24 azimuth sectors. The downcomer is modelled with 24 volume elements in the upper part and 24 axial elements in the lower one.

5. *How is the lower plenum modelled?*

   There are 2 axial layers of 24 volumes each.

6. *How are the upper plenum and upper head modelled?*

   The upper plenum is modelled by 3 axial layers $\times$ 12 volumes each and 12 volumes in the outlet ring.

II. Core thermal-hydraulic model

1. *How many thermal-hydraulic channels/cells do you have in the core?*

   Channels: 24, bypass channels: 24.

2. *What is the number of axial nodes?*

   Ten (10) nodes in the heated core and 3 nodes in each axial reflector.

III. General

1. *Are you using vessel boundary conditions?*

   Both the vessel boundary condition problem and the full plant problem were solved. The presented in-vessel distributions refer to the vessel boundary condition problem.

2. *User assumptions?*

ORNL (RELAP5-3D)

I. Vessel thermal-hydraulic model

1. *Type of model?*
   Coarse 3-D.

2. *Vessel thermal-hydraulic nodalisation. How are the channels/T-H cells chosen?*
   There are 6 azimuth sectors and 5 radial nodes. See Frisani (2006) for details.

3. *How is the vessel mixing modelled?*
   Coarse 3-D simulation without turbulence.

4. *How are the inlet ring and downcomer modelled?*
   Coarse 3-D without turbulence.

5. *How is the lower plenum modelled?*
   Coarse 3-D without turbulence.

6. *How are the upper plenum and upper head modelled?*
   Coarse 3-D without turbulence.

II. Core thermal-hydraulic model

1. *How many thermal-hydraulic channels/cells do you have in the core?*
   Nodes per horizontal cut: 18 (6×3), bypass channels: 6.

2. *What is the number of axial nodes?*
   Ten (10).

III. General

1. *Are you using vessel boundary conditions?*
   Yes.

2. *User assumptions?*
   N/A

PSU (TRACE)

I. Vessel thermal-hydraulic model

1. *Type of model?*
   Coarse 3-D.

2. *Vessel thermal-hydraulic nodalisation. How are the channels/T-H cells chosen?*
   The vessel is modelled in 3-D cylindrical geometry using 6 azimuth sectors and 5 radial cells.

3. *How is the vessel mixing modelled?*
   Coarse-mesh 3-D simulation without turbulence.

4. *How are the inlet ring and downcomer modelled?*
   Three-dimensional modelling.

5. *How is the lower plenum modelled?*
   Three-dimensional modelling.

6. *How are the upper plenum and upper head modelled?*
   Three-dimensional modelling.

II. Core thermal-hydraulic model

1. *How many thermal-hydraulic channels/cells do you have in the core?*
   The core is modelled in 3-D cylindrical geometry using 6 azimuth sectors and 3 radial cells.

2. *What is the number of axial nodes?*
   Ten (10).

III. General

1. *Are you using vessel boundary conditions?*
   Yes.

2. *User assumptions?*
   N/A

UNIPI (RELAP5-3D)

I. Vessel thermal-hydraulic model

1. *Type of model?*

   Coarse 3-D.

2. *Vessel thermal-hydraulic nodalisation. How are the channels/T-H cells chosen?*

   See Items 3-5 below and Frisani (2006) for details.

3. *How is the vessel mixing modelled?*

   Coarse 3-D simulation without turbulence in the downcomer and the lower plenum.

4. *How are the inlet ring and downcomer modelled?*

   The downcomer is modelled with one 3-D thermal-hydraulic volume. There are 20 azimuth sectors, 1 radial node and 20 axial nodes in the downcomer.

Figure D.1: Nodalisation scheme of UNIPI RELAP5-3D model

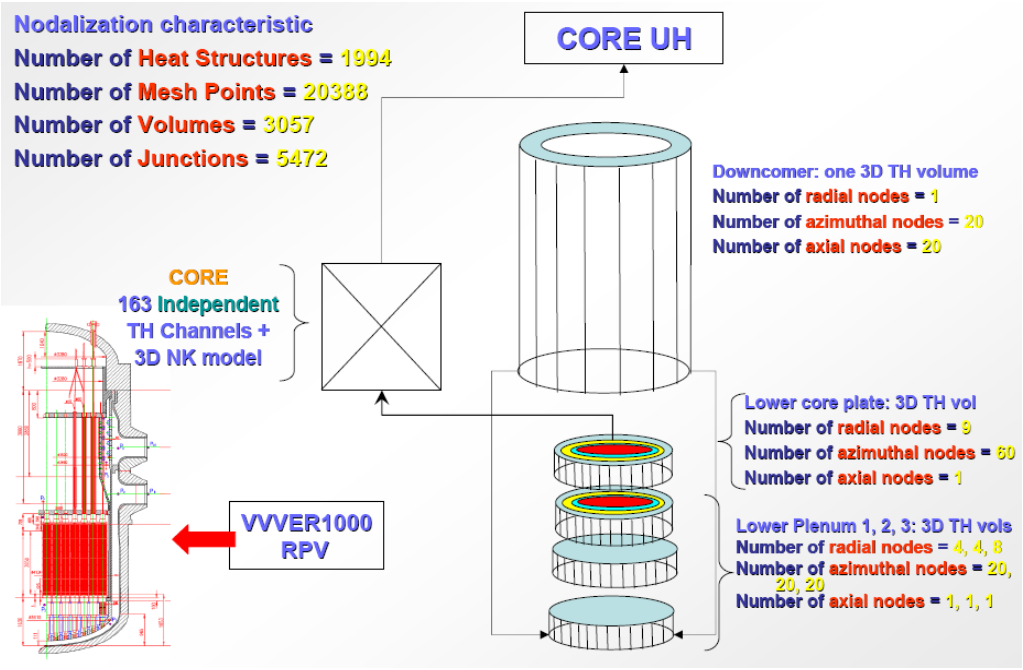

5. *How is the lower plenum modelled?*

   The lower plenum is modelled with 4 thermal-hydraulic 3-D volumes. The first 2 have 20 azimuth nodes, 4 radial nodes and 1 axial node. The second has 20 azimuth nodes, 4 radial nodes and 1 axial node. The third has 20 azimuth nodes, 8 radial nodes and 1 axial node. The lower core plate is modelled separately with 60 azimuth nodes, 9 radial nodes and 1 axial node.

6. *How are the upper plenum and upper head modelled?*

   The upper plenum is modelled with pipes and branches. Before flowing into the hot legs, the coolant is homogenised and all the hot leg temperatures have the same values.

II. Core thermal-hydraulic model

1. *Number of thermal-hydraulic channels in the core?*
   Independent thermal-hydraulic channels: 163.

2. *Number of axial nodes?*
   Twelve (12).

III. General

1. *Are you using vessel boundary conditions?*
   Yes.

2. *User assumptions?*
   N/A

Appendix E: Deviations of CFD computed-to-experimental core inlet temperatures

Figure E.1: CEA TRIO_U results – core inlet temperature deviations from plant data

Yellow – overestimated; green, blue – underestimated; no colour – deviation ≤ 1.2 K

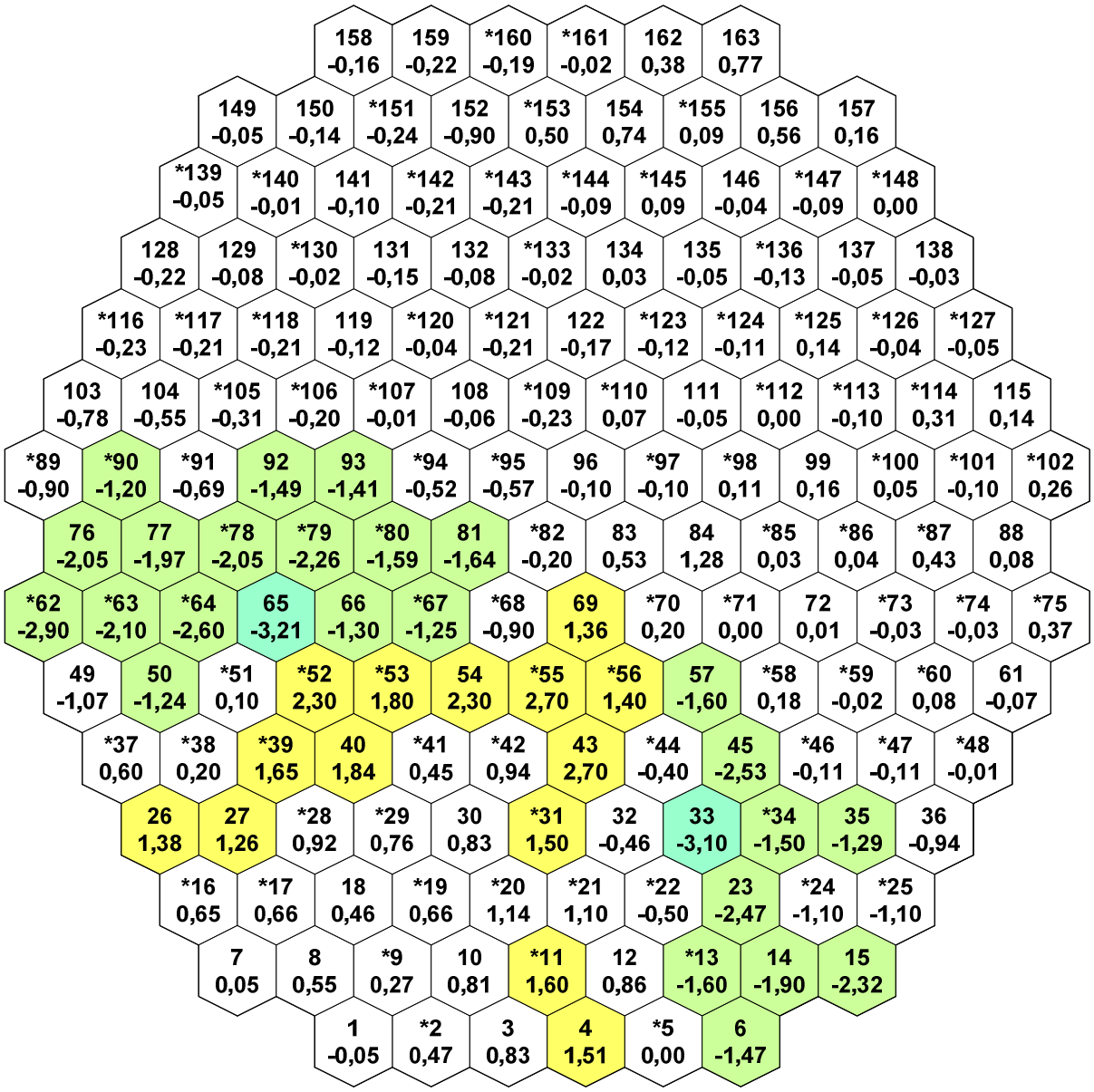

Figure E.2: BUTE CFX 10 SST results – core inlet temperature deviations from plant data

Yellow – overestimated; green, blue – underestimated; no colour – deviation ≤ 1.2 K

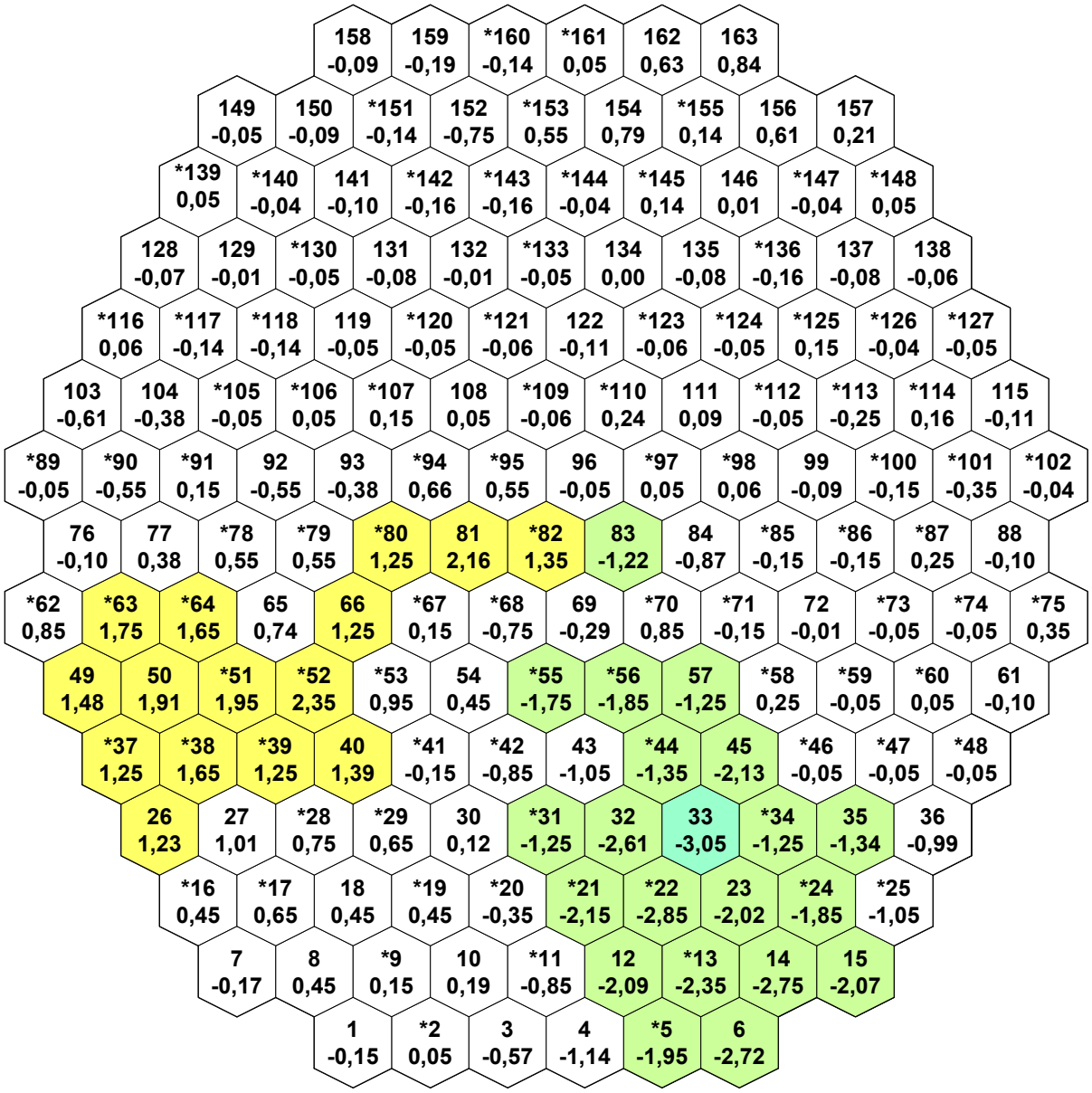

Figure E.3: FZK CFX 5 k-ε results – core inlet temperature deviations from plant data

Yellow, red – overestimated; green, blue – underestimated; no colour – deviation ≤ 1.2 K

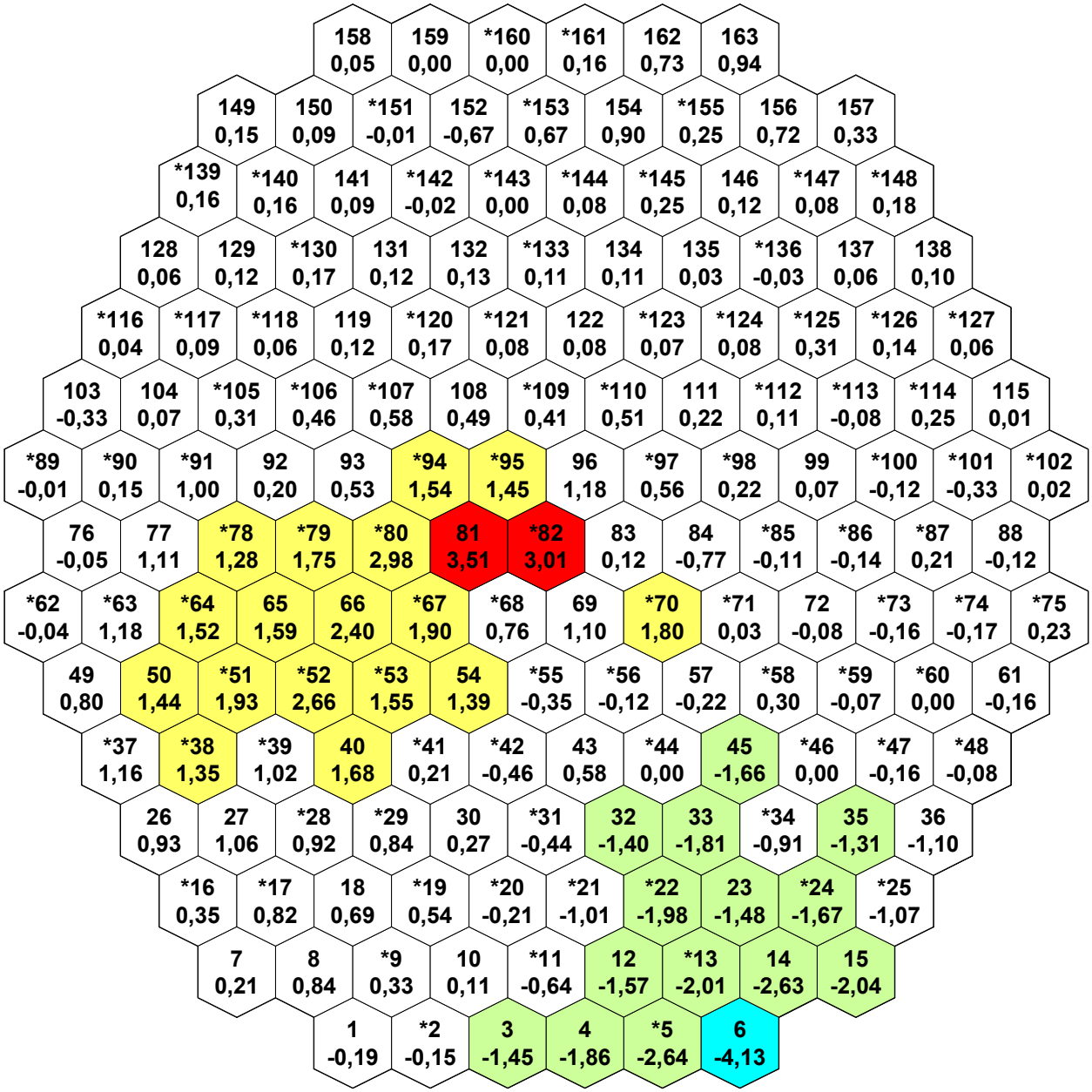

Figure E.4: UNIPI CFX 10 k-ε results – core inlet temperature deviations from plant data

Yellow, red – overestimated; green, blue – underestimated; no colour – deviation ≤ 1.2 K

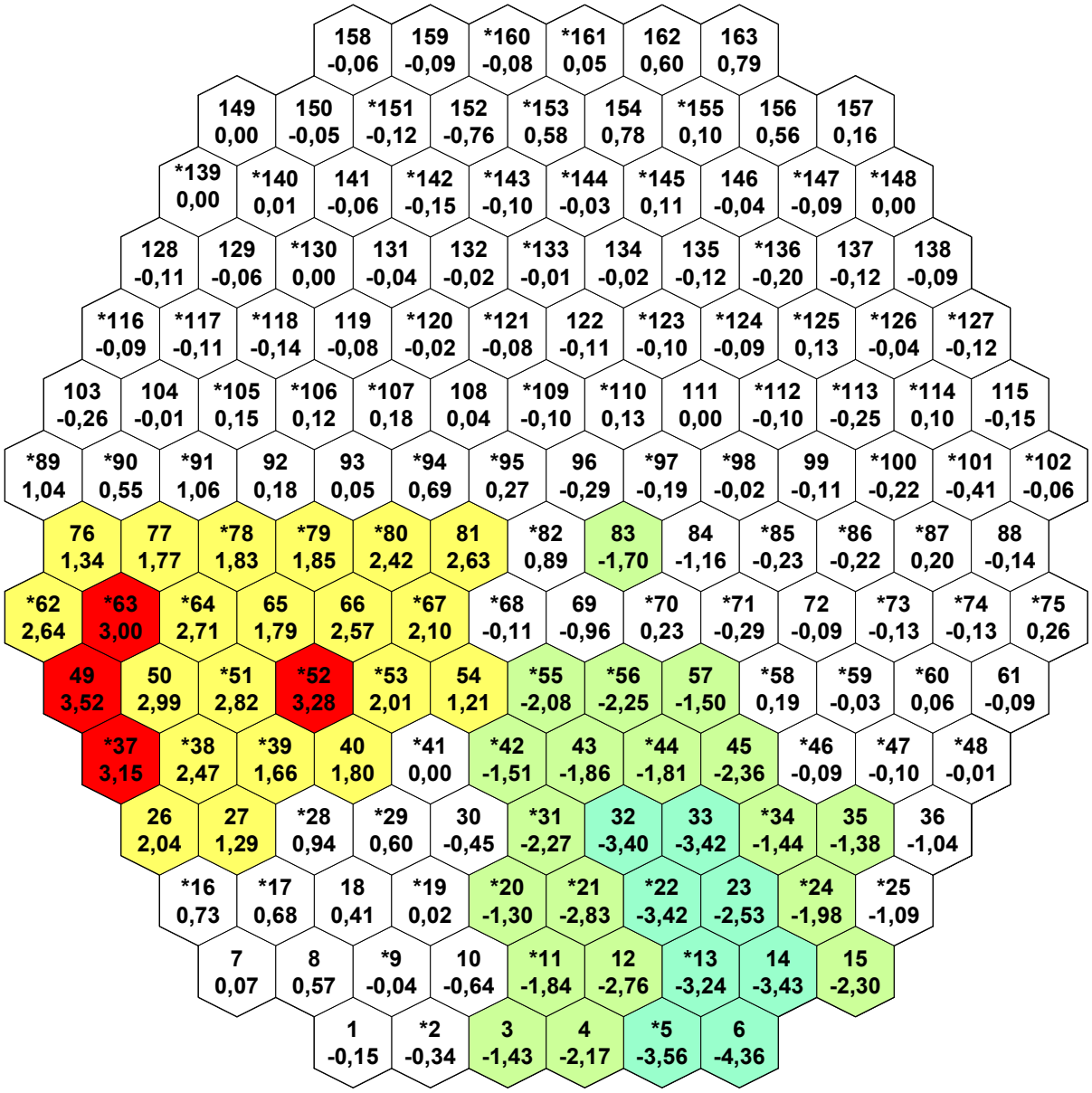

Figure E.5: EREC REMIX k-ε results – core inlet temperature deviations from plant data

Yellow, red – overestimated; green, blue – underestimated; no colour – deviation ≤ 1.2 K

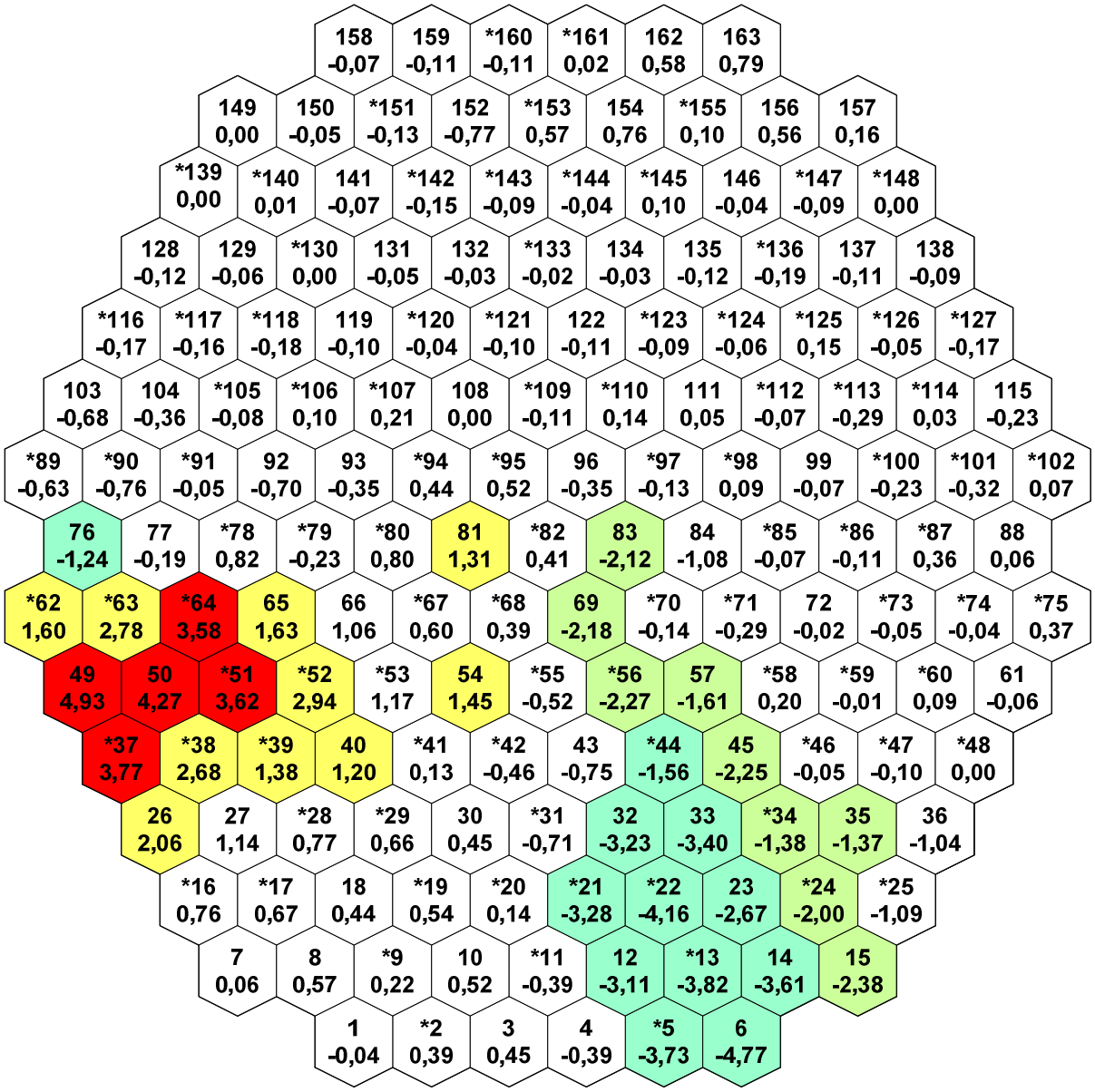

Figure E.6: FZD CFX 10 SST results – core inlet temperature deviations from plant data

Yellow, red – overestimated; green, blue – underestimated; no colour – deviation ≤ 1.2 K

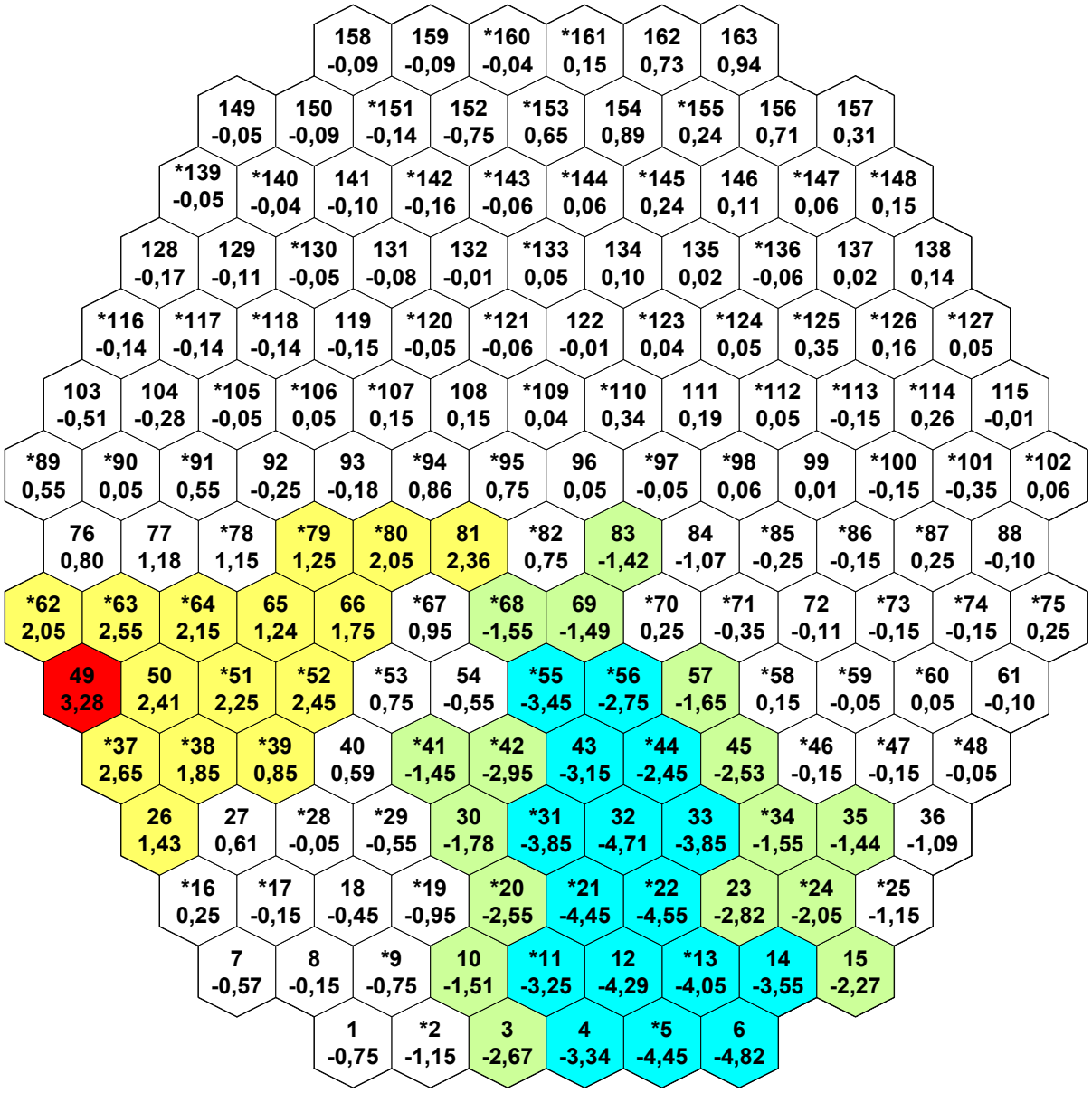

Figure E.7: FLUENT k-ω results – core inlet temperature deviations from plant data

Yellow, red – overestimated; green, blue – underestimated; no colour – deviation ≤ 1.2 K

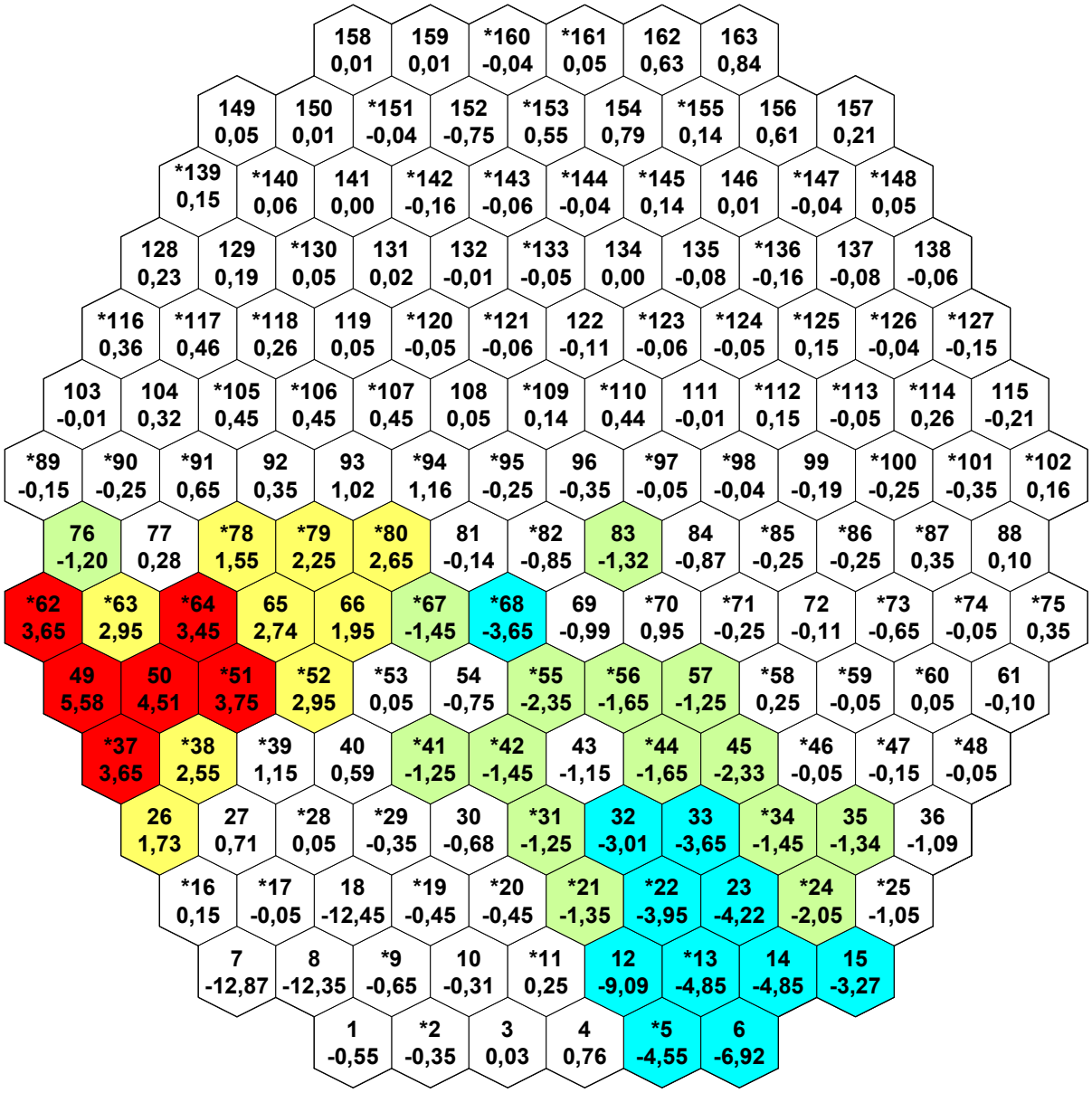

Appendix F: Deviations of coarse-mesh computed-to-experimental core inlet temperatures

Figure F.1: INRNE CATHARE2 – core inlet temperature deviations from plant data

Yellow, red – overestimated; green, blue – underestimated; no colour – deviation ≤ 1.2 K

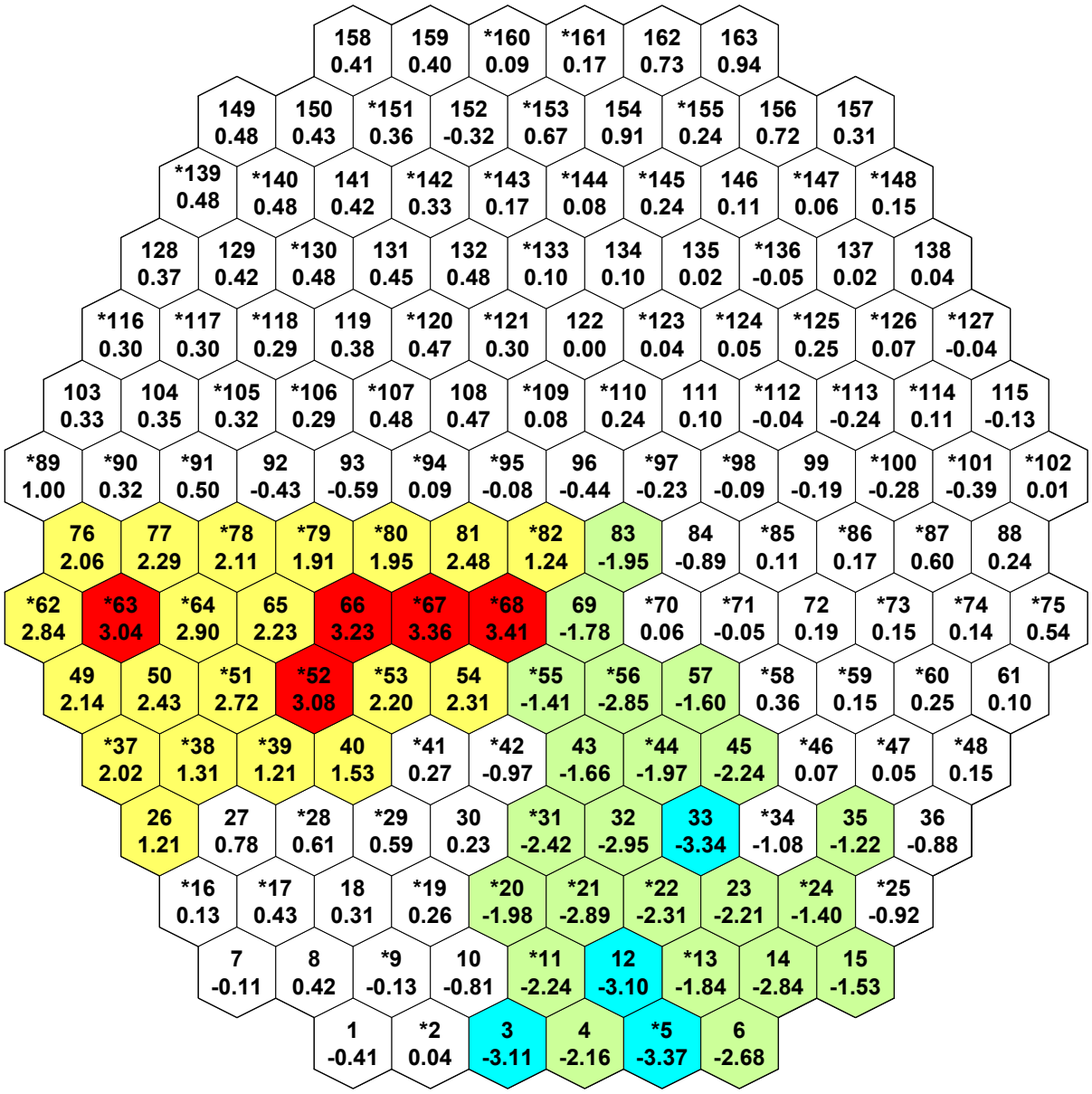

Figure F.2: GRS/KI ATHLET/BIPR – core inlet temperature deviations from plant data

Yellow, red – overestimated; green, blue – underestimated; no colour – deviation ≤ 1.2 K

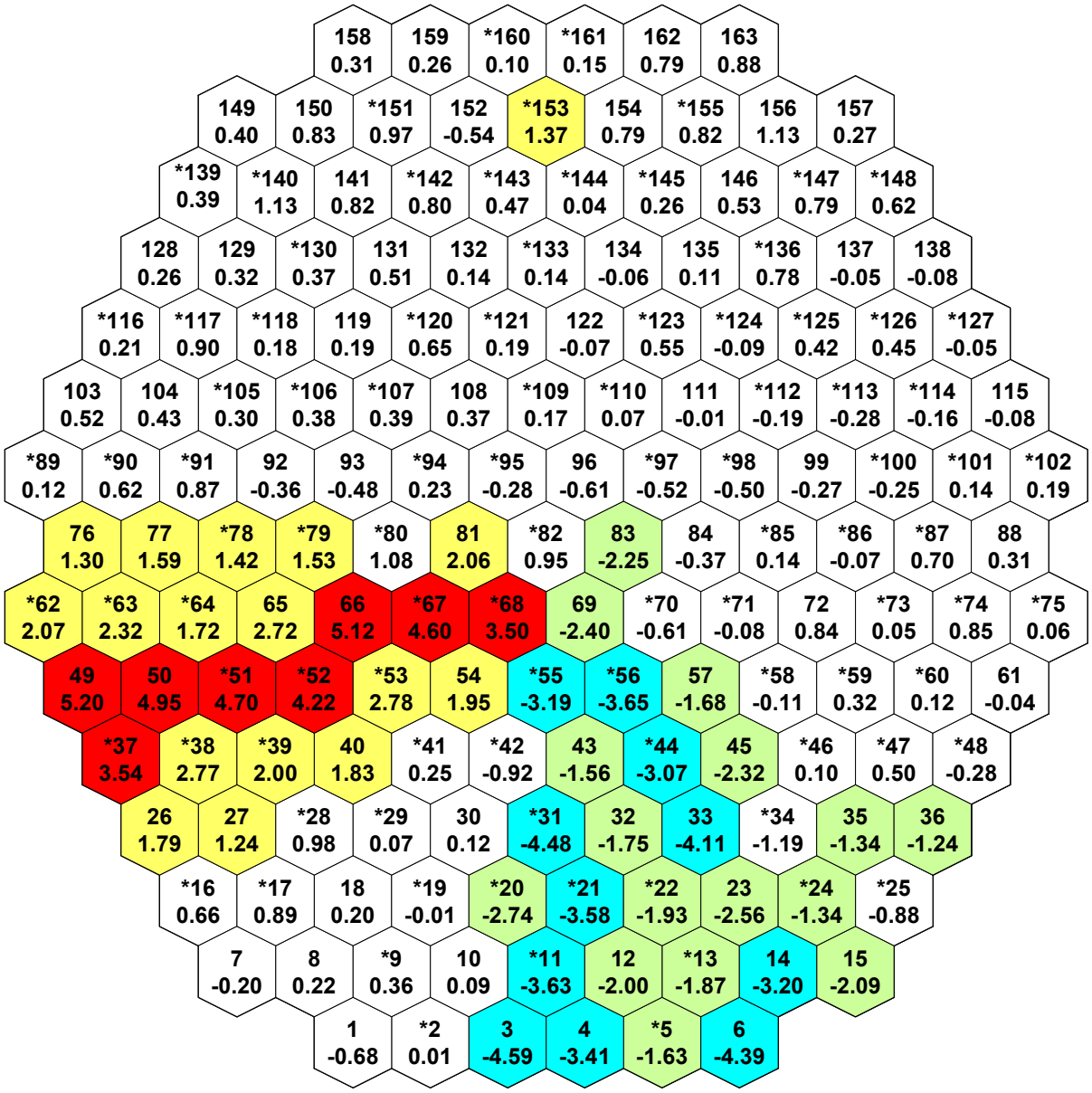

Figure F.3: UNIPI RELAP5-3D – core inlet temperature deviations from plant data

Yellow, red – overestimated; green, blue – underestimated; no colour – deviation ≤ 1.2 K

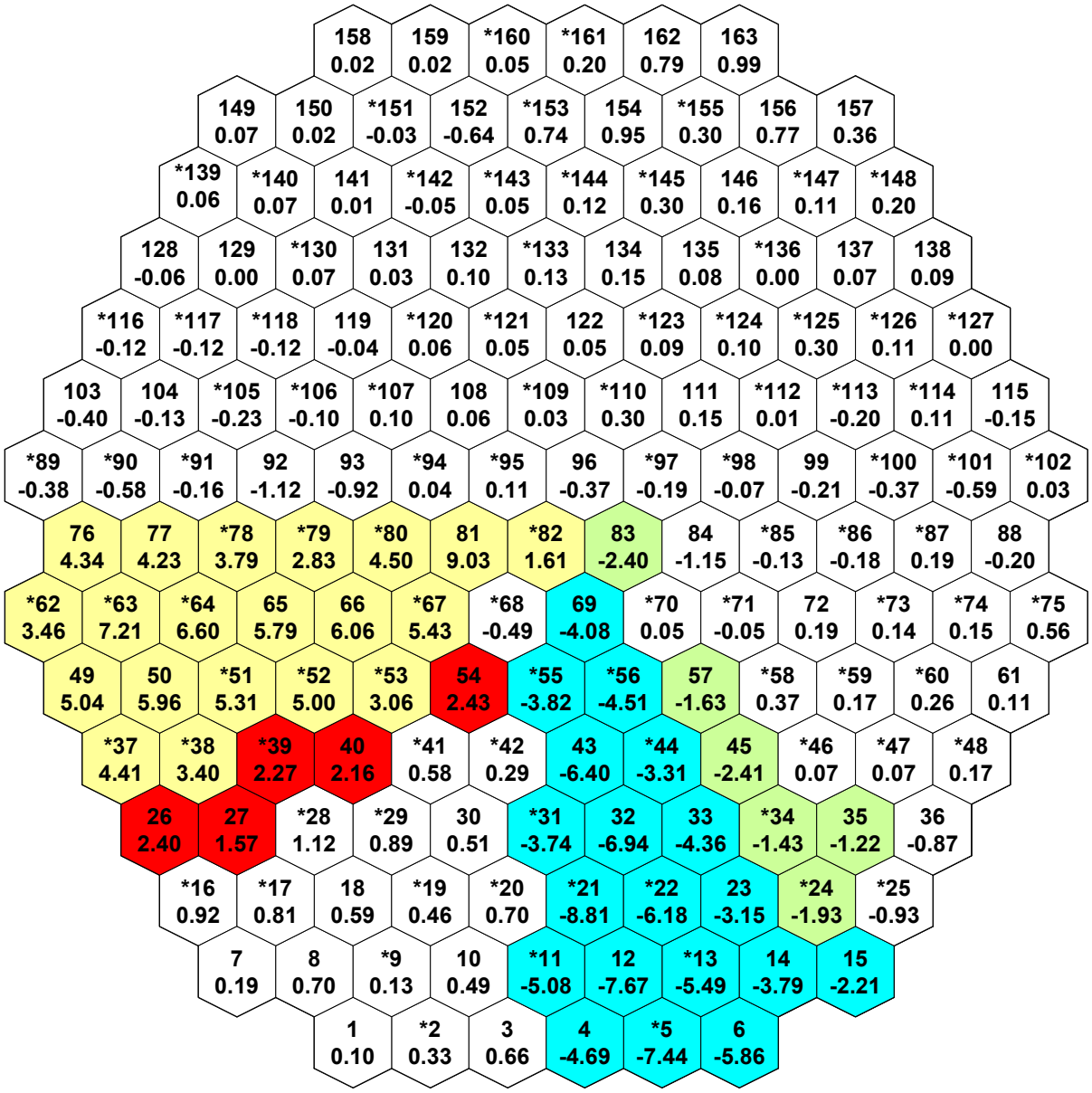

Figure F.4: KU RELAP5-3D – core inlet temperature deviations from plant data

Yellow, red – overestimated; green, blue – underestimated; no colour – deviation ≤ 1.2 K

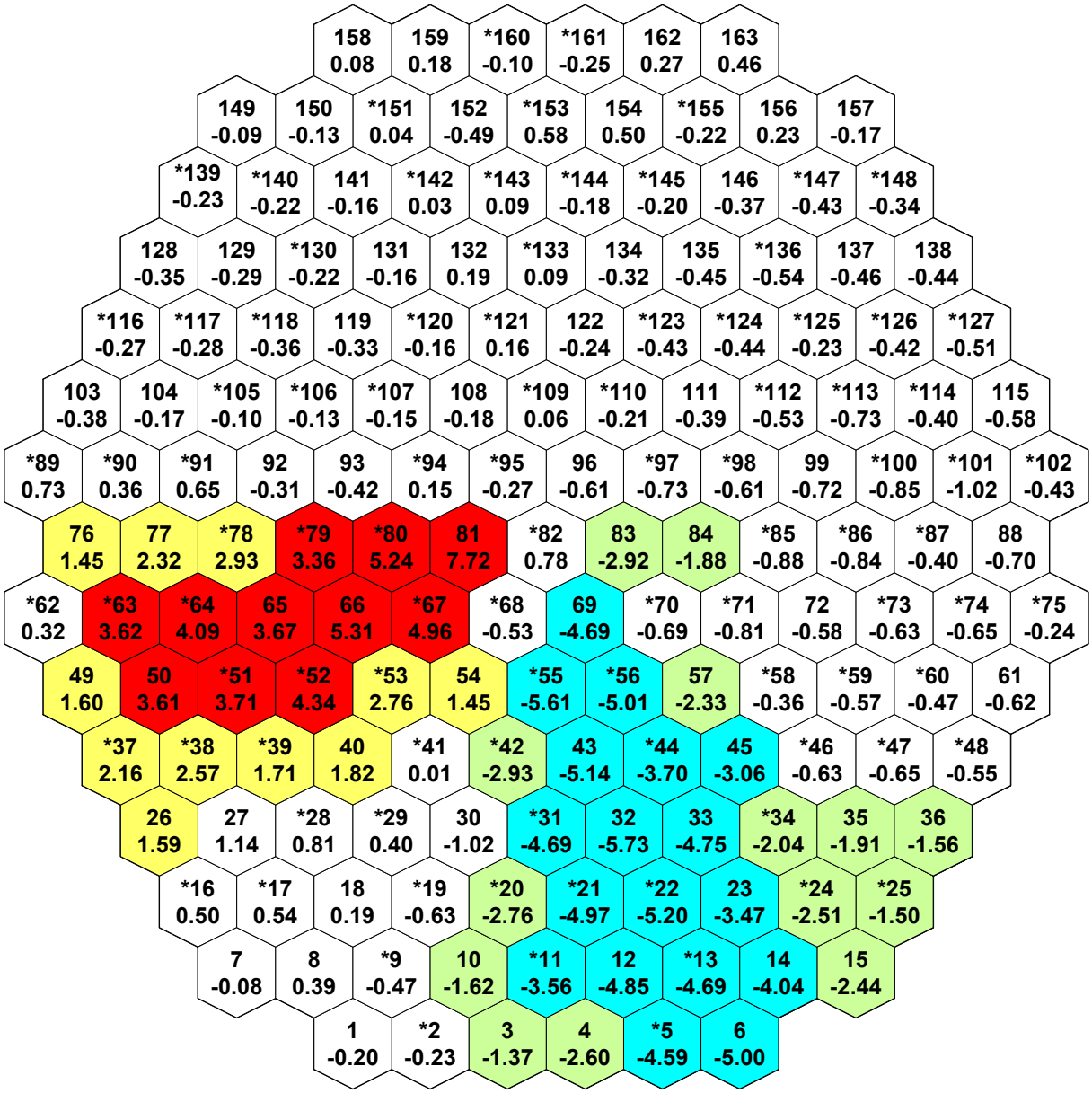

Figure F.5: PSU TRACE – core inlet temperature deviations from plant data

Yellow, red – overestimated; green, blue – underestimated; no colour – deviation ≤ 1.2 K

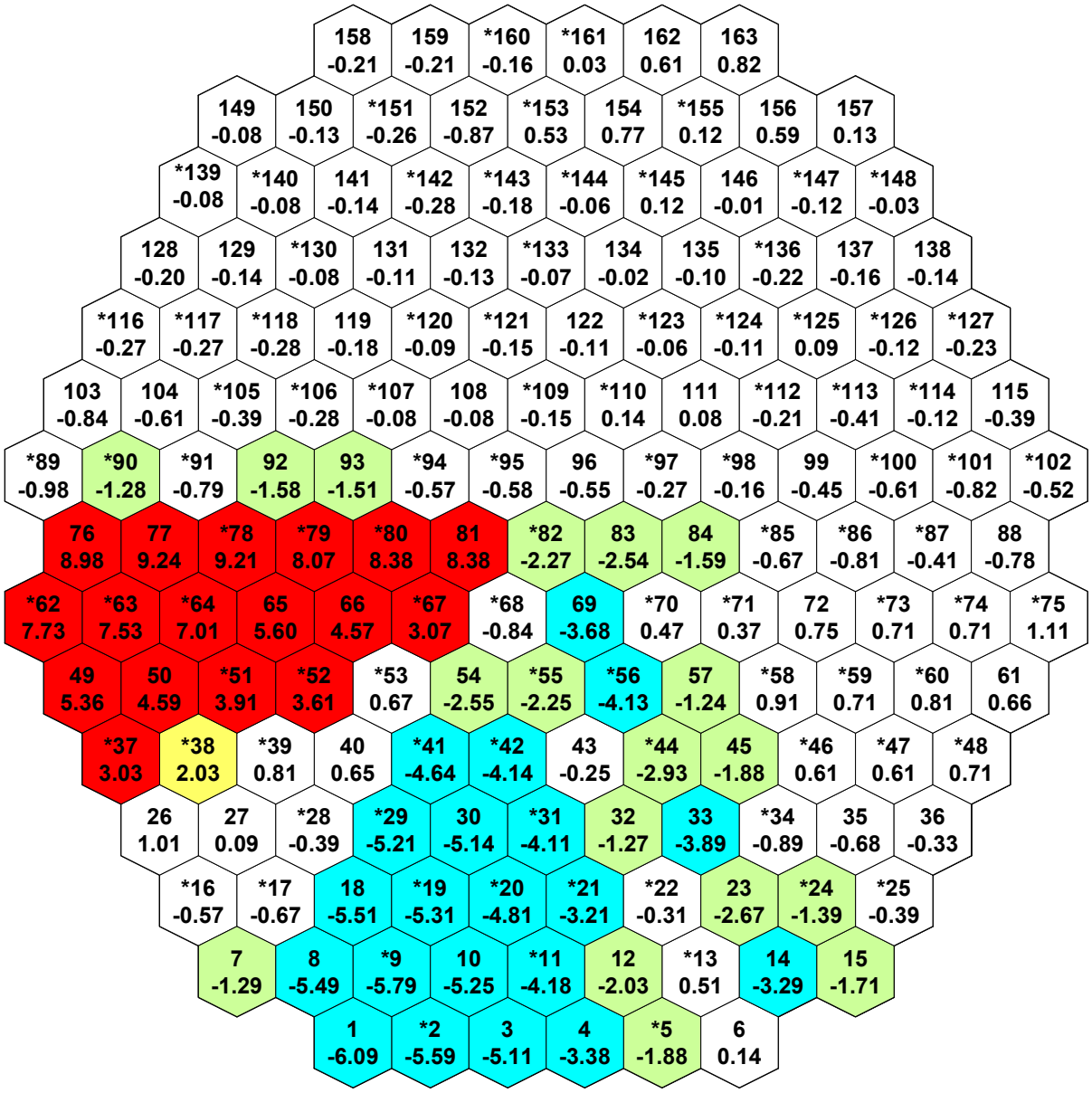

OECD PUBLICATIONS, 2 rue André-Pascal, 75775 PARIS CEDEX 16
PRINTED IN FRANCE